R005-01
B 会場 ：9/24　PM1 （13:45-15:30）
13:45〜14:00

大型研究プロジェクト「太陽地球系結合過程の研究基盤形成」

#山本　衛 [1)], 小川　泰信 [2)], 塩川　和夫 [3)], 吉川　顕正 [4)], 岩井　一正 [5)]
([1] 京大・生存圏研,([2] 極地研,([3] 名大 ISEE,([4] 九大/理学研究院,([5] 名大 ISEE

Large-scale research project ”Study of coupling processes in the solar-terrestrial system”

#Mamoru Yamamoto[1)],Yasunobu Ogawa[2)],Kazuo Shiokawa[3)],Akimasa Yoshikawa[4)],Kazumasa Iwai[5)]
([1]Research Institute for Sustainable Humanosphere, Kyoto University,([2]National Institute of Polar Research,([3]Institute for Space-Earth Environmental Research, Nagoya University,([4]Department of Earth and Planetary Sciences, Kyushu University,([5]Institute for Space-Earth Environmental Research, Nagoya University

The Earth receives energy from the Sun by radiation and by the solar wind (the flow of high-speed particles) and balances the energy by emitting infrared radiation. The material exchange between the Earth and surrounding space exists. We aim to unify and quantitatively understand the coupling processes of the solar-terrestrial system. Combining space plasma physics and the Earth’s atmospheric and hydrosphere science, we study the vast area as one complex system. It is to contribute to space utilization and to enhance the prediction of space and atmospheric changes. We pursue observations, theory, and simulations to accomplish the studies. In this research program, we develop an observation system that measures the entire region of the solar wind, electromagnetic plasma, and atmosphere. We are proposing this large research project to Roadmap 2023 of the Ministry of Education, Culture, Sports, Science and Technology (MEXT). In the project we set the following five research topics.

(1) Equatorial fountain

The energy and material flows that occur in all height regions of the equatorial atmosphere are named as ”Equatorial Fountain.” These processes from the bottom also cause various effects in the upper atmosphere. We establish Equatorial MU Rdar (EMU radar) in Indonesia as main instrument for the studies.

(2) Energy inputs into polar upper atmosphere and its response

The energy/particle inflow results in auroral Joule heating and ion drag of the atmosphere. The ion outflow from the polar ionosphere controls ambient plasma constituents in the magnetosphere. We will contribute the international EISCAT_3D radar project that has started in northern Scandinavia since 2017.

(3) Solar wind propagation process

In order to clarify the acceleration and propagation processes of the solar wind from the sun and to accurately predict its impact on the Earth, we develop a next-generation solar wind observation system and start observations. Clarifying the solar wind acceleration mechanism and dramatically improving the prediction accuracy of the scale and arrival time of the solar wind affecting the Earth.

(4) Global network of observation and data

We develop a global observation network of compact radio and optical remote sensing equipment from the equator to polar region.

(5) Integrated analysis of observational data centered on IUGONET

The data from the above observations are accumulated in the data-sharing system (IUGONET). A comprehensive analysis of the coupling process of the solar-terrestrial system will be conducted through the construction of an integrated database and analysis system that links domestic and international satellite missions and numerical models.

地球は太陽からの放射エネルギーと太陽風を受け、逆に赤外放射を行い物質が流入・流出する複合系で構成される。我々は太陽地球系の結合過程を統一し定量的な理解を目指す。宇宙惑星科学と大気水圏科学を結合し、広大な領域を複合システムとして研究し、宇宙利用や大気変動予測に貢献する。稠密で継続的な観測と理論・シミュレーションの協働が必須であり、太陽風、電磁気圏、大気圏の全域を測る地上観測を整備する。今回、以下の 5 つの研究項目を含む大型研究を文部科学省のロードマップ 2023 に提案した。研究プログラムの概要を報告する。

1. 赤道ファウンテン：赤道を中心とする地球大気の上下結合

赤道では、積雲対流と呼ばれる大気擾乱が活発である。赤道域の全ての高度層で現れる、エネルギーと物質の流れを「赤道ファウンテン」として捉え、その変動を、観測で明らかにする。そのため赤道域でも大気変動が最も強くなるインドネシアの赤道直下に赤道 MU レーダー（EMU: Equatorial MU Radar）を設置する。

2. 極域の磁気圏・電離圏・大気圏へのエネルギー流入と応答過程

太陽風に起因するエネルギーによる極域特有の現象を解明する。太陽風のエネルギーは姿を変えて、下層の大気や低緯度方向に輸送される。極域における大気の宇宙空間への流出の解明にも取り組む。スカンジナビア北部に EISCAT_3D レーダー（European Incoherent SCATter 3 Dimensional Radar）を建設する。

3. 太陽風伝搬過程

太陽から放出された太陽風の加速・伝搬過程を明らかにし、地球に対する影響を正確に予測するため、次世代太陽風観測装置を開発し、観測を開始する。太陽風加速機構を明らかにし、太陽面爆発が地球に影響を与える規模と到来時刻の予報精度を飛躍的に向上させる。

4. グローバル結合過程

小型の観測機器を多点に設置して、赤道から極域を南北につなぐ広域地上観測ネットワークを整備し、衛星観測、データベース、数値モデルと複合して、極と赤道を繋ぐ大気圏・電離圏・磁気圏のグローバルなエネルギーの流れを解明する。

5. IUGONET を中心とする観測データ統合解析

上記の観測からのデータをデータ共有システム (IUGONET) に適用し、国内外の衛星観測や数値モデル等と連携した統合データベース・解析システムの構築を通じて太陽地球系の結合過程を総合解析する。

R005-02
B 会場 ：9/24　PM1 （13:45-15:30）
14:00〜14:15

Es 層形成過程の中性大気とプラズマ大気の同時観測による解明: RIDE キャンペーン

#齊藤　昭則[1)], 松岡　彩子[2)], 坂崎　貴俊[1)], 阿部　琢美[3)], 齋藤　義文[3)], 石坂　圭吾[4)], 田川　雅人[5)], 横田　久美子[5)], 熊本　篤志[6)], 小嶋　浩嗣[7)], 栗田　怜[7)], 横山　竜宏[7)], 村田　直史[8)], 斎藤　享[9)], 高橋　透[9)], 西岡　未知[10)], 安藤　慧[10)], 細川　敬祐[11)], 中田　裕之[12)],Liu　Huixin[13)], 木暮　優[13)], 西山　尚典[14)], エジリ　ミツム[14)]
([1] 京都大・理・地球物理,[2] 京都大学,[3] ＪＡＸＡ宇宙科学研究所,[4] 富山県大・工,[5] 神戸大学大学院工学研究科,[6] 東北大・理・地球物理,[7] 京都大学 生存研,[8]JAXA,[9] 電子航法研,[10] 情報通信研究機構,[11] 電通大,[12] 千葉大・工,[13] 九大・理・地惑,[14] 極地研,[15]NICT,[16] 九大・理・地惑,[17] 千葉大・工,[18] 電通大,[19] 極地研

Elucidation of sporadic E layers by simultaneous observation of the neutral and ionized atmospheres: RIDE rocket campaign

#Akinori Saito[1)],Ayako Matsuoka[2)],Takatoshi Sakazaki[1)],Takumi Abe[3)],Yoshifumi Saito[3)],Keigo Ishisaka[4)],Masato Tagawa[5)],Kumiko Yokota[5)],Atsushi Kumamoto[6)],Hirotsugu Kojima[7)],Satoshi Kurita[7)],Tatsuhiro Yokoyama[7)],Naofumi Murata[8)],Susumu Saito[9)],Toru Takahashi[9)],Michi Nishioka[10)],Satoshi Andoh[10)],Keisuke Hosokawa[11)],Hiroyuki Nakata[12)],Huixin Liu[13)],Masaru Kogure[13)],Takanori Nishiyama[14)],Mitsumu K Ejiri[14)]
([1]Department of Geophysics, Graduate School of Science, Kyoto University,[2]Graduate School of Science, Kyoto University,[3]Institute of Space and Astronautical Science, Japan Aerospace Exploration Agency,[4]Faculty of Engineering, Toyama Prefectural University,[5]Graduate School of Engineering, Kobe University,[6]Department of Geophysics, Graduate School of Science, Tohoku University,[7]Research Institute for Sustainable Humanosphere, Kyoto University,[8]Japan Aerospace Exploration Agency,[9]Electronic Navigation Research Institute,[10]National Institute of Information and Communications Technology,[11]Graduate School of Informatics and Engineering, University of Electro-Communications,[12]Graduate School of Engineering, Chiba University,[13]Department of Earth and Planetary Science, Graduate School of Science,Kyushu University,[14]National Institute of Polar Research,[15]National Institute of Information and Communications Technology,[16]Department of Earth and Planetary Sciences , Kyushu University,[17]Department of Electrical and Electronic Engineering, Graduate School of Engineering, Chiba University,[18]Graduate School of Communication Engineering and Informatics, Graduate School of Informatics and Engineering, University of Electro-Communications,[19]National Institute of Polar Research

Rocket Investigation of Daytime E-region (RIDE) campaign is to directly observe the neutral atmosphere, plasma atmosphere, the electric field, and the magnetic field that generates the sporadic E layer with the S-310-46 sounding rocket from Uchinoura in the summer of 2024. The objectives of this sounding rocket experiment are as follows:

(1) Elucidate phenomena in which the interaction between neutral atmosphere and plasma is important by combining direct observations by the sounding rocket with a numerical model and ground-based observations.
(2) Complete measurement packages of the neutral atmosphere, plasma, and electromagnetic fields for sounding rockets and satellites.
(3) Develop human resources for future deployment.

The daytime sporadic E layer around 100 km altitude is the target of the campaign. Elucidation of the interaction between the neutral and plasma atmospheres, which is thought to be the cause of this phenomenon, will lead to the forecast of the sporadic E layer, which has an impact on social systems such as radio propagation disturbance. Although there is a wide range of ionospheric phenomena in which the interaction between neutrals and plasma is important, their elucidation has not been sufficiently advanced due to the difficulty of simultaneous observation of both atmospheres. In this experiment, comprehensive direct measurements of the neutral atmosphere, plasma atmosphere, and electromagnetic field will be made at 90-130 km altitude during the ascent and descent of the S-310-46 rocket at 11-14 local time in summer at mid-latitudes. This local time range is when the Es layer is expected to reach an altitude of around 105 km as it develops and the interaction between the neutral and plasma atmospheres is expected to be intense. Combined with numerical model predictions, the contribution of the electric field and wind in the formation of the Es layer can be clarified. In addition to this direct measurement by the rocket, ground-based observations at multiple locations will be conducted to evaluate the temporal evolution and spatial extent of the Es layer observed by the rocket and its effect on the anomalous propagation of radio waves used in air navigation and other social systems.

R005-03
B 会場 ：9/24　PM1 （13:45-15:30）
14:15〜14:30

#熊本　篤志 [1)], 阿部　琢美 [2)], 小嶋　浩嗣 [3)], 栗田　怜 [4)], 田中　孝治 [2)], 加藤　雄人 [1)]
([1] 東北大・理・地球物理,[2] ＪＡＸＡ宇宙科学研究所,[3] 京大,[4] 京都大学 生存研

Development of 1U-size impedance probe for cube satellite missions

#Atsushi Kumamoto[1)],Takumi Abe[2)],Hirotsugu Kojima[3)],Satoshi Kurita[4)],Koji Tanaka[2)],Yuto Katoh[1)]
([1]Department of Geophysics, Graduate School of Science, Tohoku University,[2]Institute of Space and Astronautical Science, Japan Aerospace Exploration Agency,[3]Kyoto university,[4]Research Institute for Sustainable Humanosphere, Kyoto University

Impedance probe has been used for measurements of the electron number density of the ionospheric and magnetospheric plasma in many sounding rocket experiments and several satellites missions. Its accuracy within several percent in the electron number density measurement is a clear advantage with respect to other observation methods. It has not been, however, applied yet in cube satellite missions which are increasing recently.

A small satellite mission for demonstrative experiments of wireless power transmission from Low Earth Orbit (LEO) satellites to the ground started in Dec. 2022. In the experiments planned in 2025, in addition to the performance of the power transmission, the effects of power transmission to the background plasma are required to be evaluated. So, the plasma monitor instruments such as impedance probe, Langmuir probe, and plasma wave receiver are also planned to be installed not only on mother satellite but also 6U-size daughter satellite, which is ejected from the mother satellite for additional power transmission experiments between two satellites in space. The impedance probe for previous sounding rockets (e.g. SS-520-3 NEI/PWM) would be applicable as is to the mother satellite. However, for installation to the daughter satellite, downsizing of the impedance probe instrument to 1U size is required.

Downsized impedance probe is also required in another mission: PCUBE (Probing, Controlling, and Understanding of radiation Belt Environments). The purpose of PCUBE is to investigate the contributions of the density ducts in the magnetosphere on the loss processes of the radiation belt electrons on the basis of observation with LEO cube satellite, and to make suggestions for future active experiments controlling density ducts and radiation belt electrons. In order to measure the precipitating electrons and density structures of the ducts, electron analyzer and impedance probe are planned to be installed on the cube satellite. The launch of the cube satellite is planned in 2026.

For two cube satellite missions mentioned above, development of 1U-size impedance probe has been started since Dec. 2022. In addition to the downsizing of electric circuit unit, shorter probe than the current one (1.2 m) would be preferable in order to avoid the limitations in attitude control of cube satellites. Plasma measurements test with shorter probes (0.3m and shorter) is planned using Space Chamber Laboratory of JAXA/ISAS in Sept. 2023.

R005-04
B 会場 ：9/24　PM1 （13:45-15:30）
14:30〜14:45

観測ロケット搭載超高層大気観測用真空計に関する研究

#飛田　奈々美 [1)], 阿部　琢美 [2)], 三宅　亙 [1)], 田中　真 [1)]
(1 東海大・工,(2 ＪＡＸＡ宇宙科学研究所,(3 東海大・工

The study of an ionization gauge for observing the upper atmosphere on a sounding rocket

#Nanami Tobita[1)],Takumi Abe[2)],Wataru Miyake[1)],Makoto Tanaka[1)]
(1Tokai University,(2ISAS/JAXA,(3Tokai University

Various phenomena occur in the lower thermosphere, but many of them are not well understood because of the complexity of particle motion. To understand these phenomena, it is necessary to accurately measure physical quantities. We use an ionization gauge, which is small, relatively simple in structure, and reliable, as a means of measuring atmospheric pressure in the thermosphere on board a sounding rocket. We have installed an ionization gauge onboard the sounding rocket “S-520-32” to get information on the neutral atmosphere in the lower part of the thermosphere by measuring the atmospheric pressure during the flight. To obtain information on the atmospheric inflow observed on the sounding rocket from the pressure measurement by the ionization gauge, an ionization gauge container was developed so that one can detect the direction of the atmospheric inflow on the rocket. In other words, it is necessary for the container to have a structure that the inside pressure changes depending on the inflow direction.

The pressure sensor was installed in the fabricated ionization gauge container and was mounted on the S-520-32 sounding rocket to measure atmospheric pressure during flight. The rate of change decreased when the pressure reached about 10^{-2} Pa at about 80 seconds after launch, and continued to gradually decrease until about 460 seconds. This gradual pressure change is probably related to the outgassing from the inner wall of the container where the ionization gauge sensor was housed. From about 87 seconds, sinusoidal changes in the measured pressure value with rocket spin were observed. This result shows that countermeasures against outgassing are necessary to measure atmospheric pressure at high altitudes.

In this presentation, we describe further development of the ionization gauge to be installed on the S-310-46 sounding rocket, which is scheduled to be launched in the next year, by discussing the installation configuration and necessary improvement of this ionization gauge system.

First, the direction of the atmospheric flow during the flight of the S-310 rocket was calculated using the attitude and orbit data of the S-310-44 sounding rocket, which was launched from USC. In general, the thermal velocity of atmospheric particles is enough smaller than the velocity of the rocket, so the direction of the atmospheric flow observed on the rocket is in the opposite direction of the velocity vector of the rocket. The information obtained from our calculation is the incident angle of the atmospheric inflow to the ionization gauge with respect to the rocket axis during a rocket flight. In general, measurements of sounding rockets are more important during ascent than during descent, when the rocket is affected by the wake.

Next, using the obtained angle of incidence of atmospheric flows during rocket flight, changes in measured pressure were analyzed and compared when the angle between the rocket axis and the gas inlet of the ionization gauge was changed. When the incident angle of atmospheric flows and the angle between the axis and the gas inlet is approximately equal, the measured pressure was the largest. This is because the measured pressure is maximum when the atmospheric inflow is parallel to the axis of the ionization gauge container.

The onboard ionization gauge container has a closed structure and is assumed to be affected by dynamic pressure in addition to the static pressure of the atmosphere. If the gas inlet of the ionization gauge is at an angle of more than 90 degrees to the direction of rocket velocity leading to rocket spin, the increase in gas velocity due to rocket velocity has no effect on the pressure measurement. In this case, only the atmospheric static pressure is measured, and this value is the minimum value in one spin of the rocket. Because of the supersonic speed of the rocket, the dynamic pressure is greater than the static pressure, and the measured pressure is expected to vary with the spin of the rocket during flight. The maximum pressure is measured when the dynamic pressure has the largest effect on the measured pressure, i.e., when the axis of the ionization gauge container coincides with the velocity vector of the rocket. To determine how much the pressure is expected to change during rocket spin, the relative difference between the minimum and maximum pressure in the change in measured pressure of rocket spin was calculated. At altitudes of 100-120 km during rocket ascent, the percentages were all greater than 15%. If the difference between the minimum and maximum pressures is sufficiently large, it is possible to estimate the incident angle of the atmospheric inflow on the sounding rocket.

Furthermore, we analyze if the ionization gauge system can detect a velocity shear of the neutral wind, which is probably related to the sporadic E, as a meaningful change in the observed data. Assuming that a horizontal wind of 100 m/s in the lower thermosphere, the magnitude of the pressure changes was calculated. It was found that a pressure difference of 1-9% is expected at altitudes of 100-120 km during rocket ascent if the horizontal wind with a velocity of 100 m/s exists.

熱圏下部では様々な現象が発生しているが，粒子の運動が複雑であるため未解明の現象が多い．それらを理解するため

に物理量を精確に実測する必要がある．我々は観測ロケット上で熱圏大気圧力を測定する手段として，小型で構造が比較的単純，かつ信頼性のある真空計を用いている．観測ロケットに真空計を搭載し，飛翔中に測定された大気圧力から，熱圏下部の中性大気に関する情報の推定を行なうこととした．真空計による圧力測定から観測ロケット上で観測される大気の流れに関する情報の取得を可能にするために，ロケット上で観測される大気流の方向検知が可能な真空計の容器，すなわち風が到来する方向によって内部の圧力が変動するような測定を可能にする構造の真空計容器を製作している．

製作した真空計容器内にセンサを収納し，観測ロケット S-520-32 号機に搭載して飛翔中の大気圧力を測定した．打上げから約 80 秒で圧力値が 10^{-2} Pa 程度に達すると変化率が減少し，緩やかな勾配で 460 秒まで減少した．この緩やかな圧力変化は，真空計センサが収納された容器内壁からのアウトガスの影響によって容器内部の圧力が下がらなかったために見られた傾向であると考えられる．約 87 秒からはロケットのスピンに伴う測定圧力値の正弦波的な変化を確認した．S-520-32 号機で取得した結果より，高高度で大気圧力を測定するためにはアウトガス対策を施す必要があると分かった．

本研究では，来年度に打上げが予定されている観測ロケット S-310-46 号機に搭載される真空計のために，搭載方法や観測ロケット上で予想される測定圧力の変化に係る解析を行なった．

まず，S-310 型ロケットの飛翔中に流入する大気流の方向について，内之浦宇宙空間観測所より打上げられた，観測ロケット S-310-44 号機の姿勢データと軌道情報を使用して計算を行なった．一般に，大気粒子の熱速度はロケットの速度ベクトルよりも十分に小さいため，ロケット上で観測される大気流の方向はロケットの速度ベクトルの逆方向になる．この計算により得られた角度情報は，ロケットの飛翔中に真空計に入る大気流の機軸に対する入射角である．一般に観測ロケットの測定は，ウェークの影響を受ける下降時より上昇時の測定の方がより重要である．S-310-44 号機の上昇時，高度 100〜120 km では機軸方向に対して 10〜15 度の方向から大気流が流入する可能性が高いとの結果を得た．

次に，取得したロケットの飛翔中に流入する大気流の入射角を用いて，機軸と真空計のガス流入口の間の角度を変更した場合の測定圧力の変化について解析し，比較を行なった．大気流の入射角と，機軸とガス流入口の間の角度が概ね一致した場合に，測定される圧力が最大になる．これは，大気流が真空計のガス流入口の正面から流入した際に測定圧力が最大になるためである．

搭載する真空計容器は内部が閉構造になっており，大気の静的な圧力に加え，動的な圧力による影響を受けるものと仮定している．ロケットスピンによって真空計のガス流入口がロケットの速度方向に対して 90 度以上の角度をなす方向では，ロケットの速度によるガス流入速度の増加が圧力測定に影響を及ぼさない．この場合，大気の静圧のみが測定され，この値はロケットの 1 スピンの変化の中の最小値となる．ロケット速度が超音速であるため，動圧は静圧よりも大きく，ロケットの飛翔中はスピンに応じて測定される圧力が変化すると予想される．測定圧力に動圧が最も大きく影響する時，すなわち真空計の方向がロケットの速度ベクトルと一致した時に最大圧力が測定される．このロケットスピン中での圧力変化がどの程度になると予想されるかを求めるために，ロケットスピンによる測定圧力の変化の中での最小圧力と最大圧力の相対的な差を計算した．ロケット上昇時における高度 100〜120 km では，その割合はいずれも 15% 以上であった．この最小圧力と最大圧力の差が十分に大きければ，変化する大気の入射角を推定することが可能になる．

さらに，観測するスポラディック E 層に関係があると考えられている中性風の速度シアがある場合，観測データにそれが現れるかについて解析を行なった．ロケット飛翔中に 100 m/s の水平風が存在すると仮定し，測定される圧力変化を計算した．水平方向の風を考慮した場合とロケット速度に起因する動圧のみ考慮した場合は，ロケット上昇時の高度 100〜120 km では 1〜9% 程度の圧力差が生じることが分かった．

R005-05
B 会場 ：9/24　PM1 （13:45-15:30）
14:45〜15:00

極域における夜光雲の地上観測計画

#遠藤　哲歩 [1)], 鈴木　秀彦 [1)], 川上　莉奈 [1)], 増田　歩音 [1)]
([1] 明治大

A plan for a ground-based observation of noctilucent clouds in the polar region.

#Akiho Endo[1)],Hidehiko Suzuki[1)],Rina Kawakami[1)],Ayune Masuda[1)]
([1]Meiji University

Noctilucent cloud (NLC) images often contain very fine wavy structures ranging from several kilometers to several tens of kilometers. These are thought to reflect small scale local atmospheric disturbances in the upper atmosphere. Satellite imaging data cannot resolve these fine structures, and thus, ground-based imaging is an effective method to study the relationship between fine structures in NLC and background disturbances in the upper mesosphere. However, previous NLC observations have been conducted mainly in the Northern Hemisphere, as represented by Northern Europe [e.g. P.Dalin et al., AnnGeophys.,2019] and the North American continent [e.g. James M.Russell III et al., JGR, 2014]. In contrast, there are very few observations in the Southern Hemisphere. The reason for this asymmetry is that most of the best observation latitudes in the Southern Hemisphere are in the ocean, and most of the land area of Antarctica is under the influence of the midnight sun, which makes it difficult to detect NLCs because of a bright background sky condition. Therefore, opportunities for NLC observations in the Southern hemisphere are quite limited. We have examined the feasibility to overcome this problem by developing an optical imager specialized for noctilucent cloud observations [Nakamura et al., 2021]. Noctilucent clouds are known to have a spectral peak at 400-500 nm in their radiance [Fogle and Rees,1972]. On the other hand, the background spectrum in twilight sky attenuates in wavelengths shorter than 680nm. Therefore, there is the optimum wavelength band for noctilucent cloud observation with the best signal-to-noise ratio (SNR) near this wavelength band. In this study, the most suitable bandpass for NLC observations is proposed based on the ground spectral data acquired in the polar regions in twilight time. We also report the expected observation period in the summer season if the new imager is installed in Syowa Station (69.00S, 39.58E), Antarctic.

夜光雲を地上から撮像すると、その雲の形状は数 km-数十 km という非常に細かい波状構造を含む事例が多く、これは超高層大気に常に存在する小規模の局所的な大気擾乱を反映していると考えられている。人工衛星観測からの撮像データはこの微細な構造を捉えることが出来ず、夜光雲の地上からの撮像は、超高層大気擾乱の水平空間構造の高分解能解析を可能とする現状唯一の手段である。しかし、これまでの夜光雲撮像例は北欧 [P.Dalin et al., AnnGeophys.,2019 等] や北アメリカ大陸 [James M.Russell Ⅲ et al., JGR,2014 等] に代表される北半球に集中し、南半球での観測例は極めて少ない。これは、北半球に比べ南半球の観測最適緯度帯の大部分が海域である事や、陸域にあたる南極大陸の殆どが南極圏であるために、白夜の影響から観測好機が極めて短期間である事が障壁となっているためである。本研究ではこの問題を、明るい背景光下でも観測が可能な夜光雲特化型のイメージャーを開発することにより打開できないか検討を重ねてきた [中村他,2021]。夜光雲の輝度スペクトルのピークは 400-500 nm にある事が知られている [Fogle and Rees,1972]。一方で、夜光雲が出現する時間帯である薄明時の背景光スペクトルは、680nm をピークに短波長側で減衰する。従って、この波長帯付近に最も高い信号対雑音比 (SNR) が期待される夜光雲観測に最適な波長帯が存在する。本研究では単バンド観測で夜光雲の検出に最も有利な帯域の選定を、極域で実測した薄明時の地上分光スペクトルのデータに基づいて行った。本発表では、この検討結果をもとに、昭和基地 (69.00° S,39.58° E) での夜光雲地上観測を想定した際に期待される観測期間拡大日数の推定結果および観測計画について報告する。

R005-06
B 会場 ：9/24　PM1 （13:45-15:30）
15:00〜15:15

#渡部　蓮 [1)], 津田　卓雄 [1)], 青木　猛 [1)], 雁金　沙弥香 [1)], 野澤　悟徳 [2)], 川端　哲也 [2)], 斎藤　徳人 [3)], 川原　琢也 [4)]
([1] 電通大,[2] 名大・宇地研,[3] 理化学研究所,[4] 信州大・工

A self-build FPGA-based data acquisition system for an upgrade of the Tromsoe sodium lidar

#Ren Watabe[1)],Takuo Tsuda[1)],Takeshi Aoki[1)],Sayaka Karigane[1)],Satonori Nozawa[2)],Tetsuya Kawabata[2)],Norihito Saito[3)],Takuya Kawahara[4)]
([1]University of Electro-Communications,[2]Institute for Space-Earth Environment Research, Nagoya University,[3]RIKEN,[4]Faculty of Engineering, Shinshu University

The sodium (Na) resonance scattering lidar is a laser remote sensing system that can detect Na in the upper mesosphere and lower thermosphere (80-110 km altitudes). The Na lidar installed in Tromsoe, Norway, is equipped with a laser diode (LD)-pumped laser system, which is highly stable and long-lifetime. The power of the LD laser is 4 W with a repetition rate of 1 kHz. Because of such a high-power laser, the Tromsoe lidar is capable of simultaneous five-beam observations in five directions. The inter-pulse period (IPP) is 1 msec, so the corresponding height coverage of this lidar is 0-150 km. Thus, the Tromsoe lidar is designed for observations of Na layers at 80-110 km, so-called the normal Na layers. On the other hand, recent observations by other lidars have revealed low-density Na events at higher altitudes (above 110 km, up to 170 km). Such Na events are expected to provide good opportunities for observations at the thermospheric heights. However, the current height coverage of the Tromsoe Na lidar is insufficient for observations of such Na events at higher altitudes.

To improve the height coverage of Tromsoe Na lidar, we propose a time-delayed multi-beam observation method. In the conventional method (i.e., the simultaneous multi-beam method), the laser pulses are split into multi directions, and each pulse is transmitted in each direction simultaneously. In contrast, in the proposed method, laser pulses are transmitted in each direction with a time delay. As a result, longer IPP can be obtained, which allow us to have a larger height coverage. Moreover, the laser pulses do not have to be split in this method, and thus the signal-to-noise ratio (SNR) can be improved, compared with the conventional method. These improvements are expected to be effective for observations of low-density Na events at upper altitudes. In order to implement this method, we need a more flexible data acquisition system, which fits to such a time-delayed multi-beam observation. In addition, a system for high-speed switching in the laser pulse direction is also needed.

In the present work, we have been working on a self-build FPGA-based system that includes a multi-channel data acquisition system and a precise time delay control system. In the initial stage, we developed an FPGA-based data acquisition system, which has the same functions as the commercial data acquisition system. As a performance test of the developed system, test observations were conducted by using the Na lidar at Tromsoe in mid-February 2023. From comparisons between the developed and the commercial systems, it is found that Na signals were successfully detected by the developed system, and its obtained signals were well consistent with those from the commercial system. Furthermore, as for the limit in the counting of faster signals, the developed system achieved a limit of ˜17,000, while the commercial system had a limit of ˜15,000. These results suggest that the developed system has a better dynamic range than the commercial system. In the presentation, we will show an overview of the proposed method and the results of the performance tests in the developed system. The current status of further developments for additional functions will be also reported.

R005-07
B 会場 ：9/24　PM2 （15:45-18:15）
15:45〜16:00

#大山　伸一郎 [1,2], 細川　敬祐 [3],Vanhamaki　Heikki[4],Aikio　Anita[4], 坂野井　健 [5],Cai　Lei[4],Virtanen　Ilkka[4], 塩川　和夫 [1], 西谷　望 [1], 新堀　淳樹 [1], 小川　泰信 [2]
([1] 名古屋大学宇宙地球環境研究所,[2] 国立極地研究所,[3] 電気通信大学,[4] オウル大学,[5] 東北大学

IMF dependence of midnight bifurcation of the thermospheric wind based on nine winter measurements in Tromsoe, Norway

#Shin-ichiro Oyama[1,2],Keisuke Hosokawa[3],Heikki Vanhamaki[4],Anita Aikio[4],Takeshi Sakanoi[5],Lei Cai[4],Ilkka Virtanen[4],Kazuo Shiokawa[1],Nozomu Nishitani[1],Atsuki Shinbori[1],Yasunobu Ogawa[2]
([1]Institute for Space-Earth Environmental Research, Nagoya University,[2]National Institute of Polar Research,[3]The University of Electro-Communications,[4]University of Oulu,[5]Tohoku University

The ionosphere is partially ionized plasma, but the particle minority of ions plays an important role in controlling dynamics of the thermosphere. Particle collision is the fundamental process for momentum transfer from ionospheric ions to thermospheric neutral particles. The ionospheric plasma flow pattern at high latitudes depends on the direction of the interplanetary magnetic field (IMF), and the pattern may be projected on the thermospheric wind. However, the dependence is not yet well understood. This study derived statistical experimental features regarding the dependence of the thermospheric wind at an F-region altitude, analyzing data for nine winter seasons from a Fabry-Perot interferometer (630 nm) and a Dynasonde in Tromsoe, Norway. The wind pattern around midnight is different from the ionospheric plasma convection, in accordance with the IMF direction. The zonal wind bifurcates immediately before midnight for IMF By$<$0, but for By$>$0, it inverts gradually into the postmidnight sector. Neutral wind streams, originating from higher latitudes, may cause the dependence because of anti-sunward plasma flow distortion in the polar cap. In summary, this study concludes that the zonal wind bifurcation at auroral latitudes is caused by the ion velocity bifurcation, and that advection from the polar cap region affects the wind response time to the ion velocity bifurcation.

R005-08
B 会場 ：9/24　PM2 （15:45-18:15）
16:00〜16:15

#西山　尚典[1)], 鍵谷　将人[2)], 小川　泰信[1)], 津田　卓雄[3)], 岩佐　祐希[4)], 古舘　千力[3)],Dalin　Peter[7)],Partamies Noora[6)], 土屋　史紀[2)], 野澤　悟徳[5)],Sigernes　Fred[6)]
([1] 極地研,[2] 東北大・理・惑星プラズマ大気研究センター,[3] 電通大,[4] 産総研・計量標準総合センター,[5] 名大・宇地研,[6]University In Centre Svalbard,[7]Swedish Institute of Space Physics,[8] 東北大・理・惑星プラズマ大気

A multi-event study of auroral intensifications in N2+ (0,0) Meinel band at 1.1 um observed by the NIRAS-2 and the NIRAC

#Takanori Nishiyama[1)],Masato Kagitani[2)],Yasunobu Ogawa[1)],Takuo Tsuda[3)],Yuki Iwasa[4)],Senri Furutachi[3)],Peter Dalin[7)],Noora Partamies[6)],Fuminori Tsuchiya[2)],Satonori Nozawa[5)],Fred Sigernes[6)]
([1]National Institute of Polar Research,[2]Planetary Plasma and Atmospheric Research Center, Graduate School of Science, Tohoku University,[3]University of Electro-Communications,[4]National Metrology Institute of Japan, AIST,[5]Institute for Space-Earth Environment Research, Nagoya University,[6]University In Centre Svalbard,[7]Swedish Institute of Space Physics,[8]Planetary Plasma and Atmospheric Research Center, Graduate School of Science, Tohoku University

Dayside aurora and polar patch are the key phenomena for understanding of the dayside magnetosphere-ionosphere-atmosphere coupling process. These phenomena are being monitored by ground-based optical instruments in high latitude region corresponding to polar cap and cusp, but the observations are done at limited geographic location and in limited season for avoiding strong photon intensity of sky background. Alternatively, active/passive radio remote sensing such as HF/VHF/UHF radar, GNSS and LF wave receiver are effective, but spatial and temporal resolutions by those measurements are not sufficient generally in comparison to optical measurements.

We present simultaneous observations of N_2^+ Meinel (0,0) band (hereafter, N_2^+ (M)) aurora by cutting-edge short wavelength infrared (SWIR) imaging spectrograph (NIRAS-2) and monochromatic camera (NIRAC) installed at Kjell Henriksen Observatory (78^{o}N, 16^{o}E). NIRAS-2 is a 2-D imaging spectrograph with a fast optical system and high spectral resolutions to challenge twilight/daytime aurora measurements from the ground. It is designed for SWIR wavelength from 1.1 to 1.3 microns in which sky background intensity is weaker than in visible subrange. In addition, NIRAC have been developed focusing on aurora emissions of N_2^+ (M). N_2^+ (M) is about two orders brighter than the N_2 1st negative band at 427.8 nm (Remick et al. 2001), which means that the band can be a good indicator of energetic electron precipitations. Total optical system is fast (F-number 1.5) and its FOV (84^o x 68^o) is slightly wider than that of the NIRAS-2. Thus, the NIRAC is used as a twin instrument to the NIRAS-2 to help in interpreting meridional scan data obtained from the NIRAS-2.

On January 21 2023, N_2^+ (M) intensification of associated with a band-shape aurora structure was observed by the NIRAS-2 and the NIRAC by temporal resolutions of 30 seconds and 20 seconds, respectively. Additionally, the European incoherent scatter Svalbard Radar (ESR) also observed electron density variations at the same time. Electron density measured at altitude ranges from 100 km 120 km changed in the same way as N_2^+ (M) intensity, which implies that a primary source of N_2^+ (M) emissions is direct collisions of N_2 by precipitating electrons penetrating down to around 100 km altitude (up to 10 keV). However, the observation also demonstrated moderate correlations between N_2^+ (M) intensity and electron density above 140 km, which implies that different N_2^+ (M) generation process, N_2 charge exchange with O^+, may work up to near 160 km and make a non-negligible contribution to N_2^+ (M) emissions. This hypothesis would be verified with further radar observations or stereo imaging observations useful to estimate the vertical distribution of the emission layers.

The observed N_2^+ (M) spectrum show fine structures due to N_2^+ rotational motions and it was successfully reproduced by common molecular models for diatomics and non-linear least squares fitting. The estimated N_2^+ rotational temperature with 30-sec cadences mostly ranges from 200 to 400 K, which agrees with one in NRLMSIS 2.1 at 100 and 120 km altitude, respectively. During a period where strong aurora intensification was seen, the rotational temperature was about 210 K with an error of 15 K (1-sigma). In addition, the ESR demonstrated that a peak altitude of electron density also got down to 100 km. These results are consistent with that a center altitude of N_2^+ (M) emission layer gets lower associated with more energetic particle precipitations. In this study, further analysis results based on the above case study and several similar events will be presented.

R005-09
B 会場 ：9/24　PM2 （15:45-18:15）
16:15〜16:30

#古舘　千力 [1)], 西山　尚典 [2)], 津田　卓雄 [1)], 小川　泰信 [2)], 堤　雅基 [2)],Partamies Noora[3)], 野澤　悟徳 [4)],Sigernes Fred[3)]
([1] 電通大,[2] 極地研,[3]University Centre in Svalbard,[4] 名大・宇地研

Atmospheric wave variability in the upper mesosphere based on ground-based observations of OH airglows (˜1.3 μ m) in Longyearbyen

#Senri Furutachi[1)],Takanori Nishiyama[2)],Takuo Tsuda[1)],Yasunobu Ogawa[2)],Masaki Tsutsumi[2)],Noora Partamies[3)],Satonori Nozawa[4)],Fred Sigernes[3)]
([1]University of Electro-Communications,[2]National Institute of Polar Research,[3]University Centre in Svalbard,[4]Institute for Space-Earth Environment Research, Nagoya University

The energy and momentum of the atmospheric waves, such as atmospheric gravity waves, tides, and planetary waves, can drive the zonal and/or meridional winds in the mesosphere and lower thermosphere (MLT), which are considered to be closely related to the general circulation in the whole atmosphere. Thus, it is important to observe the activities of such atmospheric waves in the MLT region, for more precise modeling research. Many observations of such atmospheric waves have been done for many years. In particular, recent polar-orbit satellites have been providing global observations. On the other hand, in addition to such satellites, higher resolution observations by ground-based observations are also important to resolve smaller- or shorter-scale waves. For example, tides with higher frequencies (8- and 6-hours periods) in polar regions have not been fully studied and poorly understood

As for the temperature observations from the ground, the rotational temperature of OH airglow has been extensively investigated in the past over 60 years. Recently, short-wavelength infrared OH airglow observations using InGaAs FPA (Focal Plane Array) have been reported. The OH airglow intensity in this region is stronger than that in the visible subrange, and thus more advanced airglow observations (e.g., with higher time resolution) can be expected. However, observations using the short-wavelength infrared OH bands are still limited so far, especially in the polar region. In addition, auroral contamination is one of the difficulties in airglow observations in the polar region. For example, there is a report that temperature measurements using the OH (3,1) band (˜1.5 μ m) at Syowa Station, Antarctic (69.0 ºN, 39.6 ºN) included an underestimation of the temperature possibly by ˜40 K due to auroral contamination. Therefore, a more robust method is needed for OH temperature observations in the polar region.

In this research, we propose spectroscopic observations of the OH airglow in ˜1.3 μ m, which would be expected to be more robust to such auroral contamination. We have developed a brand new Near-InfraRed Aurora and airglow Spectrograph-2 (NIRAS-2). It is an imaging spectrograph with InGaAs 2D FPA, which has a wide FOV of 55 degrees with a resolution of 0.11 degrees, and its wavelength resolution is variable with combinations of three slits, 30-, 60-, and 90- μ m, and two volume phase holographic gratings, 950- and 1500-lpmm. OH airglow observations are mainly performed using the low-dispersion 950-lpmm grating with 60- μ m slits. The wavelength range is from 1195 to 1350 nm, targeting the OH (7,4) and (8,5) bands and O_2 IR band with a spectral resolution of 1.1 nm. The preliminary test observation in NIPR, Tokyo, showed that the signal-noise ratio is better than its predecessor, NIRAS. The temperature data, estimated from the OH (8,5) band (˜1.3 μ m) in the 10-minute integration, were well comparable with those from NRLMSISE-00. The estimated temperature error was a few K, which is significantly better than that from NIRAS.

NIRAS-2) was installed at The Kjell Henriksen Observatory (KHO), Longyearbyen (78.1 ºN, 16.0 ºN) in late November 2022. Continuous 24-hour observations of the OH bands were made with 30-second exposures from November 23 to December 26, 2022, and then the OH observations were also routinely done for continuous two weeks in every month from January to March 2023. OH rotational temperatures derived from the 30-minute integrations are in a good agreement with the OH (6,2) rotational temperatures obtained from the spectrometer of the University Centre in Svalbard and the temperature obtained from Aura/Microwave Limb Sounder. Moreover, we are working on data analysis to investigate the activities of atmospheric waves, mainly atmospheric tides and gravity waves. In the preliminary analysis, we found clear 6- and 8-hour wave activities in both the OH (7,4) and OH (8,5) bands data with 5-min resolutions. These results would be similar to the previous results obtained at Eureka (80 ºN) [Oznovich et al., 1997]. For further investigation, the results from the temperature observations will be then compared with wind observations from the co-located Nippon/Norway Svalbard Meteor Radar (NSMR) [Hall et al., 2002]. In the presentation, we will show these results and give a more detailed discussion.

R005-10
B 会場 ：9/24　PM2 （15:45-18:15）
16:30〜16:45

VortEx キャンペーン中における北極域 MLT 領域風速変動

#野澤　悟徳 [1)], 小川　泰信 [2)], 堤　雅基 [2)],Lehmacher　Gerald A[3)]
[(1] 名大・宇地研,[(2] 極地研,[(3] クレメンス大学

Variations of winds from 70 to 120 km in the polar MLT region during the VortEx campaign

#Satonori Nozawa[1)],Yasunobu Ogawa[2)],Masaki Tsutsumi[2)],Gerald A Lehmacher[3)]
[(1]Institute for Space-Earth Environment Research, Nagoya University,[(2]National Institute of Polar Research,[(3]Clemson University

The Vorticity Experiment (VortEx) campaign was conducted from 17 to 25 March 2023 in northern Scandinavia. At 21:00 UT and 21:02 UT on March 23, two rockets were successfully launched (https://andoyaspace.no/news-articles/lift-off-for-nasa-vortex/) from Andoya (69.3 deg. N, 16.0 deg. E). TMA (Trimethylaluminum) observations were made (see Figure). The campaign was designed to study mesoscale structures in the wind field in the lower Thermosphere (90-120 km). The EISCAT UHF radar, which has a capability to derive wind velocities between 90 and 120 km, was successfully operated at Tromsoe (69.6 deg. N, 19.2 deg. E) during the campaign. We gathered 130 hours of EISCAT Special experiment (SP) time from Japan, UK, Sweden, Norway, Germany (DLR) and Peer-reviewed Program (EISCAT), and made EISCAT UHF radar observations during the campaign for 12 hrs every night from 17 to 25 March; we utilized scanning modes (so-called CP-2 type). Co-located MF radar and meteor radar at Tromsoe also made wind observations in the upper Mesosphere (70-100 km), and also meteor radar at Alta (69.97 deg. N, 23.24 deg. E) as well. We analyzed the wind data, and derived wave components in the upper Mesosphere and the lower Thermosphere. We will report observational results, in particular focusing on variations of the semidiurnal tide between 70 and 120 km in the polar MLT region.

Vorticity Experiment (VortEx) キャンペーンが、2023 年 3 月 17 日から 25 日に実施され、3 月 23 日 21:00 UT および 21:02 UT にアンドーヤロケットレンジ (69.3 度 N, 16.0 度 E) から連続して 2 つのロケットが北西に向けて発射され (https://andoyaspace.no/news-articles/lift-off-for-nasa-vortex/)、TMA(Trimethylaluminum) 観測等が実施された（図参照)。このロケットキャンペーンの目的は、上部中間圏・下部熱圏 (90-120 km; MLT 領域) におけるメソスーケル風速構造および乱流の解明である。このロケットキャンペーンに呼応して、複数のレーダー、イメージャー等の地上観測装置が稼働した。我々のグループは、トロムソ (69.6 度 N, 19.2 度 E) における地上観測を実施した。EISCAT UHF レーダーの特別実験を、3 月 17 日から 25 日にかけて毎晩 12 時間実施した（計 108 時間)。この EISCAT レーダー特別実験には、日本、英国、ノルウェー、スウェーデン、ドイツ（DLR）および EISCAT Peer-reviewed Program から実験時間が提供された。EISCAT UHF レーダー観測モードは、いわゆる CP-2 タイプのスキャンニングモード（3 点ないし 4 点を 10 分間でスキャン）を採用し、特に大きな問題なく 9 晩実施できた。この観測データにより下部熱圏高度 (90-120 km) での中性風速が導出できる。トロムソでは、MF レーダー（名大 ISEE、ノルウェー北極大学（以下、UiT)、サスカッチャン大学による共同運営)、流星レーダー（NIPR、UiT 共同運営）も問題なく稼働し、風速データを取得した。また、アルタ (69.97 度 N, 23.24 度 E）流星レーダー（名大 ISEE、UiT 共同運営）も問題なく稼働した。これらの風速データを合わせることにより、高度 70 km から 120 km の風速変動を調べることができる。講演では、観測結果の概要を述べた後、半日潮汐波の変動を中心に報告する。

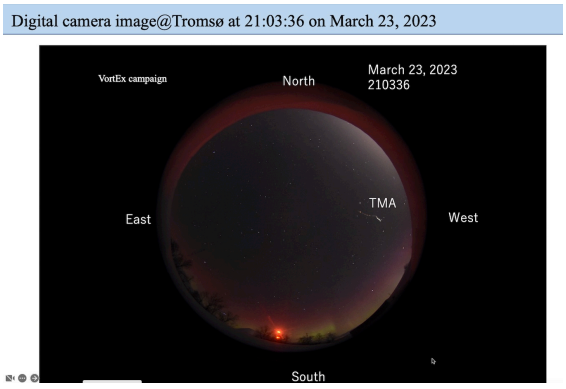

R005-11
B 会場 ：9/24　PM2 （15:45-18:15）
16:45〜17:00

中波レーダーを使った流星エコー観測に基づく高分解能風速観測

#堤　雅基[1)],Renkwitz Toralf[2)],Chau Jorge[2)]
[(1] 極地研,[(2]Leibniz Institute of Atmospheric Physics

High resolution wind observations based on MF radar meteor echo measurements

#Masaki Tsutsumi[1)],Toralf Renkwitz[2)],Jorge Chau[2)]
[(1]National Institute of Polar Research,[(2]Leibniz Institute of Atmospheric Physics

The MF (middle frequency) radar at Syowa Station (69S, 39E), Antarctic, has been applied to meteor wind observations since 1999 [Tsutsumi and Aso, JGR, 2005], and recently redeveloped further to improve its time/spatial resolutions. Because the duration of meteor echoes is proportional to the square of the radio wavelength, the duration of MF (2-3 MHz) meteor echoes is more than 100 times longer than that of usual VHF (~30 MHz) meteor echoes, indicating that the actual observation time of MF radar meteor measurement can be significantly longer than that of a VHF system and that a more continuous and dense measurement is possible under a geomagnetically quiet condition where MF radio wave can travel without significant absorption or retardation. The redeveloped technique show horizontal wind velocities can be estimated with a highly improved time resolution of about 10 minutes in the height region of 80-115 km, and can even be resolved horizontally every 50 km or so within the 10 minutes. Such resolutions are unprecedentedly high as meteor wind measurements [Tsutsumi, SGPESS fall meeting, 2022; Tsutsumi et al., JPGU 2023].

This technique is now being further applied to MF radars at the northern mid-to-high latitudes, Saura (69N, 16E) and Juliusruh (54N, 13E), routinely operated by Leibniz Institute of Atmospheric Physics. These radars are well equipped with an interferometer capability with 9 and 6 receiver channels, respectively. We have found that existing archived data of these radar systems can, at least partly, be applicable to the meteor echo analyses as those we have done with the Syowa system. Some preliminary results of wind analyses are to be presented, and a future plan is also to be discussed. The high resolution wind measurements by these radars would especially be beneficial for small scale atmospheric gravity wave studies in the mesosphere and lower thermosphere.

R005-12
B 会場 ：9/24　PM2 （15:45-18:15）
17:00〜17:15

城里におけるＯＨ大気光イメージング観測で検出された停滞性波動イベントの解析

#石井　智士 [1)], 鈴木　秀彦 [2)]
([1] 立教大,[2] 明治大

Analysis of stationary wave events detected by OH airglow imaging observation at Shirosato

#Satoshi Ishii[1)],Hidehiko Suzuki[2)]
([1]Rikkyo University,[2]Meiji university

The mountain wave (MW) is an atmospheric gravity wave generated by orographic forcing. Since the source of MW is fixed at the ground, it is considered an important factor affecting atmospheric circulation in the upper atmosphere, coupled with the seasonally changing lower-level wind field. Although various observations and numerical experiments have been conducted to understand the excitation and propagation characteristics of MWs, few previous studies have focused on the propagation process of MWs excited by small-scale mountains and the frequency of propagation into the upper atmosphere. Ishii et al. (2022) analyzed satellite image data in which wave cloud generated by MWs were observed. Also, they used reanalysis data (MERRA-2) and investigated the relationship between lower-level wind directions and orientations of mountain ridges around the world. It was found that mountain waves are more likely to occur when the angle between the wind direction and the orientation of the mountain ridge is between 60 and 90 degrees. Based on the analysis results, they estimated that many small-scale (˜100 km) MWs hotspots are scattered throughout the world. In Japan, Tohoku region and Hokkaido are showed as MWs hotspots.

In this study, we have observed OH airglow to detect MWs which propagate from the troposphere to the mesopause region at Shirosato, Ibaraki Prefecture (36.5 ^{o}N, 140.3 ^{o}E) from August 2021. The field of view (F.O.V.) of the imager is approximately 100 km in the east-west direction and 200 km in the north-south direction. Because Shirosato is located in the northern part of Ibaraki Prefecture, the southern part of the Tohoku region is also included in the F.O.V. The imager consists of a consumer color digital camera (ILCE - 6000, SONY), a fisheye lens and a long pass filter. The color digital camera had removed the originally installed filters that cut off infrared radiation. We detected two stationary wave events in January 2022. Both waves were observed for one to two hours and had horizontal wavelengths of 20 to 30 km. They were also similar in that the wavenumber vector direction was tilted approximately 40 and 49 degrees to the north when east was 0 degrees. In this presentation, we will report the results of observations from August 2021 to September 2022 and from April 2023. In addition, by using the topography data and the reanalysis data as a vertical profile of the background atmospheric field at the observation period, we will discuss the excitation sources and vertical propagation possibilities of the two stationary waves. We will consider the frequency of generation and propagation into upper atmosphere of small-scale mountain waves.

地形性大気重力波である山岳波は励起源が地上に固定されているため、季節変動する下層風と相まって超高層大気の循環に一定の規則を与える重要な因子だと考えられている。山岳波の特性を理解するために、様々な観測や数値実験が実施されてきたが、小スケール地形によって励起される山岳波動の超高層大気への伝搬頻度については先行研究例が少ない。Ishii et al. (2022) では、衛星画像に写る山岳波由来の波状雲の解析、及び再解析データ（MERRA-2）を下層の風速場として、下層の風向と地形の稜線方向との関係が調査された。その結果、山岳の稜線方向と風向が 60〜90 度の関係になっている地域では山岳波が励起されやすいと示され、小規模（〜100 km）ながらも頻繁に山岳波を励起するホットスポットが世界中に点在していると推定された。特に、日本においては東北地方と北海道が山岳波のホットスポットであると示された。

本研究では、高度約 85 km の中間圏界面領域に発光ピークを持つ OH 大気光を地上からイメージング観測し、下層から中間圏界面領域に伝搬する山岳波を検出している。2021 年 8 月より茨城県城里町（北緯 36.5 度、東経 140.3 度）に OH 大気光イメージャーを設置し観測を継続している。観測視野は、東西方向に約 100km、南北方向に約 200km であり、城里町は茨城県北部に位置しているため、東北地方南部の中間圏界面領域を観測視野に含む。このイメージャーは民生用のカラーデジタルカメラ（ILCE - 6000、SONY）、魚眼レンズ、ロングパスフィルターで構成されている。民生用のカラーデジタルカメラには、赤外線をカットするフィルターが取り付けられているが、このフィルターを除去することで、近赤外領域で発光するＯＨ大気光を検出している。2021 年 8 月から 2022 年 9 月までの観測期間のうち、2022 年 1 月に地上からは停滞して観測されるという山岳波の性質を持った波動イベントを 2 例検出した。その波動はどちらも 1 〜 2 時間にわたって観測され、水平波長が 20〜30 km、波数ベクトル方向は、東を 0 度としたときに北に約 40 度と約 49 度傾いた方向であるという似た特徴を持つイベントであった。

本発表では、2021 年 8 月〜2022 年 9 月と 2023 年 4 月から再開した城里町におけるＯＨ大気光イメージング観測の結果を報告する。また、検出された停滞性の波動イベントについては、再解析データを観測当時の背景大気場の鉛直プロファイルとして用いることで、地形と下層風の関係、風速や温位の鉛直プロファイルを示し波動の励起源や鉛直伝搬可能性について議論し、小スケール山岳波動の超高層大気への励起伝搬頻度について考察する。

R005-13
B 会場 ：9/24　PM2 （15:45-18:15）
17:15〜17:30

高エネルギー粒子降リ込みの大気影響理解のための昭和基地における多輝線ミリ波同時観測の現状と今後の計画

#水野　亮 [1)], 中島　拓 [1)], 長濱　智生 [1)], 溝口　玄真 [1)], 後藤　宏文 [1)], 片岡　龍峰 [2)], 田中　良昌 [2)], 小池　陸斗 [2)], 江尻　省 [2)], 冨川　喜弘 [2)], 鈴木　ひかる [3)], 土屋　史紀 [3)], 村田　功 [3)], 笠羽　康正 [3)],ISEE EPC　融合研究コンソーシアム [1)]

([1] 名大・宇地研,[2] 極地研,[3] 東北大学

Current Status and Future Plans of MM-wave Multi-line Observation at Syowa to Understand the Effect of EPP on the Atmosphere

#Akira Mizuno[1)],Taku Nakajima[1)],Tomoo Nagahama[1)],Gemma Mizoguchi[1)],Hirofumi Goto[1)],Ryuho Kataoka[2)],Yoshimasa Tanaka[2)],Rikuto Koike[2)],Mitsumu K Ejiri[2)],Yoshihiro Tomikawa[2)],Hikaru Suzuki[3)],Fuminori Tsuchiya[3)],Isao Murata[3)],Yasumasa Kasaba[3)],ISEE EPC Interdisciplinary Research Consortium[1)]

([1]Institute for Space-Earth Environmental Research, Nagoya University,[2]National Institute of Polar Research,[3]Tohoku University

It is well-known that energetic particle precipitation into the polar regions induced by the solar activity ionizes atmospheric molecules, and the subsequent ion chemistry produces NO_x and HO_x, leading to depletion of ozone.

We have been conducting long-term monitoring using a millimeter-wave spectrometer in two spectral lines of nitric oxide (NO) and ozone (O_3) above Syowa Station since 2012 to clarify the atmospheric response to the energetic particle precipitation. However, we could not observe both lines simultaneously due to the limitation of the instantaneous bandwidth of the millimeter-wave spectrometer, the two lines were observed alternately by switching the frequency setting of the receiver system. To overcome this situation, a multi-frequency millimeter-wave spectrometer using a waveguide-type frequency multiplexer was developed and installed at Syowa Station in 2020. Simultaneous observation of multiple emission lines in the 230-250 GHz band, including CO additionally, was realized for the first time in the ground-based millimeter-wave observations. But the originally planned performance was not achieved, due to some problems with damages of parts and an incomplete cooling system setup. In 2022, we made a quick overhaul of the observing system, such as expansion of the FFT spectrometer bandwidth from 2.0 GHz to 2.5 GHz, improvement of the IF circuit design, and reassemble the cooling system. And finally, the spectrometer achieved originally planned performance.

Frequency switching method was used for the observations, which is less sensitive to sky inhomogeneities due to cloudlets etc. because the same elevation angle is always observed and able to reduce dead time caused by rotational motion of the switching mirror to change the elevation angles. CO in the 230 GHz band, two ozone spectra (J=$7_{1,7}$-$6_{0,6}$ and J=$10_{2,8}$-$10_{1,9}$) and six NO spectra (F=7/2-5/2, 5/2-3/2, 3/2-1/2 with J=5/2-3/2 for each p_{ul}=-→ + and + → -) in the 250 GHz band were detected significantly, while NO_2 in the 247 GHz band and HO_2in the 250 GHz band were not detected so far.

Comparison of time series data of daily averaged NO column density with the flux of high-energy electrons (0-degree telescope data of POES/METOP satellites) between August to the end of October 2022 shows that NO enhancement occurred five times corresponding to the electron precipitations. The decay time of the NO column density after the steep increase by the electron precipitation tends to shorten as the daylight hours increase from winter to spring, suggesting that the length of decay time of NO column density reflects the photodissociation process.

The ozone data is currently being analyzed in collaboration with the Tohoku University group. Since the current retrieval program was optimized to derive the stratospheric ozone amount, development of new analytical algorithms to improve the accuracy of deriving ozone column densities above the mesosphere is a key issue.

In this presentation, we will report the current performance as a remote sensing instrument, problems that have become apparent after one-year operation of routine observations, issues in future data analysis, and plans for future observations in the Arctic polar cap region using the same type of mm-wave spectrometer system.

太陽活動にともない極域に降り込んだ高エネルギー粒子が、大気分子を電離しイオン反応を介して NO_x, HO_x などを生成しオゾンを破壊することが知られている。

我々は、高エネルギー粒子が降り込んだ際の大気側の応答を明らかにするため、2012 年よりミリ波分光放射計を用い、昭和基地上空の一酸化窒素およびオゾンの２つの線スペクトルで長期モニタリングを行なってきた。しかし、ミリ波分光を分光計の瞬時帯域幅の制限から２つの輝線を同時観測することはできず、周波数設定を切り替えながら交互に観測を行ってきた。この状況を打開するため、導波管型周波数マルチプレクサを用いた多周波ミリ波分光計システムを開発し、昭和基地に設置し 2020 年にさらに CO を加えた 230-250GHz 帯の多輝線同時観測を地上ミリ波観測において世界で初めて実現させた。しかし、部品の故障や不完全な冷却系セットアップの問題があり、当初計画していた性能が達成されずにいた。そこで、2022 年に FFT 分光計の帯域を 2.0GHz から 2.5GHz に拡張し、IF 回路の改良、冷却系の再組み立てをおこない、ほぼ所期の性能が達成でき 2022 年の 7 月から定常観測を開始した。

観測には、同じ高度角を観測するため雲などの空の非一様性の影響を受けにくく、高度角の切り替えに伴うデッドタイ

ムの少ない周波数スイッチングを用いた。230GHz 帯の CO、250GHz 帯の 2 本のオゾン (J=$7_{1,7}$-$6_{0,6}$ と J=$10_{2,8}$-$10_{1,9}$) および 6 本の NO のスペクトル (J=5/2-3/2 の F=7/2-5/2, 5/2-3/2, 3/2-1/2 の 3 本が p_{ul}=－→＋と＋→－ 2 組で計 6 本) が有意に検出できたが、その一方 247GHz 帯の NO_2、250GHz 帯の HO_2 は現時点で検出されていない。

2022 年 8 月から 10 月末までの NO 柱密度日平均値の時系列データと高エネルギー降下電子のフラックス (POES/METOP 衛星の 0 度望遠鏡データ) との比較をおこなったところ、電子の降り込みに対応する NO の増加が 5 回ほど見られた。冬から春にかけて日照時間が伸びるに伴い、降下電子で増加した NO 柱密度の減衰時間が短くなる傾向が見られ、NO 柱密度の減衰時間は光解離過程を反映していると考えられる。

オゾンデータについては、現在東北大学のグループと共同で解析を進めており、特にこれまで成層圏のオゾン量導出に重点を置いて開発されてきたリトリーバルプログラムを改良し、中間圏以上の柱密度を精度良く抽出する方法を開発することが課題となっている。

発表では、観測装置としての達成度を示すと共に、約 1 年間の定常観測を終え明らかになってきた問題点・課題、今後のデータ解析における課題、今後の同型の装置を用いた北極極冠域での観測計画などについて報告する予定である。

R005-14
B 会場 ：9/24　PM2 （15:45-18:15）
17:30〜17:45

Aura/MLS 衛星データによる日食時の中高層大気微量分子応答の統計解析

#楊　天量 [1,2)], 長濱　智生 [2)], 水野　亮 [2)], 中島　拓 [2)]
([1] 名古屋大学理学研究科,[2] 名大・宇地研

Statistical Analysis of the Earth's Atmospheric Molecular Constituents Response during a Solar Eclipse Using Aura/MLS Data

#Tianliang Yang[1,2)],Tomoo Nagahama[2)],Akira Mizuno[2)],Taku Nakajima[2)]
([1]Graduate School of Science, Nagoya University,[2]Institute for Space-Earth Environmental Research, Nagoya University

A solar eclipse is a familiar natural phenomenon characterized by a short-term obscuration of solar radiation. It can provide a unique perspective of a natural experiment on the short-term variations of the middle and upper atmosphere during a short-term change in solar radiance. However, limited research or survey has been conducted on this short-term variability. For example, Imai et al. (2015) used JEM/SMILES data to assess the impact of the January 15, 2010, annular solar eclipse on the mesospheric ozone. However, there are few examples of observations on the variation of atmospheric molecular constituents in the stratosphere and mesosphere during solar eclipses. This study examined the relationship between eclipse obscuration rate and ozone variability for all eclipses from 2004 to 2023 using Aura/MLS data. We used the vertical ozone distribution data (version 4.2) with AURA/MLS, and the obscuration rate at the time of the eclipse was calculated for each observation point. Ozone variability was determined as the difference from the ozone data from orbits before and after the eclipse. In the case of the total eclipse on December 14, 2020, we found that ozone concentrations increased at altitudes of 58 km to 67 km during the eclipse. This is generally consistent with the results of Imai et al. (2015). Imai et al. (2015) also noted that the relationship between solar radiation variability and ozone variability is due to differences in the mechanism of OH production at different altitudes. However, our statistical analysis shows that the rate of ozone variability when the obscuration rate is significant is lower than the relationship noted by Imai et al. (2015), which suggests that when the occultation rate is significant in an eclipse, ozone loss due to OH may continue for a relatively long time and suppress ozone increase.

R005-15
B 会場 ：9/25　AM1 （9:00-10:30）
9:00〜9:15

#高田　雅康 [1)], 関　華奈子 [2)], 小川　泰信 [1)], 桂華　邦裕 [3)]
([1] 極地研,[2] 東大理・地球惑星科学専攻,[3] 東大・理

Properties of ionospheric low-altitude ion upflows during CIR- and CME- driven magnetic storms based on the EISCAT observations

#Masayoshi Takada[1)],Kanako Seki[2)],Yasunobu Ogawa[1)],Kunihiro Keika[3)]
([1]National Institute of Polar Research,[2]Department of Earth and Planetary Science, Graduate School of Science, University of Tokyo,[3]Department of Earth and Planetary Science, Graduate School of Science, The University of Tokyo

Molecular ions (O_2^+/NO^+/N_2^+) in the ring current of the terrestrial magnetosphere have been observed during the magnetic storms [e.g., Klecker et al., 1986; Seki et al., 2019]. These ions originate from the low-altitude ionosphere. In the ionosphere, upward ion transports (upflows) supply sources of the ions outflowing to the magnetosphere. Since the molecular ions usually exist in the low-altitude (<300 km) ionosphere and can be affected by neutral winds, the generation mechanisms and properties of ion upflows to transport molecular ions are different from those of O^+ [e.g., Ogawa et al., 2010; Yamazaki et al., 2017]. In particular, their dependence on solar activities is one of the important properties to understand formation mechanisms of the ion upflows. In a previous study by Ogawa et al. [2019], the characteristics of O^+ ion upflows in the polar ionosphere were investigated during CIR- and CME-driven magnetic storms by using EISCAT radars. They reported that the upflows during CIR- and CME-driven storms have different dependence on magnetic local time. For the CIR-driven storms, upward ion flux around noon was pronounced, while it was enhanced around midnight during the CME-driven storms. Their study focused on the ion upflows in the altitude range between 400 and 500 km, where O^+ is the dominant species, and responses of the ion upflows to the different type of magnetic storms in the low-altitude ionosphere, where molecular ions exist, are far from understood. The purpose of this study is thus to understand properties of ion upflows in the low-altitude polar ionosphere during CIR- and CME- driven magnetic storms based on the long-term EISCAT observations.

We used data from the EISCAT ultra high frequency (UHF) radar at Tromso (Invariant Latitude: 66.12' N) and Svalbard 42m antenna radar (ESR) at Svalbard (Invariant Latitude: 75.10' N) during CIR- and CME-driven magnetic storms from 1996 to 2015. We used 5-minute time resolution data when the radar was looking along the magnetic field line. The ionospheric parameters such as electron density, ion velocity, and ion and electron temperatures were averaged between 250 and 350 km and we screened data to exclude unrealistic values. The results show that ion upflows in the low-altitude ionosphere were mainly detected in the dayside and nightside at Tromso during both CIR- and CME- driven magnetic storms. On the other hand, the upward flux at Svalbard was not enhanced in nightside but remarkable in dawnside after CIR-driven storms, whereas it increased from the low-altitude region in the nightside only after CME-driven large storms. The ion upflows were detected in the duskside at Tromso only during CME-driven large storms. We also estimated the generation mechanisms of upflows by comparing ion and electron temperatures between pre-storm time and after storm onset. The frictional heating mainly caused upflows during CME-driven storms at both locations and possibly in the dawnside during CIR-driven storms at Svalbard, whereas the precipitation mainly caused upflows during CIR-driven storms at both locations and possibly in the nightside during CME-driven small storms at Tromso.

References:

[1] B. Klecker et al., Discovery of energetic molecular ions (NO+ and O2+) in the storm time ring current, Geophys. Res. Lett., 13, 632-635, 1986

[2] K. Seki et al., Statistical Properties of Molecular Ions in the Ring Current Observed by the Arase (ERG) Satellite, Geophys. Res. Lett., 46, 8643-8651, 2019

[3] Y. Ogawa et al., Solar activity dependence of ion upflow in the polar ionosphere observed with the European Incoherent Scatter (EISCAT) Tromso UHF radar, J. Geophys. Res., 115, A07310, 2010

[4] Y. Yamazaki et al., Average field-aligned ion velocity over the EISCAT radars, J. Geophys. Res. Space Physics, 122, 5630-5642, 2017

[5] Y. Ogawa et al., Characteristics of CME- and CIR-driven ion upflows in the polar ionosphere, J. Geophys. Res. Space Physics, 124, 3637-3649, 2019

R005-16
B 会場 ：9/25　AM1 （9:00-10:30）
9:15〜9:30

#Chen　Liwei[1)], 塩川　和夫 [1)], 加藤　悠斗 [1)], 坪井　巧馬 [1)],Martin Connors[2)]
([1 名大 ISEE,([2 アサバスカ大学

Triangulation of a STEVE observed at Athabasca, Canada on Sept 3rd, 2022

#Liwei Chen[1)],Kazuo Shiokawa[1)],Yuto Kato[1)],Takuma Tsuboi[1)],Connors Martin[2)]
([1Institute for Space-Earth Environmental Research, Nagoya University,([2Athabasca University

The Strong Thermal Emission Velocity Enhancement (STEVE) is a purplish westward surging arc which attracts much attention from the scientific community since 2016. In this presentation, we present a unique triangulation campaign of a STEVE observed on Sept 3rd, 2022, at Athabasca, Canada. For the first time we show the profile of STEVE altitude variation over time in 1-min resolution, for both the visible purplish arc and the green fence structures. All these STEVE altitude properties are obtained from triangulations made by several different cameras which were operated at two ˜24 km separated observatories at Athabasca, Canada. We used two Nikon cameras to make the campaign observation. We also compare the images from Nikon cameras and an Optical Mesosphere Thermosphere Imager (OMTI) to see the difference between emissions at different wavelengths. The temporal profile of the visible STEVE arc shows that emission height around the zenith of Athabasca was stable at 150-170 km during its presence (˜0546-0633 UT), except for a short elevation to ˜200 km at 0600 UT. The green fence structures appeared at 0549 UT when the intensity of the STEVE arc started to intensify and only lasted for 7 minutes, and their altitude was maintained at ˜110 km. In this presentation, we compare these results with previous STEVE studies about STEVE common properties, its possible generation mechanism, and its relationship with other subauroral phenomena.

R005-17
B 会場 ：9/25　AM1 （9:00-10:30）
9:30〜9:45

630-nm 大気光増光の３地点同時観測に基づくサブストームに伴う中緯度への電場侵入の複数例解析

#森田　早紀 [1)], 塩川　和夫 [1)], 大塚　雄一 [1)], 西谷　望 [1)], 新堀　淳樹 [1)], 惣宇利　卓弥 [1)], 藤本　晶子 [2)], 吉川　顕正 [3)], 西岡　未知 [4)],PERWITASARI　SEPTI[4)], 山本　衛 [5)]
[(1 名大宇地研,(2 九工大,(3 九大/理学研究院,(4 情報通信研究機構,(5 京大・生存圏研

Multiple-event study of substorm electric-field penetration based on simultaneous observation of 630-nm airglow enhancements

#Saki Morita[1)],Kazuo Shiokawa[1)],Yuichi Otsuka[1)],Nozomu Nishitani[1)],Atsuki Shinbori[1)],Takuya Sori[1)],Akiko Fujimoto[2)],Akimasa Yoshikawa[3)],Michi Nishioka[4)],SEPTI PERWITASARI[4)],Mamoru Yamamoto[5)]
[(1Institute for Space-Earth Environmental Research, Nagoya University,(2Kyushu Institute of Technology,(3Department of Earth and Planetary Sciences, Kyushu University,(4National Institute of Information and Communications Technology,(5Research Institute for Sustainable Humanosphere, Kyoto University

630-nm red airglow emissions at altitudes of 200-300 km are produced by dissociative recombination of $O_2{}^+$. The emission intensity is proportional to the product of O^+ and O_2 densities. The O^+ is also proportional to the ionospheric plasma density because it is a major part of the F-region plasma in the ionosphere. Therefore, the change of the product of O^+ and O_2 densities due to the upward or downward motion of the ionosphere by a zonal electric field or a meridional neutral wind leads to the variation of the 630-nm red airglow intensity. In other words, observation of the 630-nm airglow modulation is equivalent to seeing the upward and downward motion of the ionosphere. One of the causes of moving mid-latitude ionospheric plasma is the penetration of the transient magnetospheric electric field associated with substorms. Region 1 currents dominate due to the development of a current wedge system at substorm onset, and a westward electric field penetrates at mid-low latitudes on the night side. The direction of the associated **E**x**B** drift is diagonally downward, which causes the ionospheric plasma to move to lower altitudes with higher O_2 density. This process enhances the 630-nm airglow emission. Shiokawa et al. [2000] reported only two events of two-dimensional observations of the 630-nm airglow enhancement using an all-sky camera at mid-latitudes. However, there have been no other reports of the mid-latitude 630-nm airglow modulations associated with substorms. Further, because Shiokawa et al. [2000] did not conduct a multi-observation data analysis for the 630-nm airglow enhancement, the spatial and temporal variations of the 630-nm airglow enhancement remained unknown.

In this study, we will increase the number of 630-nm airglow enhancement events with substorm by observing simultaneously with all-sky cameras installed at Rikubetsu (43.5^{o}N, 143.8^{o}E), Shigaraki (34.9^{o}N, 136.1^{o}E) and Sata (31.0^{o}N, 130.7^{o}E) in Japan. Further, we use various kinds of observation data obtained from the FM-CW radar installed at Sasaguri (33.4^{o}N, 130.3^{o}E) by Kyushu University, SuperMAGs, GNSS receiver networks, Ionosondes, the DMSP F15 satellite, and the SuperDARN Hokkaido East radar to clarify the characteristics of airglow and ionospheric variability due to electric field penetration with substorms over a wide latitudinal range.

From 2002 to 2012, there were 1,800 days of FM-CW radar observations. Among them, we found five events of simultaneous airglow enhancements at two or more stations. Substorm-like AL index decreases were observed with the onset of these airglow enhancements. The occurrence probability of ”simultaneous enhancement at two or more stations” in the “time when the weather is clear by confirming the all-sky camera on the day that FM-CW radar at Sasaguri is available” was 5.5 [hour]/6080 [hour]=0.09%, which is very rare. Three events occur during peculiar intervals, such as very large substorms or giant magnetic storms (Halloween events). This suggests that in order to cause electric field penetration and simultaneous airglow enhancement at mid- and low latitudes, there may be some necessary conditions in the substorm-like geomagnetic variations and the background solar-wind, magnetospheric and ionospheric parameters. In this presentation, we investigate possible mechanisms to cause airglow variations associated with substorm electric field penetration into the mid-latitude ionosphere, based on a combined analysis of airglow, geomagnetic field, ionospheric and TEC variations, and solar wind parameters.

630-nm 大気光は、$O_2{}^+$ の解離性再結合により生成され、典型的には電離圏 F 領域中の高度 200-300 km で赤く光っている。発光強度は、O^+ と O_2 の密度の積に比例し、この O^+ は電離圏 F 領域のプラズマの大部分を担っているため、電離圏プラズマ密度に比例する。そのため、電離圏が電場や中性風によって上下に動くことにより、O^+ と O_2 の密度の積が変化するため、その変動を 630-nm 大気光で観測することができる。つまり、630-nm 大気光を観測することは、電離圏の高度変動を見ていることと等価である。また、中緯度電離圏のプラズマが動かされる原因の 1 つとして、サブストームに伴う一時的な磁気圏電場の中緯度電離圏への侵入が挙げられる。これは、サブストーム開始に伴ってカレントウェッジ電流系が発達することにより Region 1 電流が卓越し、夜側の中低緯度では時間遅延なく西向き電場が侵入する。これに伴う **E**x**B** ドリフトが斜め下向きにかかるため、電離圏プラズマがより O_2 の密度が高い低高度に侵入し、630-nm 大気光が増光する。Shiokawa et al. [2000] は、この増光を中緯度の全天カメラを用いて 2 次元的に観測した例を 2 例報告し

た。しかし、同様の報告例はなく、各イベントに対して１か所の観測点のみの観測であり、増光の空間的な拡がりや同時性が不明であった。そこで本研究では、サブストームに伴う電場侵入により 630-nm 大気光が増光する事例を増やし、これを日本の陸別 (43.5^{o}N, 143.8^{o}E)、信楽 (34.9^{o}N, 136.1^{o}E)、佐多 (31.0^{o}N, 130.7^{o}E) に設置された全天カメラで同時に取得された観測データを使用する。さらに、九州大学が篠栗 (33.4^{o}N, 130.3^{o}E) に設置している FM-CW レーダーや SuperMAG、GNSS 受信機網、イオノゾンデ、DMSP F15 衛星、SuperDARN 北海道-陸別第 1 レーダーの観測データと比較することで、サブストームに伴う電場侵入による大気光強度と電離圏の変動特性を広い緯度範囲に渡って明らかにする。

2002 年〜2012 年の期間で、FM-CW レーダーの観測が行われている 1,800 日に対して、2 観測点以上で同時に大気光が増光している例は現時点で 5 例見つかり、増光の開始に伴いサブストームのような AL 指数の減少が見られた。このため、「篠栗の FM-CW レーダーのデータがある日で、全天カメラで確認された天気が 2 観測点以上で晴れの時間」の中で、「2 観測点以上で同時増光する」発生頻度は、5.5 [時間]/6080 [時間]=0.09% と非常にまれであることが分かった。この中の 3 例は、非常に巨大なサブストームや巨大磁気嵐（ハロウィンイベント）など特殊な場合であった。そのため、中低緯度で大気光が同時に増光するほどの電場が侵入するためには、サブストームのような地磁気変動や、背景の磁気圏・電離圏の状態、太陽風の性質に条件がある可能性がある。そこで本発表では、得られた５例に関して、大気光画像に加えて、磁場変動や電離圏高度、TEC、太陽風パラメータなどを総合的に解析し、中緯度電離圏への侵入電場に伴う大気光変動のメカニズムを考察した結果を報告する。

R005-18
B 会場 ：9/25　AM1 （9:00-10:30）
9:45〜10:00

SuperDARN レーダーを用いた Superposed Epoch Analysis による磁気嵐発生後の中緯度電離圏プラズマフローの解析

#大森　康平 [1)], 西谷　望 [1)], 堀　智昭 [1)],Shepherd Simon[2)]
([1] 名大 ISEE,([2]Thayer School of Engineering, Dartmouth College, Hanover, NH, USA

Superposed Epoch Analysis of mid-latitude ionospheric plasma flows after geomagnetic storms using SuperDARN radar observations

#Kohei Omori[1)],Nozomu Nishitani[1)],Tomoaki Hori[1)],Simon Shepherd[2)]
([1]Institute for Space-Earth Environmental Research, Nagoya University,([2]Thayer School of Engineering, Dartmouth College, Hanover, NH, USA

Disturbance Dynamo is a dynamo process caused by neutral winds resulting from Joule heating of the polar regions during a geomagnetic storm or substorm. Past studies have suggested that the Disturbance Dynamo process generates westward plasma flows in the mid-latitude ionosphere with a time delay of about 10 hours from the onset of geomagnetic storms. However, there have been few statistical studies on the effect of Disturbance Dynamo on the mid-latitude ionospheric plasma flow after geomagnetic storms, and the magnitude and time constant of the plasma flow variations caused by Disturbance Dynamo are not clear from observations. In this study, we performed Superposed Epoch Analysis based on the peaks of Dst indices using data from three SuperDARN radar observations: Christmas Valley East (CVE), Christmas Valley East (CVW), Hokkaido East (HOK), and Hokkaido West (HKW). The goal is to investigate the variation of mid-latitude ionospheric plasma flows after geomagnetic storms. The analysis covered over 300 storms between December 2006 and April 2023. The results showed that the westward plasma flow velocity tended to increase around 45-48 degrees of geomagnetic latitude with a time delay of about 10-20 hours from the peak of the Dst index. Additionally, the peak value of the Dst index and the amplitude and time delay of the plasma flow velocity increase have little correlation. More detailed analysis and discussion will be presented.

ディスターバンスダイナモは、磁気嵐やサブストームが発生した際の極域のジュール加熱によって生じる中性風が引き起こすダイナモプロセスである。過去の研究から、Disturbance Dynamo の過程で地磁気嵐の発生から 10 時間程度の時間遅れをもって中緯度電離圏に西向きのプラズマフローが発生すると考えられている。しかし、磁気嵐発生後の Disturbance Dynamo の中緯度電離圏電場への影響について統計的に調べた研究は少ない。本研究では、私たちは Christmas Valley East (CVE)、Hokkaido East (HOK)、Hokkaido West (HKW) の 3 つの SuperDARN レーダーの観測を用いて、Dst 指数のピークを基準とした Superposed Epoch Analysis を行うことで、磁気嵐発生後の中緯度電離圏プラズマフローの変動を調査した。解析は 2006 年 12 月から 2023 年 4 月の間に発生した 300 個以上の磁気嵐について行った。その結果、磁気嵐のピークから 10 − 20 時間程度の時間遅れをもって、磁気緯度 45 − 48 度の辺りで西向きプラズマフローの速度が増加する傾向が見られた。また、Dst 指数のピーク値とプラズマフロー速度の振幅や速度増加の時間遅れとの関係を調査したところ、それらの間にはあまり相関がないことが示唆された。講演ではより詳細な解析結果と考察を示す予定である。

R005-19
B 会場 ：9/25　AM1 （9:00-10:30）
10:00〜10:15

#Fu　Weizheng[1)], 大塚　雄一 [1)], 新堀　淳樹 [1)], 西岡　未知 [2)],PERWITASARI　SEPTI[2)]
(1 名大・宇地研,(2 情報通信研究機構

Assessing the performance of the double-thin-shell model for studying E-F coupling using two dense observation networks in Japan

#Weizheng Fu[1)],Yuichi Otsuka[1)],Atsuki Shinbori[1)],Michi Nishioka[2)],SEPTI PERWITASARI[2)]
(1Institute for Space-Earth Environmental Research, Nagoya University,(2National Institute of Information and Communications Technology

Electrodynamic coupling between the ionospheric E and F regions is widely accepted as the underlying mechanism for the generation of nighttime medium-scale traveling ionospheric disturbances (MSTIDs) at midlatitudes. Recently, the double-thin-shell approach has proved to be a useful tool for studying the E-F coupling process, allowing the simultaneous observation of electron density perturbations with broad and continuous coverage in both E and F regions. GEONET (GNSS Earth Observation Network System) is a dense network of ground-based GNSS receivers over Japan. However, previous results have shown that the reconstruction performance for Es with small amplitudes is limited when only GPS total electron content (TEC) measurements from GEONET are used. Fortunately, SoftBank Corp., a Japanese telecommunications provider, has recently developed a dense independent GNSS observation network to improve positioning services. The use of this network provides an opportunity to improve the resolution and accuracy of the double-thin-shell model. In this research, we analyze the potential of the improved double-thin-shell approach by incorporating multi-GNSS observation data from both GEONET and SoftBank. Solvability analysis and simulation results suggest that the spatiotemporal resolution and reconstruction performance have been greatly improved. By using real observations on July 3, 2022 for a typical nighttime MSTID event, the reconstruction results illustrate the ability and fidelity of the approach to discriminate between perturbations in the E and F regions, especially in complex background conditions near the solar terminator. Based on these assessments, we conclude that the incorporation of GEONET and SoftBank GNSS observation data holds significant potential for improving the double-thin-shell model and advancing our understanding of MSTIDs.

Acknowledgement: TEC data were obtained from RINEX files taken from GEONET and SoftBank Corporation.

R005-20
B 会場 ：9/25　AM2 （10:45-12:30）
10:45〜11:00

S-520-27 号機観測ロケットによる夜間中規模伝搬性電離圏擾乱発生時の電場観測結果

#松山　実由規 [1)], 石坂　圭吾 [2)], 山本　衛 [3)], 斎藤　享 [4)], 高橋　透 [5)], 大塚　雄一 [6)], 熊本　篤志 [7)], 田中　真 [8)], 阿部　琢美 [9)]
([1] 富山県大,[2] 富山県大・工,[3] 京大・生存圏研,[4] 電子航法研,[5] 電子航法研,[6] 名大・宇地研,[7] 東北大・理・地球物理,[8] 東海大学,[9] ＪＡＸＡ宇宙科学研究所

Electric field Observed during Nighttime Medium Scale Traveling Ionospheric Disturbance Occurrence by S-520-27 Sounding Rocket

#Miyuki Matsuyama[1)],Keigo Ishisaka[2)],Mamoru Yamamoto[3)],Susumu Saito[4)],Toru Takahashi[5)],Yuichi Otsuka[6)],Atsushi Kumamoto[7)],Makoto Tanaka[8)],Takumi Abe[9)]
([1]Toyama Prefectural University,[2]Faculty of Engineering, Toyama Prefectural University,[3]Research Institute for Sustainable Humanosphere, Kyoto University,[4]Electronic Navigation Research Institute,[5]Electronic Navigation Research Institute,[6]Institute for Space-Earth Environmental Research, Nagoya University,[7]Department of Geophysics, Graduate School of Science, Tohoku University,[8]Tokai University,[9]Institute of Space and Astronautical Science, Japan Aerospace Exploration Agency

The phenomena of propagation of electron density fluctuations are known as the Traveling Ionospheric Disturbance (TID). The TID with short periods of 30 minutes to 3 hours is called the Medium Scale TID (MSTID). The MSTID occurs during the day or night. This presentation will discuss the nighttime MSTID. The wave structure of the electron density in the nighttime MSTID in the Northern Hemisphere extends in a northwest-southeast direction and propagates in a southwest direction. In addition, the DMSP satellite observation shows that the electric field is perpendicular to the electron density wave structure (Shiokawa et al, 2003). The Perkins instability has been proposed as the generation mechanism of the MSTID. However, it cannot explain the growth rate and the propagation direction. In contrast, simulations revealed that the interaction between the ionospheric E and F regions through the Earth's magnetic field lines plays an important role (Yokoyama and Hysell, 2010). Therefore, on July 20, 2013, S-310-42 and S-520-27 sounding rockets were successively launched from Uchinoura Space Center in Japan to simultaneously observe the E and F regions connected by the Earth's magnetic field lines. In this study, the electric field observed by S-520-27 is analyzed to investigate the contribution of the electric field to the MSTID generation mechanism. This rocket was launched when the electron density structure in the northwest-southeast direction was occurring. The electric field of the northeast direction was observed in the low electron density regions and the electric field of the northwest direction was observed in the high electron density regions. The electric field was generated not only perpendicular to the wave front but also parallel to it. In this presentation, we will explain the relationship between the electron density structure and the electric field.

電離圏電子密度の変動が伝搬する現象として，伝搬性電離圏擾乱（Traveling Ionospheric Disturbance：TID）がある．特に，周期が 30 分から 3 時間程度のものを中規模伝搬性電離圏擾乱（Medium Scale TID：MSTID）という．MSTID は昼間に発生するものと夜間に発生するものがある．本発表では，夜間に発生する MSTID について議論する．北半球での夜間 MSTID の電子密度の波状構造は北西-南東方向に延び，南西方向に伝搬する．また，DMSP 衛星による観測では北西-南東方向に発生している電子密度の波状構造に対して垂直な電場が観測されている (Shiokawa et al, 2003)．MSTID の生成機構としてパーキンス不安定が提唱されたが，現象の成長率や伝搬方向などを説明することができない．これに対し，シミュレーションにより，地球磁力線を通じた電離圏 E-F 領域相互作用が重要な役割を果たすことが明らかとなった (Yokoyama and Hysell, 2010)．そこで，2013 年 7 月 20 日に S-310-42 号機と S-520-27 号機を連続して打ち上げ，地球磁力線で結ばれた F 領域と E 領域を同時観測した．電場観測装置（EFD）は S-520-27 号機に搭載され，E 領域および F 領域の電場を観測した．本研究では，S-520-27 号機で得られた電場を解析し，MSTID 生成における電場の寄与について調査する．本ロケットは，北西-南東方向の MSTID が発生しているときに打ち上げられた．電場解析の結果，電子密度の低い領域では北東方向，高い領域では北西方向の電場が存在しており，波面に垂直な電場だけでなく平行な電場が発生していた．本発表では，電子密度と電場の関係について説明する．

R005-21
B 会場 ：9/25　AM2 （10:45-12:30）
11:00〜11:15

#高橋　透 [1)], 斎藤　享 [2,3)], 山本　衛 [3,4)], 篠原　学 [4)]
([1] 電子航法研,[2] 電子航法研,[3] 京大・生存圏研,[4] 鹿児島高専

Tomographic imaging of sporadic E-layer by sounding rocket S-520-32 observation

#Toru Takahashi[1)],Susumu Saito[2,3)],Mamoru Yamamoto[3,4)],Manabu Shinohara[4)]
([1]Electronic Navigation Research Institute,[2]Electronic Navigation Research Institute,[3]Research Institute for Sustainable Humanosphere, Kyoto University,[4]National Institute of Technology, Kagoshima College

Sporadic-E (Es) layers is a thin and dense layer appearing from 90 to 120 km and have been studied over six decades. Previous studies presented that the horizontal structure of the Es layer is likely to play an important role for the generation of medium-scale traveling ionospheric disturbances (MSTIDs) due to E-F coupling via the earth's magnetic field lines.

The sounding rocket S-520-32, which aimed to observe irregularities associated with the Es layer and MSTIDs, was launched from Uchinoura Space Center (USC), JAXA (31.25 deg. N, 131.08 deg. E) at 23:20:00 JST (UT+9) on 11 August 2022. It transmitted the dual-band beacon signals (150 and 400 MHz) and received GNSS signals to separately observe the total electron content (TEC) in the E and F region during the flight. The rocket flew between the E and F-layer and reached an apogee of 270 km. It splashed into the sea around 23:28:43. During the rocket flight, the MSTIDs were seen in the TEC map derived from the GNSS receiver network around the rocket trajectory. The ionosonde in Yamagawa, Kagoshima 44 km away from USC detected the Es layer and the foEs and altitude of Es layer were approximately 4.2 MHz and 90 km.

We installed the beacon receivers at USC, Tarumizu (TRM) (31.49 deg. N, 130.70 deg. E), Kirishima (KRS) (31.73 deg. N 130.73 deg. E), and Satsumasendai (SND) (31.83 deg. N, 130.34 deg. E). These four sites almost aligned with the backward extension of the line of rocket trajectory. Thus, the tomography technique could be attempted in the line to estimate the spatial distribution of the Es layer.

The dual-band beacon signals were successfully received in all sites. The TEC values were derived from the phase difference of 150 and 400 MHz signals after removing the phase shift due to the rocket spin. The TEC observed at four sites showed a similar trend and drastically increased when the rocket reached 116 km. This indicated that the path between the receiver and the rocket crossed the Es layer. After that, the TEC values increased moderately until the rocket reached 200 km in descending interval. During the rocket went down below 200 km, the TEC values decreased and widely fluctuated, implying the horizontal structure of the Es layer.

We performed the tomography analysis with the TEC values observed at four sites. The Es layer was found to be located at 116 km in the tomography result, and its peak density was 6×10^{10} m^{-3}. The Es layer distributed around 100 km distance from the USC, but from 100 to 220 km, there was no single peak of electron density. The Es layer was found again around 220 to 300 km from the USC, but the altitude was lower by about 4 km and the peak density was smaller by 1-4$\times 10^{10}$ m^{-3} than the Es layer around 100 km from the USC.

In this presentation, we will show the observation results as well as the comparison of it with ionosonde and onboard instruments. Furthermore, we will compare the horizontal structure of the Es layer and the F-region structure to discuss the E-F coupling process.

R005-22
B 会場 ：9/25　AM2 （10:45-12:30）
11:15〜11:30

日本のイオノゾンデ観測によるスポラディック E 層の長期変動

#寺岡　宙惟 [1)],Liu　Huixin[1,2)], 西岡　未知 [3)]
([1] 九州大学,[2] 九大・理・地惑,[3] 情報通信研究機構

Study of long-term variations in the sporadic E layer by using Japanese ionosonde observations

#Sorai Teraoka[1)],Huixin Liu[1,2)],Michi Nishioka[3)]
([1]Kyushu University,[2]Department of Earth and Planetary Science, Graduate School of Science,Kyushu University,[3]National Institute of Information and Communications Technology

A sporadic E (Es) layer is one of the important ionospheric irregularities and disturbs wireless communications. In this study, We examine the long-term trend of Es density and height by using long-term data of ionosonde observations at Japanese 5 stations, i.e., Wakkanai(45.16 north latitude, 141.75 east longitude, during 1957-2022), Kokubunji(35.71 north latitude, 139.49 east longitude, during 1957-2022), Yamagawa(31.20 north latitude, 130.62 east longitude, during 1965-2022), Okinawa(26.68 north latitude, 128.15 east longitude, during 1972-2022), Syowa(69.00 south latitude, 39.60 east longitude, during 1970-2022). To derive their long-term trend, we apply a multiple regression method with the ionosonde data. The presentation focuses on variabilities of its altitude and intensity, and LT dependence. We also show trend correlations with the background ionospheric E and F layers.

スポラディック E(Es) 層は、無線通信に影響を与える電離圏の重要な現象である。本研究では、日本の 5 地点 (稚内 (北緯 45.16°, 東経 141.75°, 期間 1957-2022 年)、国分寺 (北緯 35.71°, 東経 139.49°, 期間 1957-2022 年)、山川 (北緯 31.20°, 東経 130.62°, 期間 1965-2022 年)、沖縄 (北緯 26.68°, 東経 128.15°, 期間 1972-2022 年)、昭和基地 (南緯 69.00°, 東経 39.60°, 期間 1970-2022 年)) のイオノゾンデ観測のデータを用いて Es 層の密度と高度の長期トレンドを明らかにした。これらの長期トレンドは、イオノゾンデデータに重回帰法を適用することで導出した。発表では Es 層の強度や高度の変化、そして LT 依存性に焦点を当てる。また、背景の電離圏の E 層、F 層の長期トレンドも示した。

R005-23
B 会場 ：9/25　AM2 （10:45-12:30）
11:30〜11:45

短波ドップラー観測と MU レーダーを用いたスポラディック E 微細構造の研究

#齋藤　龍之介 [1)], 細川　敬祐 [1)], 斎藤　享 [2)]
[(1] 電通大,[(2] 電子航法研

Fine structure of sporadic E: simultaneous observations with HF Doppler sounding system and MU radar in Japan

#Ryunosuke Saito[1)],Keisuke Hosokawa[1)],Susumu Saito[2)]
[(1]The University of Electro-Communications,[(2]Electronic Navigation Research Institute

Sporadic E (Es) layer is a layer of extremely high electron density that occurs mainly in summer at mid-latitudes around 100 km altitude. Es layer has been known to cause long-range anomalous propagation of radio waves in the VHF band because of the reflection due to an extreme increase of the electron density associated with Es layer. Es layer has been studied for more than half a century using various instruments because of its influence on aeronautical navigation systems and radio broadcasts that use the VHF band. It was revealed that quasi-periodic coherent radar echoes (QP echoes) were observed by using the MU radar when Es layer occurs at night during summer months (Yamamoto et al., 1991). These echoes would manifest fine-scale internal structure of Es layer during nighttime. It was also found that nighttime Es layers are related to Medium-Scale Traveling Ionospheric Disturbances (MSTIDs), which occurs at the F region altitudes. In order to understand the temporal evolution of these two phenomena, it is needed to understand the fine structure of Es layer. However, the spatial extent of the fine structure has been unclarified because the coverage of the MU radar is limited.

In this research, we used the HF Doppler (HFD) observation in order to observe Es layer in a wide area. The HFD sounding system transmits two continuous waves, 5.006 MHz and 8.006 MHz from Chofu, Tokyo and the reflected waves are received at 11 observation stations in Japan. The system can detect the vertical motion of the ionosphere and dynamical characteristics of various ionospheric phenomena from variations of the Doppler frequency and received signal intensity derived from the received signal at multiple stations. The sampling rate of the raw waveform data is 100 Hz. The temporal resolution of the Doppler frequency and received signal intensity is 10 sec. The HFD observation is known to observe characteristic (quasi-periodic) Doppler spectral traces associated with Es layer, mainly at night during the summer season. This feature would reflect the spatial structure of Es layer, which corresponds to QP echoes. If the identity of the quasi-periodic Doppler trace and QP echoes is confirmed, it would be possible to observe the fine structure of Es layer in a wide area by using the HFD sounders.

For this purpose, we conducted simultaneous observations of Es layer by using HFD and MU radar on eight nights (May 23-26 and June 6-9, 2022). During five nights, the MU radar detected clear signatures of QP echoes. In addition, we confirmed that quasi-periodic Doppler traces were observed in the HFD data obtained in Awaji station. The two observation methods would have detected same Es layer because the difference in the timing of detection was small, about 10 – 20 minutes. The time lag would have been due to the location of the reflection point of the HFD observation in Awaji, which is about 200 km away from the MU radar observation area. When the MU radar clearly detected Es layer, the difference in speed between MSTIDs and Es layer was less than 20 %. This indicates that Es layer and MSTIDs propagated in tandem. Based on this fact, the time needed for propagation of MSTIDs between observation areas of MU radar and HFD was calculated by a cross-correlation analysis of GPS-TEC data. The estimated travel time was almost equal to the time lag in the Es layer observation between the MU radar and HFD. Therefore, we conclude that the time lag of Es layer observation was due to the difference of the observation areas, which further confirms that the quasi-periodic structures in the Doppler spectra of HFD measurements are manifestations of QP echoes seen in data from coherent radars such as the MU radar.

It was confirmed that the two methods observed the internal structures of the same Es layer. Still, however, it is unclarified what kind of spatial structure of Es layer is represented by the quasi-periodic Doppler traces observed by HFD. In order to reveal the spatial structure of Es layer in a wide area, we conduct a cross-correlation analysis of received signal intensity obtained at the HFD stations around the Kanto area, where the distribution of the receiving stations is dense. Also, we plan to reconstruct 2D images of the QP echoes from the imaging observations made by the MU radar and compare them with the quasi-periodic Doppler traces seen in the HFD measurements.

スポラディック E（Es）層は、主として夏季の中緯度の高度 100 km 付近に発生する電子密度が極端に増大した層である。Es 層の発生に伴う電子密度の増大によって、通常は電離圏を突き抜ける VHF 帯の電波が反射されてしまうことから、電離圏に浅く入射した電波の長距離異常伝搬を引き起こすことが知られている。Es 層は、VHF 帯を使う航空機の制御システムやラジオ放送に影響を及ぼすことから、様々な観測機器を用いて半世紀以上にわたって研究されてきた。MU レーダーを用いた観測によって、夏季の夜間に Es 層が発生した際に、準周期的なコヒーレントレーダーエコー（QP エコー）が観測されることが分かった（Yamamoto et al., 1991）。このエコーは夜間の Es 層の微細構造を示していると考えられる。夜間の Es 層は、電離圏 F 領域で発生する現象である中規模伝搬性電離圏擾乱（Medium-Scale Traveling Ionospheric Disturbances: MSTID）と関連することが明らかになっており、この 2 つの現象の時間発展を理解するうえで

Es 層の微細構造について理解することが求められている。しかし、MU レーダーなどの干渉性散乱レーダーの観測範囲は限られているため、微細構造がどの程度の領域にわたって分布しているかは明らかになっていない。

そこで、本研究では、広域的な観測を実現するために短波ドップラー観測（HF Doppler: HFD）を用いた解析を行った。HFD 観測は、電離圏に向けて短波帯の電波を送信し、その反射波を遠隔地で受信したときに得られるドップラー周波数や受信電界強度の変化から、電離圏の上下動や電離圏現象の移動特性をリモートセンシングするシステムである。我々が運用している HFD 観測システムでは、東京都調布市から 5.006 MHz、8.006 MHz の 2 周波の連続波を送信し、全国 11 箇所で受信している。生の波形データは 100 Hz でサンプリングされており、ドップラー周波数と受信電界強度は 10 秒の時間分解能で算出されている。HFD の観測において、夏季夜間の Es 層の発生時にドップラーシフトがプラスからマイナスに変動する筋状の構造が準周期的に見られることが知られており、QP エコーに対応する Es の微細構造を反映しているものと考えられる。このドップラートレースと QP エコーの関連性（同一性）を確認できれば、HFD を用いて Es 層の微細構造を広域的に観測することが可能になる。

この目的のために、2022 年 5 月 23-26 日、6 月 6-9 日の合計 8 日間にわたり、短波ドップラー観測と、干渉性散乱レーダーの 1 つである MU レーダーを用いて、夜間の Es 層の同時観測を実施した。計 8 晩のうち、5 晩の観測において明瞭な QP エコーを得ることができた。また、同時間帯の淡路における HFD 受信データを確認したところ、準周期的なドップラートレースを確認することができた。10 – 20 分の時間差があったものの、二つの準周期的現象が概ね同じ時間帯に観測されたため、同じ Es 層を捉えられた可能性が高いと考えられる。時間差は、HFD 観測の中間反射点が MU レーダーの観測領域から 200 km 程度離れていることによって生まれていると考えられる。MSTID と Es 層 の伝搬速度を比較したところ、MU レーダーで Es 層 が明瞭に捉えられた日に限れば両者の差は最大 20 % 程度であり、Es 層と MSTID の伝搬特性は一致していたことが分かった。この事実にもとづいて、GPS-TEC のデータを相互相関解析することで MSTID が MU レーダーの観測領域から HFD の観測領域まで伝搬するのに要した時間を求めた。求められた伝搬時間は MU レーダーと HFD の間で生じた Es 層の観測時間の差とおおよそ一致していた。したがって、Es 層の観測時間の差は観測領域の違いに伴うものであると考えられ、HFD で見られる準周期的なドップラートレースが MU レーダーなどの干渉性散乱レーダーで観測される QP エコーに相当することが示された。

2 つの方法で同じ Es 層が観測できることは確認できたものの、HFD で観測できたドップラートレースが具体的に反映している空間構造や移動特性は分かっていない。そこで、観測点が多い関東近郊における HFD 観測点のデータを相互相関解析することで、Es 層の広域的な空間構造や移動特性を明らかにする予定である。また、MU レーダーで実施したイメージング観測から QP エコーの 2 次元像を復元し、HFD の観測結果との比較を行い、HFD でどの程度 Es 層の観測ができるかについても評価を行う予定である。

R005-24
B 会場 ：9/25　AM2 （10:45-12:30）
11:45〜12:00

航空航法用電波 ILS Localizer を用いたスポラディック E 層空間構造の解析

#田淵　駿平 [1)], 細川　敬祐 [1)], 斎藤　享 [2)], 山本　淳 [3)], 坂井　純 [1)], 冨澤　一郎 [1)], 高橋　透 [2)], 中田　裕之 [4)]
([1] 電通大,[2] 電子航法研,[3] 海上保安大学校,[4] 千葉大・工

Analysis of the spatial structures of the sporadic E layer using aeronautical navigation radio - ILS Localizer

#Shumpei Tabuchi[1)],Keisuke Hosokawa[1)],Susumu Saito[2)],Atsushi Yamamoto[3)],Jun Sakai[1)],Ichiro Tomizawa[1)],Toru Takahashi[2)],Hiroyuki Nakata[4)]
([1]The University of Electro-Communications,[2]Electronic Navigation Research Institute,[3]Maritime Science and Technology, Japan Coast Guard Academy,[4]Chiba University

The sporadic E (Es) layer is a phenomenon in which the electron density increases locally at an altitude of about 100 km in the ionosphere. Normally, VHF radio waves above 100 MHz are not reflected at that altitude. However, the extremely high electron density in Es sometimes reflects HF to VHF radio waves and causes anomalous propagation of such waves for a long distance. Therefore, Es layer has a potential to cause interference to radio systems such as aeronautical navigation systems. In this study, observations of Es using radio waves used for aeronautical navigation systems, in particular the ones for the Instrument Landing System Localizer (ILS LOC), have been conducted in Kure, Japan.

The ILS LOC transmits radio waves in 108-112 MHz frequency range with amplitude modulation at 90 Hz on the left side and 150 Hz on the right side of the runway as seen from the aircraft. Then, ILS provides information about the approach course to airplanes based on the difference in the intensity of these two modulations (Difference in Depth of Modulation: DDM). Since radio waves from the ILS LOC system have strong directivity, they may propagate anomalously over a long distance due to reflection by the Es layer despite its low transmission power of 10 W. Recently, it has been reported that a 110.3 MHz radio wave, which seems to have been transmitted from the Localizer Type Directional Aid (LDA) at the Hualien Airport in Taiwan, was received in Kure, using a software-defined radio receiver. However, the source of the signal has not yet been confirmed and it is still unclear how the DDM data can be used for inferring the spatial structure of the Es layer. To overcome these problems, in this study, we have been operating an ILS LOC receiver since in Kure, which was actually used in the aircraft, and the direction of arrival of the radio wave has been measured continuously.

During summer seasons, we often observe a very strong signal at 110.3 MHz at Kure, which is possibly caused by anomalous long-range propagation of VHF waves due to reflection by the Es layer. Analysis of the audio Morse code obtained from our observation revealed that the VHF signal at 110.3 MHz received in Kure was transmitted from a Localizer type Directional Aid (LDA) at Hualien Airport in Taiwan. The difference between the direction of Kure as viewed from Hualien and the beam direction of the Hualien LDA is -0.68 degree. However, the most frequent DDM angle was slightly different from the direction of Hualien. Moreover, during nearly half of the events during two summer seasons, significant fluctuations were seen in the DDM angle. The statistical analysis using two years of measurement indicates that the characteristics of the fluctuation of DDM (which is identical to the angle-of-arrival of the signal) change from case to case. This implies that Es has a potential to change the propagation direction of radio waves used for the ILS Localizer system; thus, the behavior of DDM values may be used for diagnosing the complicated spatial structure of Es.

In this presentation, we will report on the statistical analysis of the data obtained from the software receiver and ILS LOC receiver for the anomalous Es propagation events in the summer seasons of 2021 and 2022. Furthermore, by introducing a few cases of anomalous Es propagation in the summer of 2023, we will discuss how the characteristics of the DDM variation reflect the spatial structure and dynamical characteristics of the Es layer through comparison with the two-dimensional maps of Es from GPS-TEC ROTI and the radio wave observations of the Automatic Identification System (AIS) installed from ships.

スポラディック E (Es) 層は, 電離圏の高度約 100 km において局所的に電子密度が増大する現象である. 電子密度の増大に伴い, 通常電離圏 E 層において反射されることがない 100 MHz を超える VHF 帯の電波も Es 層により反射されることがある. Es 層によって反射された電波は, 長距離にわたって異常伝搬し, 航空航法システムなどの無線システムに電波干渉を引き起こす可能性がある. 我々は 2021 年から, 航空航法システム, 特に計器着陸装置ローカライザー (Instrument Landing System Localizer: ILS LOC) の電波を用いた Es 層の観測を広島県呉市において行ってきた.

ILS LOC は, 108-112 MHz の電波を航空機から見て左側に 90 Hz, 右側に 150 Hz で振幅変調して送信し, 変調度の差 (Difference in Depth of Modulation: DDM) を用いて, 進入コースに関する情報を提供している. 出力される電波は, 強い指向性を持つため, Es 層による反射で長距離にわたる異常伝搬が生じる可能性がある. 著者らのグループの最近の研究によって, 日本の広島県呉市において台湾の花蓮空港の ILS LOC 型の方向指示器 (Localizer Type Directional Aid: LDA) から送信されたと考えられる 110.3 MHz の電波のソフトウェア受信機を用いた受信事例が報告されている. 本研究では, ソフトウェア受信機に加えて航空機搭載用 ILS LOC 受信機を広島県呉市に設置し, 電波の到来方向を連続的に計測した. これにより, 異常伝搬の送信元を明らかにするとともに, ILS の DDM の値から Es 層の空間構造に関する情報を抽出するこ

とが可能かを検証した.

Es 層による異常伝搬イベントでは, ILS LOC 受信機が示す受信電界強度に変動が見られ, 航空機搭載の機器に対する Es 層の影響について確認することができた. また, 観測で得られた音声モールス信号を解析したところ, 呉で受信した 110.3 MHz の電波は, 確かに台湾の花蓮空港より送信されていることが判明した. しかし, ILS LOC 受信機によって得られた受信電波のビーム中心からの偏位の角度を統計的に解析した結果, 呉から見た実際の花蓮の方位角と電波のビーム中心の方位角の差 (− 0.68 度) とは異なる値を示す場合が多く, 数十分程度の時間スケールで DDM の値が変動することも分かった. 2021, 2022 の 2 年間の Es シーズンの観測を統計的に解析することによって, このような DDM の値が大きく変動するイベントが全体の半数近くを占め, その特性は事例毎に異なることも明らかになった. このような DDM の値の変動は, Es 層の複雑な空間構造が, 花蓮空港 LDA の電波の伝搬方向を変化させている可能性がある事を示唆しており, DDM の時間変化から Es 層の形状に関する情報を得ることが期待できる.

本発表では, これまでの 2021, 2022 で得られた Es の異常伝搬イベントについて, ソフトウェア受信機, および ILS LOC 受信機によって得られたデータを統計的に解析した結果を報告する. また, DDM の変動特性が Es 層のどのような空間構造・移動特性を反映しているかについて, 2023 年夏季に得られた Es 層の観測事例を例にとり, GPS-TEC ROTI による Es 層の 2 次元分布や船舶自動識別装置 (Automatic Identification System: AIS) の電波観測との比較を行うことで議論する.

R005-25
B 会場 ：9/25　AM2 （10:45-12:30）
12:00〜12:15

GAIA モデルと COSMIC-1 データを用いた 2009 年冬季における Es 層密度増加の発生機構の解明

#安藤　慧 [1)], 齊藤　昭則 [2)], 品川　裕之 [3)]
[(1] 情報通信研究機構,[(2] 京都大・理・地球物理,[(3] 九州大学 国際宇宙惑星環境研究センター

Investigation of wintertime sporadic E layer intensification in 2009 using COSMIC-1 and GAIA data

#Satoshi Andoh[1)],Akinori Saito[2)],Hiroyuki Shinagawa[3)]
[(1]National Institute of Information and Communications Technology,[(2]Department of Geophysics, Graduate School of Science, Kyoto University,[(3]International Research Center for Space and Planetary Environmental Science, Kyushu University

This study investigated the generation mechanisms of wintertime sporadic E layer intensification (WEsLI) occurring primarily in February 2009. It is known that EsLI shows the minimum in winter. EsLs are formed by vertical ion convergence (VIC) driven by winds, and thus, EsLI variations relate to VIC variations. Our recent simulation demonstrated that SW2 tidal amplification can cause WEsLI at mid-latitudes. However, the simulation was performed only in the mid-latitude ionosphere. The global distribution of WEsLI and its driver is not fully understood.

In this presentation, we investigated the global distribution of WEsLI using FORMOSAT-3/COSMIC in 2009-2011. Moreover, a comparison between the observed WEsLI distribution and simulated VIC distribution was conducted to reveal the generation mechanism of WEsLI in 2009. The VIC was calculated from GAIA (Ground-to-topside model of Atmosphere and Ionosphere for Aeronomy) data. WEsLI in 2009 occurred at the latitudes of 10-40 degrees N between 90 degrees E and 140 degrees W and the latitudes of 0-20 degrees N between 80 degrees W and 120 degrees W. WEsLI in the central and western Pacific areas was evident. The observed WEsLI distribution resembled the VIC distribution driven by SW2, DW1, DE2, and DE3 tides between 12 and 18 LT at 100-120 km altitudes. SW2 and DE3 tidal amplification controlled primarily the WEsLI in 2009. We will discuss the mechanisms of tidal amplifications in the presentation.

本発表では 2009 年の主に 2 月に発生したスポラディック E 層 (sporadic E layer; EsL) の数十日間にわたる密度上昇の発生機構を調査した。EsL は冬季になると密度が減少することが知られている。EsL の形成には水平風の鉛直シアによるイオンの鉛直圧縮が重要であるため、イオンの鉛直圧縮の変動が EsL の密度変動と密接に関係していると考えられてきた。我々は最近の研究で、SW2 tides の鉛直シアが強くなることが、中緯度帯において冬季の EsL 密度の上昇を発生させていることを EsL の数値計算により見出した。しかし、その研究では中緯度帯にのみ焦点を当てており、冬季 EsL の密度上昇が中緯度帯以外でも発生しているのか、また発生していたとして SW2 tides が駆動源となっているのかは調査されなかった。

本発表では 2009-2011 年の FORMOSAT-3/COSMIC (COSMIC-1) による電波掩蔽による EsL 観測を用いることで、2009 年の冬季の EsL 密度上昇の分布を調査した。また、得られた分布を全球大気モデル GAIA (Ground-to-topside model of Atmosphere and Ionosphere for Aeronomy) から計算した中性風の潮汐波成分が駆動する鉛直イオン収束分布と比較した。2009 年の冬季の EsL 密度上昇は、東経 90 度-西経 140 度の北緯 10-40 度と西経 80 度-120 度の北緯 0-20 度付近とで特に発生していた。特に太平洋中部から西部の北緯 10-40 度での EsL 密度上昇が顕著であった。地方時では 12-18 時付近において、高度では 120 km 以下において特に観測されていた。2009 年の冬季の EsL 密度上昇の分布は SW2、DW1、DE2、DE3 tides が 12-18 時に駆動する鉛直イオン収束分布とよく一致していた。1 日潮汐波は主に低緯度帯の、半日潮汐波は中緯度帯の鉛直イオン収束を駆動していた。これらの潮汐波成分のうち、特に SW2 と DE3 が冬季 EsL の突発的密度上昇に寄与していた。これらの結果に加えて、潮汐波の振幅増加の物理機構を議論する。

R005-26
B 会場 ：9/25　PM1 （13:45-15:30）
13:45〜14:00

#中山　雅晴 [1)], 大矢　浩代 [2)], 土屋　史紀 [3)], 塩川　和夫 [4)], 野崎　憲朗 [5)]
([1] 千葉大学,[2] 千葉大・工・電気,[3] 東北大・理・惑星プラズマ大気,[4] 名大宇地研,[5] 電通大

Horizontal inhomogeneity of the D-region ionosphere detected by OCTAVE VLF/LF observations network during X-class solar flares

#Masaharu Nakayama[1)],Hiroyo Ohya[2)],Fuminori Tsuchiya[3)],Kazuo Shiokawa[4)],Kenro Nozaki[5)]
([1]Department of Electrical and Electronics Engineering, Graduate School of Engineering, Chiba Univ.,[2]Department of Electrical and Electronics Engineering, Graduate School of Engineering, Chiba Univ.,[3]Planetary Plasma and Atmospheric Research Center, Graduate School of Science, Tohoku University,[4]Institute for Space-Earth Environmental Research, Nagoya University,[5]The University of Electro-Communications

When solar flares occur, electron density in the ionosphere (60-100 km altitudes) increases because of intense X-rays. So far, relationship between VLF (3-30 kHz) and X-ray flux has been reported (Paulin et al., 2010), although there are few reports for horizontal inhomogeneity of the reflection height in the D-region ionosphere. The purpose of this study is to reveal horizontal homogeneity of electron density in the D-region ionosphere during X-class solar flares using multi-path VLF/LF (30-300 kHz) transmitter signals of “Observation of CondiTion of ionized Atmosphere by VLF Experiment (OCTAVE)” network. The OCTAVE network is our originally worldwide VLF network for monitoring the D-region phenomena such like solar flares, energetic electron precipitation, and acoustic waves and atmospheric gravity waves associated with earthquakes and volcanic eruption. When solar flares occur, VLF/LF amplitude and phase vary with decreasing the reflection height. The transmitters used in this study were NWC (21.817S, 114.167E, 19.8 kHz), JJI (32.05N, 130.82E, 22.2 kHz), JJY (37.37N, 140.85E, 40.0 kHz; 33.47N, 130.18E, 60.0 kHz), and BPC (34.63N, 115.83E, 68.5 kHz). The receivers were located at RKB (Rikubetsu, Hokkaido, 43.45N, 143.77E), ZAO (Zao, Miyagi, Japan, 38.10N, 140.53E), SGR (Sasaguri, Fukuoka, Japan, 33.63N, 130.51E), KAG (Tarumizu, Kagoshima, Japan, 31.59N, 130.55E), and PTK (Pontianak, Indonesia, 0.003N, 109.37E), which are part of OCTAVE network. When the class of solar flares is X2.2, X2.7 and X4.9, amplitudes of variations in the VLF/LF amplitude (Δ A) and phase (Δ P) were 2.9-24.9 dB and 24.8-420.0 degrees, respectively. Using wave-hop method, we estimated reduction in reflection height (Δ h) from the observed Δ A and Δ P. The Δ h were estimated to be 1.0-12.9 km for 16 paths, and showed that Δ h tends to increase with solar zenith angle in large solar flares. In addition, we estimated the increase in electron density (Δ N) with azimuth angle using IRI-2016 model. As a result, the difference of Δ N with the propagation direction was confirmed. Δ N of west to east propagation path was larger than that of east to west one. In this presentation, we will discuss the horizontal inhomogeneity of the reflection height during solar flares taking into account difference of VLF east-west propagation.

R005-27
B 会場 ：9/25　PM1 （13:45-15:30）
14:00〜14:15

特異的減少傾向を持つ赤道ジェット電流の発生特性について

#池末　暉 [1)], 吉川　顕正 [2)], 藤本　晶子 [3)]
(1 九州大学,(2 九大/理学研究院,(3 九工大

Research on the characteristics of equatorial electrojet occurrence with a peculiar decreasing trend

#Hikaru Ikesue[1)],Akimasa Yoshikawa[2)],Akiko Fujimoto[3)]
(1Kyushu university,(2Department of Earth and Planetary Sciences, Kyushu University,(3Kyushu Institute of Technology

During quiet magnetic field activity, various current structures exist in the dayside ionosphere, including Sq current, the strong eastward current EEJ (Equatorial ElectroJet) and CEJ (Counter ElectroJet) that flow in the opposite westward direction. (e.g., Stening;1992, Rastogi;1973, Yamazaki & Maute;2017)

EEJ driven by an eastward electric field are usually observed with an increased amplitude compared to the Sq current due to the Cowling effect. However, there is a phenomenon in which the EEJ amplitude is equal to or smaller than that of the Sq current during quiet magnetic field activity. We defined this phenomenon as a “peculiar EEJ” and analyzed it to understand the characteristics and causes of its occurrence.

We used the magnetic field data observed at Ancon and Huancayo in Peru as equatorial stations and Eusebio as an off-dip equatorial station in Brazil. Comparing between the amplitudes of the equatorial stations (Ancon and Huancayo) for EEJ amplitude and the off-dip equatorial station (Eusebio) for lower latitude magnetic field amplitude which corresponds to Sq current variations, we found that the peculiar EEJ was classified into roughly three types: (1) undeveloped type, which is characterized with a full lack of EEJ amplitude, (2) sudden type, which shows a sudden drop of EEJ amplitude than lower latitude magnetic field amplitude, and (3)other types.

The five-year analysis from 2016 to 2020 resulted that there are 57 events as the peculiar EEJ and the event number of each type: undeveloped type, sudden type, other types are 21, 16, 20, respectively. The occurrence of the peculiar EEJ has seasonal dependence: the undeveloped type in the summer solstice, the sudden type in the winter solstice. We suspect that the seasonal dependence of EEJ and Sq current for the undeveloped type and the seasonal dependence of CEJ for the sudden type may play a significant role in, respectively. In this presentation, I will report the results of further analysis using TEC, which represents electron density, and ROTI, an electron density disturbance index, and discussion on the occurrence characteristics and factors of the peculiar EEJ.

太陽静穏時、昼側電離層では Sq 電流や、東向きに卓越した EEJ、その反対の西向きに流れる CEJ をはじめとする様々な電流構造が存在する。(e.g., Stening;1992, Rastogi;1973, Yamazaki & Maute;2017)

東向き電場により駆動される EEJ は、Cowling 効果によりその背景に拡がる Sq 電流と比べて振幅が増大されて観測されることが通常である。しかしながら、磁気擾乱がないのにもかかわらずこの EEJ 振幅が Sq 電流と同等、ないしはそれ以下になる現象も存在する。我々はこの現象を“特異型 EEJ”と定義し、その発生特性と要因の解明を目的とした解析を行った。

磁場観測点は赤道上のステーションとしてペルーのアンコンとワンカヨ、赤道上外のステーションとしてブラジルのユーゼビオを用いた。☒赤道上の磁場変動と赤道外上の磁場変動（Sq）を比較することで、特異型 EEJ を大きく EEJ が異様に卓越できていないという特徴を持つ未発達型: ①と EEJ に突発的な落ち込みを見せる突発型: ②、その他: ③の 3 種類に分類した。また、2016-2020 年の 5 年分について解析を行った結果、それぞれの発生頻度は特異型 EEJ 発生日が 57 日、具体的には未発達型が 21 イベント、突発型が 16 イベント、その他が 20 イベントであった。それぞれの型については①の未発達型が夏至周辺に多く、②の突発型が冬至周辺に多いという季節依存性をもつことが明らかになった。現時点ではこれらの要因として、①については赤道ジェット電流と Sq 電流の季節依存性、②については CEJ の季節依存性が大きくかかわっているのではないかと考えている。

本講演では、抽出した特異型 EEJ についての発生特性・要因について電子密度を表す TEC や電子密度擾乱指数 ROTI などを用いた更なる解析と考察を行った結果について報告する予定である。

R005-28
B 会場 ：9/25　PM1 （13:45-15:30）
14:15〜14:30

半球間沿磁力線電流（IHFAC）に現れる準６日波の変動

#高山　久美 [1)], 吉川　顕正 [2)], 三好　勉信 [3)]
([1] 九大,[2] 九大/理学研究院,[3] 九大・理・地球惑星

Quasi-6-Day Wave Modulation of the Inter-Hemispheric Field-Aligned Currents (IHFACs)

#Kumi Takayama[1)],Akimasa Yoshikawa[2)],Yasunobu Miyoshi[3)]
([1]Kyushu University,[2]Department of Earth and Planetary Sciences, Kyushu University,[3]Department of Earth and Planetary Sciences, Faculty of Sciences, Kyushu University

The quasi-6-day wave is a type of atmospheric wave generated by the latent heat heating associated with the cumulus convection activity in the tropics [Miyoshi and Hirooka, 1999]. It propagates upward and affects the equatorial electrojet (EEJ) in the ionosphere, which has been confirmed from satellite observations [Yamazaki et al., 2018]. In addition, TIME-GCM calculations shows that the EEJ reaches its maximum intensity around the equinoxes [Liu et al., 2014]. Inter-hemispheric field-aligned currents (IHFACs) flow from the ionosphere of one hemisphere to the other through the magnetosphere, to resolve the non-uniformity of ionospheric currents with divergent spatial structure that occurs between hemispheres [Fukushima, 1979]. The direction of the IHFACs changes in the morning, noon, and evening, and its intensity is highest in February and August [S. Yamashita and T. Iyemori, 2002].

In this study, we used ground magnetic field data from MAGDAS, GSI, and INTERMAGNET to clarify the effects of the quasi-6-day wave on the Sq current and the IHFACs. The ground magnetic field data used are the north-south (H) and east-west (D) magnetic field components at 15 stations within the 210 geomagnetic longitude band and -42 to +35 geomagnetic latitude during the 2007-2011 magnetic quiet period. Principal component analysis is a statistical analysis method that can extract large components from any data and reveal its internal structure. We applied this method to the data to extract the Sq-EEJ current system from the H/D components in the mid-low latitude region, and the IHFACs variation from the D component in the magnetic equator. The amplitude of the variation with a period of about 6 days was extracted, and this was taken to be the quasi-6-day wave. To show the latitudinal and seasonal structure of the quasi-6-day wave, the average amplitude for each month over the 5-year timespan was calculated.

The results show that, in addition to the EEJ, the equatorial IHFAC and the mid-low latitude Sq currents are affected by the quasi-6-day wave. It was also found that both the H and D components show seasonal variations, becoming stronger around the equinoxes. This is consistent with the seasonal dependence of the quasi-6-day wave. The foci of the Sq current system are affected only by the D component, indicating that the quasi-6-day wave on the D component increases in proportion to the amplitude of the Sq current system. More results and discussion will be presented in this presentation.

準 6 日波は大気波動の 1 つで、熱帯における積雲対流活動に伴う潜熱加熱によって発生し [Miyoshi and Hirooka, 1999]、上方に伝播、電離圏の赤道ジェット電流 (EEJ) に影響を与えることが衛星観測から確認されている [Yamazaki et al., 2018]。また TIME-GCM による計算から Equinox 前後で最大振幅となる [Liu et al., 2004] ことがわかっている。半球間沿磁力線電流（IHFAC）は、半球間で生じる発散的な空間構造を持つ電離層電流の非一様性を解消するために、片側半球の電離圏から磁気圏を通ってもう一方の半球に流れる電流である [Fukushima, 1979]。朝、昼、夜で向きが変化し、２月と８月に電流強度が最大となることが示されている [S. Yamashita and T. Iyemori, 2002]。

本研究では、地上磁場観測データを用いて、Sq 電流および IHFAC に現れる準 6 日波の影響を明らかにした。使用した地上磁場データは、MAGDAS、国土地理院、INTERMAGNET の 2007〜2011 年の磁気的静穏期における、地磁気経度 210° 帯、地磁気緯度-42° 〜＋ 35° 内の 15 観測点の南北 (H) および 東西 (D) 成分である。解析手法として、データから大規模な成分を分離・抽出し、内部構造を明らかにすることができる主成分分析を各観測点/各成分に適用することにより、中低緯度領域の H/D 成分から Sq-EEJ 電流系、および磁気赤道域のＤ成分から IHFAC による変動成分を抽出し、その変動成分から約６日周期の変動の振幅を取り出した。また、各月でその振幅を５年平均することで、準 6 日波による電離層電流変動の緯度構造と季節変動を示した。

その結果、EEJ に加えて、赤道域の IHFAC、および中低緯度の Sq 電流が準 6 日波の影響を受けていることがわかった。また、H/Ｄ成分ともに春分/秋分前後に強くなる季節変動を示すことを明らかにした。これは準６日波の季節依存性と一致する。また電気伝導度が高くなる夏半球に強く現れていること、および Sq 電流の渦中心は D 成分のみに影響が見られることから、Sq 電流系の振幅に比例して増大していることがわかる。詳しい結果および考察は本発表で述べる予定である。

R005-29
B 会場 ：9/25　PM1 （13:45-15:30）
14:30〜14:45

プラズマバブル発生に関するＣＥＪの影響

#加藤　彰紘 [1)], 吉川　顕正 [2)], 藤本　晶子 [3)]
[(1] 九大,[(2] 九大/理学研究院,[(3] 九工大

CEJ Effects on Plasma Bubble Generation

#Akihiro Kato[1)],Akimasa Yoshikawa[2)],Akiko Fujimoto[3)]
[(1]Kyushu university,[(2]Department of Earth and Planetary Sciences, Kyushu University,[(3]Kyushu Institute of Technology

Plasma bubbles are ionospheric disturbances that occur in the magnetic equatorial region and are caused by Rayleigh-Taylor instabilities. Therefore, an eastward electric field that enhances the equatorial electrojet current (EEJ) is a prerequisite for plasma bubble generation, and the occurrence of the counter electrojet current (CEJ) with a westward electric field is thought to suppress plasma bubble generation [e.g., Uemoto et al., 2010]. However, the relationship between the equatorial electrojet current structure and plasma bubble generation is not yet fully understood, as is spread-F, which appears by plasma bubbles even during CEJ generation and has been observed in Peru, South America [Akiyama et al., 2018].

We analyzed ground-based magnetic field data on CEJ occurrence dates to investigate whether EEJ/CEJ-induced magnetic field variations can be used as an indicator of plasma bubble generation. In this study, we analyzed the EEJ monitoring index, EUEL, the S4-index, and ionosonde data, which indicate scintillation, for plasma bubble events in Peru. The following results were obtained.

(1) On magneticaly quiet day (Kp $\leqq$ 3), the correlation between the EUEL integrated over 17-19 LT (Pre-sunset IEUEL) and S4-index showed that plasma bubble events were suppressed when the pre-sunset IEUEL was negative.
(2) On magneticaly quiet day (Kp $\leqq$ 3), the correlation between the EUEL and plasma bubble events at sunset shows that when the H component becomes positive again after the occurrence of a CEJ, the ionospheric F-layer height h'f increases and a spread-F of about S4-index = 0.3-0.8 is generated.
(3) Furthermore, on magneticaly disturbance days (Kp $>$3) plasma bubble generation events were also identified in the case of large CEJ growth after sunset .

The result of (1) indicate that there were CEJs that generate westward currents, making it difficult for plasma bubbles to develop.
The result in (2) may have been caused by the eastward electric field becoming stronger around sunset (PRE: pre-reversal enhancement). On the other hand, when the magnetic field was southward at sunset, h'f did not increase sufficiently (below 300 km) and a spread-F of less than S4-index=0.4 occurred. Therefore, the generation of plasma bubbles with large scintillation was related to the eastward-facing electric field at sunset.
The trend in (3) is currently being analyzed.

Based on the above results, the influence of the CEJ on plasma bubble generation will be discussed in this presentation.

プラズマバブルは磁気赤道域で起こる電離圏擾乱現象で、レイリー・テイラー不安定性によって発生する。そのため、赤道ジェット電流 (EEJ) を強化するような東向き電場が必要条件であり、西向き電場を伴うカウンタージェット電流 (CEJ) が発生すると、プラズマバブルの発生は抑制されると考えられる [e.g. Uemoto et al., 2010]。 しかし、南米のペルーにおいて、CEJ 発生時でもプラズマバブルによって現れるスプレッド F が確認される [Akiyama et al., 2018] など、赤道ジェット電流構造とプラズマバブルの発生に関係性はまだ十分に理解されていない。

そこで我々は、CEJ 発生日の地上磁場データを解析し、EEJ/CEJ による磁場変動がプラズマバブルの発生指標となり得るかどうかを調べた。本研究では EEJ モニタリング指数である EUEL と、シンチレーションを示す S4-index とイオノゾンデを用いて、ペルーにおけるプラズマバブルイベントについて解析を行った。以下の結果が得られた。

（1）磁気静穏日（K $\leqq$３）IEUEL の 17〜19LT（夕方側）を積分した値（Pre-sunset IEUEL）と S4-index の相関を見ると、Pre-sunset IEUEL がマイナス時、プラズマバブルの発生が抑制された。
（2）磁気静穏日（Kp $\leqq$３）日没時のＥＵＥＬとプラズマバブルの相関を見ると、CEJ 発生後の日没時に磁場が北向きに戻るとき、電離圏 F 層高度 h'f は上昇し、S4-index=0.3-0.8 程度のスプレッド F が発生している。
(3) さらに、磁気擾乱日（Kp ＞３）の日没後に CEJ が大きく成長する場合においても、プラズマバブルの発生イベントが確認された。

(1) の結果は、西向き電場である CEJ が発生しており、プラズマバブルが発達しにくい状況であったと示唆される。

(2) の結果は、日没前後で東向き電場が強くなる現象（PRE：pre-reversal enhancement）によって発生したものではないかと考えられる。一方、日没時に磁場が南向きであるとき、h'f は十分に上昇せず (300km 以下)、S4-index=0.4 未満のスプレッド F が発生した。したがって、シンチレーションが大きいプラズマバブルの発生には、日没時の東向き電場が関係していると考えられる。

(3) の傾向については、現在解析中である。

本発表では、上記の結果に基づき、プラズマバブル発生に関するＣＥＪの影響について議論する。

R005-30
B 会場 ：9/25　PM1 （13:45-15:30）
14:45〜15:00

#Abadi　Prayitno[1)]
([1]BRIN

The Use of Ionosonde for Forecasting Post-Sunset Equatorial Plasma Bubbles: An Observational Experiment in Southeast Asia

#Prayitno Abadi[1)]
([1]Indonesian National Research and Innovation Agency

Equatorial plasma bubbles (EPBs) can negatively affect space-based technological systems. This study investigates the potential of ionosonde to forecast the occurrence of post-sunset EPBs in the zonal direction using observational data from four ionosondes near Southeast Asia's magnetic Equator. A logistic regression model was used to establish a relationship between the probability of post-sunset EPB occurrence and the evening vertical plasma drift (v). Results show that the probability of EPB occurrence is close to zero, or the EPB cannot be generated when v is negative. Conversely, when v is stronger than 30 m/s, the probability of EPB occurrence is greater than 0.90, meaning that EPB almost always occurs. The probability of EPB occurrence is 1 when v is greater than or equal to 40 m/s. Using this model, the study found that a single ionosonde in the Equator can optimally forecast the occurrence of EPBs up to a longitudinal distance of 30 deg from its position. The accuracy of ionosonde in predicting the occurrence of EPBs above its location is approximately 0.80, and the accuracy decreases by 10% for forecasting EPB occurrence at longitudinal distances of 30 deg. The results of this study enhance our knowledge of the connection between the evening vertical plasma drift and the emergence of post-sunset EPBs by utilizing the data obtained from the ionosonde. In addition, the study offers an essential insight into the recommended coverage range of ionosonde for predicting EPB occurrence in the zonal direction, which can be utilized to strengthen the regional space weather services.

R005-31
B 会場 ：9/25　PM1 （13:45-15:30）
15:00〜15:15

#斎藤　享 [1)], 高橋　透 [2)], 吉原　貴之 [3)]
([1] 電子航法研,[2] 電子航法研,[3] 電子航法研究所

Strong ionospheric irregularities in sunlit conditions and its impact on GNSS-based navigation systems

#Susumu Saito[1)],Toru Takahashi[2)],Takayuki Yoshihara[3)]
([1]Electronic Navigation Research Institute, MPAT,[2]Electronic Navigation Research Institute, MPAT,[3]Electronic Navigation Research Institute, MPAT

Ionospheric delay which is proportional to the ionospheric total electron content (TEC) and scintillation caused by small-scale irregularities are main error sources in GNSS. While ionospheric delays with large spatial scales can be corrected well by the differential correction technique, it is difficult to correct when the ionospheric delay significantly changes in space. The plasma bubble is the primary cause of such small-scale but large amplitude variation in the low magnetic latitude region.

Since the plasma bubble is know to occur in the night, most often from sunset to midnight, and rarely occur in the sunlit condition, some GNSS-based air navigation systems are operated from sunrise to sunset to avoid the impacts by the plasma bubble. While a few reports of plasma bubble occurrences around sunrise have been reported, their impacts on GNSS-based air navigation systems have not been well studied.

From 20:00 to 22:30 UTC on 27 February 2023 (from 04:15 to 06:45 LT), strong ionospheric irregularities were observed in Ishigaki (24.4N, 123.3N, 19.6 Mag.Lat). The irregularities were observed even after the local sunrise for more than 30 minutes. The event was characterized by irregular variation of the ionospheric delay (TEC) with occasional depletion of it and strong scintillation, which are the characteristics of the plasma bubble. At the same time, the background ionospheric delay (TEC) was enhanced in the western side of Japan. It was in the recovery phase of a magnetic storm commenced on 26 February 2023. These observational results indicate that the ionospheric delay (TEC) depletions with irregularities were embedded in the TEC enhancement that looked similar to the event known as the storm induced plasma stream (Maruyama et al., 2013).

By using closely separated GNSS receivers at Ishigaki Airport, the characteristics of the spatial variation of the ionospheric delay (TEC) are estimated, and their impact on GNSS-based air navigation systems are evaluated.

R005-32
B 会場 ：9/25　PM2 （15:45-18:15）
15:45〜16:00

ペナルティ付き動体検出に基づいた時系列イオノグラム画像における電離圏エコー抽出モデルの開発

#廣重　優 [1)], 藤本　晶子 [1)], 池田　昭大 [2)], 阿部　修司 [3)], 吉川　顕正 [4)]
(1 九工大,(2 鹿児島高専,(3ROIS-DS,(4 九大/理学研究院

Extraction model of ionospheric echoes for time-series ionogram images based-on penalized motion detection

#Yu Hiroshige[1)],Akiko Fujimoto[1)],Akihiro Ikeda[2)],Shuji Abe[3)],Akimasa Yoshikawa[4)]
(1Kyushu Institute of Technology,(2Kagoshima National College of Technology,(3Joint Support-Center for Data Science Research,(4Department of Earth and Planetary Sciences, Kyushu University

The ionosphere affects the operation of various systems, such as satellite and shortwave communications. For example, fluctuations in the ionospheric environment cause disturbances such as satellite positioning errors and absorption of shortwave radio waves. Therefore, it is important for space weather forecasting to continuously observe the ionospheric environment in quasi-real time, in order to alert and mitigate propagation disturbances. One of the methods of ionospheric observation is ionogram, which provides the height distribution of electron density in the ionosphere. However, ionograms contain not only ionospheric echoes but also noise due to measurements and computational processing. Those noises in ionograms are more abundant than the ionospheric echoes and comparable in the intensity to the ionospheric echoes.

The purpose of this work is to develop a method to generate ionogram images that are robust to such noise and easy to measure parameters of ionospheric echoes. We propose a method to remove noise from ionograms and extract only the ionospheric echoes automatically based on motion detection algorithm. By focusing on the time variability of the ionospheric environment, we apply Background Subtraction Algorithm, one of the motion detection methods, to the parameter scaling of the echoes.

Proposed model consists of two processing parts: weak signal reduction and penalized motion detection. As a preprocessing step, a threshold based on the distribution of ionospheric echoes was established for each ionogram image, and weaker signals were removed. Then, the motion detection was performed on the denoised ionogram time series data to separate signals into ionospheric echoes and background noise. The motion detection method used in this work is a background subtraction method with a penalty based on echo characteristics. We evaluated our model on 960 ionograms with high noise content (January 1, 2019, Sasaguri, Japan, using FMCW radar). We found that the penalized motion detection can extract ionospheric echoes from ionograms with a large amount of noise.

R005-33
B 会場 ：9/25　PM2 （15:45-18:15）
16:00〜16:15

イオノゾンデ同化 GNSS 電離圏 3 次元リアルタイムトモグラフィ解析の改良と事例解析

#野﨑　太成 [1)], 斎藤　享 [2)],Ssessanga　Nicholas[3)], 山本　衛 [4)]
([1] 京大・情・通信,[2] 電子航法研,[3] オスロ大学物理学科 4D-Space,[4] 京大・生存圏研,[5] 京大・生存圏研

Improvement of 3-D ionospheric tomography based on GNSS-TEC with ionosonde data assimilation and case analysis

#Taisei Nozaki[1)],Susumu Saito[2)],Nicholas Ssessanga[3)],Mamoru Yamamoto[4)]
([1]Course of Communications and Computer Engineering, Kyoto University,[2]ENRI, National Institute of Maritime, Port, and Aviation Technology,[34]D-Space, Department of physics, University of Oslo, Norway,[4]Research Institute for Sustainable Humanosphere, Kyoto University,[5]Research Institute for Sustainable Humanosphere, Kyoto University

Structures of the electron density in the ionosphere cause reflection, absorption, and delay of radio waves, which can lead to interference in radio communications. Therefore, the observation of the ionospheric electron density is of great importance. One of the methods to derive the ionospheric density profiles is the GNSS tomography, which estimates the three-dimensional structure of the ionosphere from the GNSS-TEC observation data.

The original algorithm employed to cover the Japanese archipelago and the nearby surrounding region was the constrained least-squared fitting method implemented by Seemala et al. (2014) and Saito et al. (2017). The method used the spatial gradient of the electron density as the constraint, and in addition, introduced boundary conditions at the top and the bottom to stabilize the results. While the original algorithm was stable and useful, it had problems with negative electron density in the solution and overestimated the ionospheric peak height when the ionospheric height was low.

To solve these problems, Ssessanga et al. (2021) proposed an algorithm based on a 3D-VAR method by assimilating ionosonde data. We further improved this algorithm by adjusting the background error covariance matrix(B), which specifies the correlation of voxels in vertical and horizontal directions.

This study presents the analysis results of improved algorithm based on GNSS-TEC plus ionosonde data. The peak-height of electron density is much more improved compared with the GNSS-only tomography algorithm.

We will also report case studies of 3-D ionospheric structure including those of the traveling ionospheric disturbance (TID) associated with the Tonga eruption in January 2022 derived by the improved algorithm.

R005-34
B 会場 ：9/25　PM2 （15:45-18:15）
16:15〜16:30

2022 年 1 月 15 日のトンガ火山噴火に伴う大気圏・電離圏変動のシミュレーション研究

#品川　裕之 [1)], 三好　勉信 [2)]
[(1] 九州大学国際宇宙惑星環境研究センター,[(2] 九大・理・地球惑星

Simulation study of atmosphere-ionosphere variations associated with the eruption of Tonga volcano

#Hiroyuki Shinagawa[1)],Yasunobu Miyoshi[2)]
[(1]International Research Center for Space and Planetary Environmental Science, Kyushu University,[(2]Department of Earth and Planetary Sciences, Faculty of Sciences, Kyushu University

On 15 January 2022 significant variations in the ionosphere and the atmosphere were observed worldwide, which is clearly associated with the eruption of Hunga Tonga-Hunga Ha'apai in Tonga. In this event, various kinds of phenomena have been reported: (1) generation and propagation of atmospheric waves such as acoustic-gravity waves, Lamb waves, and Pekeris waves, (2) TIDs (traveling ionospheric disturbances) concentrically propagating from the eruption site, (3) significant depletion of TEC(total electron content) near the eruption site, (4) oscillations in TEC and the geomagnetic field with a period of several minutes corresponding to acoustic resonance mode in the atmosphere, (5) variations in TEC/geomagnetic field in the magnetic conjugates, (6) global neutral wind variations, and (7) occurrence of equatorial plasma bubbles.

To reproduce and understand the atmospheric-ionospheric disturbances driven by the eruption of the volcano, various simulation studies have been recently made. At the present time, some of the studies have successfully reproduced Lamb waves and some gravity waves, producing traveling ionospheric disturbances (TIDs), and global thermospheric wind variations. However, most of the present studies use a hydrostatic atmospheric model, which is unable to include vertical compressibility of the atmosphere. Therefore, those models cannot reproduce acoustic shock waves, upward propagation of acoustic waves, and atmospheric oscillation with a period of a few minutes generated by the vertical acoustic resonance. Although there are a few simulation studies using a nonhydrostatic atmospheric model, various approximations and assumptions are made to express the atmospheric disturbances driven by the volcanic eruption. At the moment, existing atmosphere-ionosphere models related to the volcanic eruption are not very realistic.

To better reproduce the atmosphere-ionosphere variations driven by the volcanic eruption, we employed an axisymmetric 3-D nonhydrostatic atmospheric model and the whole atmosphere-ionosphere coupled model GAIA. In this simulation, a sudden temperature change in the eruption point is given to the nonhydrostatic atmospheric model, and then the calculated neutral wind variations are incorporated into GAIA to simulate ionospheric variations driven by the eruption.

We found that the simulation can produce various kinds of atmospheric waves generated by the eruption, such as acoustic waves, gravity waves, Lamb waves, Pekeris waves, and TIDs concentrically propagating from the eruption site, and atmospheric oscillations with a period of a few minutes. In addition, the results indicate that the eruption generates supersonic shock waves in the volcanic region, leading the extremely large vertical oscillations in the thermosphere and ionosphere. However, there are still quantitative disagreements between observations and simulations about TEC variations in the magnetic conjugate region of the eruption site, and significant TEC decrease near the Tonga region after the eruption.

We will present the results of the simulation and discuss similarities and differences between simulations and observations.

2022 年 1 月 15 日のトンガのフンガ・トンガ＝フンガ・ハアパイ火山噴火では顕著な大気圏・電離圏変動が観測され、それに伴うさまざまな現象が報告されている。主なものとしては、(1) 音波、重力波、Lamb 波、Pekeris 波などの大気波動の生成と伝搬、(2) 噴火地点を中心として同心円状に広がって伝搬する TID(伝搬性電離圏擾乱)、(3) 噴火後の震源付近での TEC(total electron content) 減少、(4) 数分周期の大気音波共鳴モードに対応する TEC/地磁気振動、(5) 磁気共役点での TEC/地磁気変動、(6) グローバルな中性風変動、(7) プラズマバブルの発生、などがある。

これらの現象の再現と解明のために、最近、さまざまな大気圏・電離圏シミュレーションによる研究が行われている。現時点で、Lamb 波とそれに伴う重力波、同心円状に伝搬する TID や、グローバルな熱圏風系の変動などは概ね再現できている。しかし、これまでの研究は主に静力学平衡の大気モデルを用いたものであり、鉛直方向の大気の圧縮性による影響が入っていないため、噴火直後の衝撃波や音波の上方伝搬、音波共鳴による数分周期の大気の振動などは再現できていない。また、非静力学モデルを用いた研究もあるが、噴火の入力方法などでさまざまな近似や仮定を用いており、まだ十分に現実的なモデルにはなっていない。

我々は、軸対称全球３次元非静力学平衡大気圏モデルと全領域大気圏-電離圏結合モデル GAIA を組み合わせることにより、トンガの噴火に伴う大気圏・電離圏変動の数値シミュレーションを行った。このシミュレーションでは、非静力学大気圏モデルに火山噴火の地点で急激な温度変化を与え、その後の中性風速度変動を求め、その結果を GAIA の背景風に加えることによって、火山噴火に起因する大気圏・電離圏変動を求めた。

このシミュレーションの結果、火山噴火に伴う衝撃波、音波、重力波、Lamb 波、Pekeris 波などの大気波動やそれらに起因する TID、数分周期の音波共鳴振動などが概ね再現された。また、噴火地点の直上では、超音速の衝撃波の上方伝搬や、鉛直方向の非常に激しい熱圏・電離圏振動が起きていたことが示唆された。しかし、電場を介した磁気共役点での TEC 変動や、噴火直後の震源付近の TEC 減少など、定量的には観測と一致しない点もあることがわかった。

本発表では、シミュレーション結果と観測の比較を行い、その類似点と相違点について議論を行う予定である。

R005-35
B 会場 ：9/25　PM2 （15:45-18:15）
16:30〜16:45

#大矢　浩代 [1)], 土屋　史紀 [2)], 鴨川　仁 [3)], 鈴木　智幸 [3)],Chum Jaroslav[4)], 高村　民雄 [5)]
([1] 千葉大・工・電気電子,[2] 東北大・理・惑星プラズマ大気,[3] 静岡県立大学,[4] チェコ科学アカデミー・大気物理研究所,[5] 千葉大・環境リモセン

Variations in the D-region ionosphere after the 2022 Tonga volcanic eruption using AVON VLF/LF transmitter signals

#Hiroyo Ohya[1)],Fuminori Tsuchiya[2)],Masashi Kamogawa[3)],Tomoyuki Suzuki[3)],Jaroslav Chum[4)],Tamio Takamura[5)]
([1]Graduate School of Engineering, Chiba University,[2]Planetary Plasma and Atmospheric Research Center, Graduate School of Science, Tohoku University,[3]University of Shizuoka,[4]Institute of Atmospheric Physics, Czech Academy of Sciences,[5]Center for Environmental Remote Sensing, Chiba University

The Hunga Tonga-Hunga Haʻapai volcano in Tonga (in southern Pacific, 20.54S, 175.38W) explosively erupted around 04:10 UT on 15 January, 2022, and large pressure variations occurred from the volcano. Large and medium scale traveling ionospheric disturbances (LSTID and MSTID) due the eruptions were observed (Themens, 2022), which were caused by Lamb wave excited by the eruptions. In addition to the Lamb wave, Pekeris waves were generated by the eruption (Watanabe et al., 2022). The Lamb waves are a kind of acoustic one, and propagate horizontally with phase velocity of ˜310 m/s. On the other hand, Pekeris waves are internal resonance mode that propagate horizontally with phase velocity of ˜240 m/s. The Pekeris waves have anti-phase between upper and lower stratopause, while the Lamb waves are in-phase vertically. The energy of the Pekeris waves is closed between stratopause and mesopause, so amplitude of Pekeris waves becomes large in the height range of 45-85 km. However, variations in the D-region ionosphere due to the Lamb and Pekeris waves associated with the eruptions has not been revealed at all. In this study, we investigate variations in VLF/LF transmitter signals and atmospheric electric field (or potential gradient) to understand coupling between the D-region ionosphere and atmosphere associated with Tonga volcanic eruptions of 15 January, 2022. The VLF/LF transmitters used in this study were JJY(60 kHz, Japan), JJI(22.2 kHz, Japan), and BPC(68.5 kHz, China). The receivers were Tainan (TNN, 23.07N, 120.12E) in Taiwan, where is one of Asia VLF observation network (AVON). We used 0.1-s sampling amplitude data. Unfortunately, there were no phase data for all paths on that day. The minimum distances of the JJI-TNN, JJY60kHz-TNN, and BPC-TNN propagation paths from the Tonga volcano were 8167.7 km, 8311.6 km, and 8499.9 km, respectively. The atmospheric electric field has been observed in Chiba University (CHB), (35.63N, 140.10E), Japan, and Studenec (STU), Czech Republic (50.26N, 12.52E). The distances of CHB and STU from the Tonga volcano were 7789.5 km and 16634.7 km, respectively. At arrival times of Lamb (˜307 m/s) and Pekeris waves (˜235 m/s), both variations in VLF/LF amplitudes were observed. The period of the variations was 3.3-16.7 min. (1-5 mHz). Amplitude of the variations in VLF/LF amplitudes due to Pekeris wave was larger than that due to Lamb wave, which is consistent with simulation of neutral winds. At arrival time of Pekeris wave, variations in atmospheric electric field were seen at CHB and STU in spite of ground-based observations. Period of the variations in atmospheric electric field due to Pekeris wave was 1.7-16.7 min. (1-10 mHz). Ground-based geomagnetic data at Kakioka also showed similar variation with the VLF/LF amplitudes. Electron density in the D-region varied by Lamb and Pekeris waves. The atmospheric electric field on the ground may vary via global electric circuit, because amplitude of Pekeris wave is very small on the ground. In this presentation, we will discuss the mechanism of the phenomena in detail.

R005-36
B 会場 ：9/25　PM2 （15:45-18:15）
16:45〜17:00

トンガ海底火山噴火により発生・伝搬した Lamb 波の異方性と電離圏電子密度擾乱分布異方性の関係

#家森　俊彦 [1)], 青山　忠司 [2)], 横山　佳弘 [3)],Pangsapa　Vijak[4)],Jarupongsakul　Thanawat[4)], 佐納　康治 [5)], 小田木洋子 [1)], 田中　良和 [1)], 田口　聡 [1)], 齊藤　昭則 [1)], 穂積　Kornyanat[6)]
([1] 京大,[2] エフ・ファクトリー,[3] スウェーデン宇宙科学研究所,[4] チュラロンコン大学,[5] 朝日大学,[6]NASA/ゴダード宇宙飛翔センター

Anisotropy of Lamb wave generated by the Tonga volcanic eruption and its relation to anisotropic distribution of Ne fluctuations

#Toshihiko Iyemori[1)],Tadashi Aoyama[2)],Yoshihiro Yokoyama[3)],Vijak Pangsapa[4)],Thanawat Jarupongsakul[4)],Yasuharu Sano[5)],Yoko Odagi[1)],Yoshikazu Tanaka[1)],Satoshi Taguchi[1)],Akinori Saito[1)],Kornyanat Hozumi[6)]
([1]Kyoto University,[2]F-Factory Co., Ltd.,[3]Swedish Institute for space physics,[4]Chulalongkorn University,[5]Asahi University,[6]NASA/GSFC

The eruption of the Tonga submarine volcano on January 15, 2022 generated the Lamb wave which orbited the Earth a few times. The global ionospheric electron density disturbance observed as GPS-TEC variation was generated along with the passage of the wave. A clear difference in amplitude and frequency of the TEC variation can be seen between the west side of the volcano (Asian region).and the east side (America region). That is, large-amplitude and short-period (<300 sec) GPS-TEC fluctuations were widely observed after the passage of the Lamb waves in Asia, while the amplitudes were relatively small in the Americas. Various factors, such as the difference in local time when Lamb waves pass, are conceivable, but from the analysis of pressure data, it was found that the amplitude and waveform of the Lamb waves themselves, which are the cause, have a fairly clear anisotropy. An attempt is made to quantitatively compare the magnitude and spectrum of barometric and TEC fluctuations.

2022 年 1 月 15 日のトンガ海底火山噴火に伴って生成され地球を周回した Lamb 波の通過に伴って全球的に引き起こされた電離圏電子密度擾乱には火山の西側 (アジア域) と東側 (アメリカ域) で明瞭な振幅や周波数分布の違いが見られる。西側に伝搬した Lamb 波が通過したアジア域では、大振幅の短周期 (<300 sec) GPS-TEC 変動が広く観測されたが、東側に伝搬した Lamb 波が通過したアメリカ域では振幅が比較的小さい。Lamb 波通過時の local time の違いなど様々な要因も考えられるが、気圧データの解析から、原因となる Lamb 波自体の振幅や波形にかなり明瞭な異方性のあることが判明した。Lamb 波に伴う気圧変動と TEC 変動の大きさおよびスペクトルを定量的に比較することを試みる。

R005-37
B 会場 ：9/25　PM2 （15:45-18:15）
17:00〜17:15

#中田　裕之 [1)], 細川　敬祐 [2)], 斎藤　享 [3)], 大塚　雄一 [4)], 冨澤　一郎 [2)]
([1] 千葉大・工,[2] 電通大,[3] 電子航法研,[4] 名大・宇地研

Periodic Oscillations of Doppler Frequency Excited by the Traveling Ionospheric Disturbances Associated with the Tonga Eruption

#Hiroyuki Nakata[1)],Keisuke Hosokawa[2)],Susumu Saito[3)],Yuichi Otsuka[4)],Ichiro Tomizawa[2)]
([1]Graduate School of Engineering, Chiba University,[2]Graduate School of Communication Engineering and Informatics, University of Electro-Communications,[3]Electronic Navigation Research Institute,[4]Institute for Space-Earth Environmental Research, Nagoya University

The enormous eruption of the Hanga Tonga-Hunga Ha'apai volcano on January 15, 2022 caused atmospheric waves with propagating the Earth, inducing ionospheric disturbances across diverse temporal and spatial scales. A High-Frequency Doppler (HFD) sounding system in Japan identified distinctive ionospheric disturbances exhibiting periodic oscillations in the Doppler frequency with an approximate period of 4 minutes. This study investigated these periodic oscillations by comparing them with the observed Total Electron Content (TEC) data from the Global Navigation Satellite System (GNSS). The observed periodic oscillations in Doppler frequency showed distinct S-letter shaped variations, indicating the passage of Traveling Ionospheric Disturbances (TIDs) around the reflection point of the HFD sounding system. These periodic oscillations were prior to the arrival of tropospheric Lamb waves triggered by the Tonga eruption. Analysis of the GNSS TEC data made clear that the TID responsible for the periodic oscillations was stimulated by tropospheric Lamb waves at the conjugate point in the southern hemisphere. Specifically, the electric field perturbations generated by Lamb waves in the southern hemisphere are projected along magnetic field lines to the sensing area of the HFD system in the northern hemisphere. The periodic oscillations were observed only in the path between the Chofu transmitter and the Sarobetsu receiver. This observational results suggests an elongated meridional structure for the TID. The Doppler frequency variations were estimated using a simplified model of TID propagation and the resulting motion of the reflection points. The vertical motion of the reflection point associated with the periodic oscillations was estimated to be approximately 1 km. Periodic fluctuations with a duration of approximately 4 minutes are occasionally observed in conjunction with earthquakes, known to be attributed to the resonance of acoustic mode waves propagating between the ground and the lower ionosphere. Thus, a comparable resonance structure in the southern hemisphere, induced by the passage of tropospheric Lamb waves triggered by the Tonga eruption, emerges as a plausible source of the TID detected in the northern hemisphere.

R005-38
B 会場 ：9/25　PM2 （15:45-18:15）
17:15〜17:30

あらせ衛星と GNSS-TEC データ解析に基づく、2022 年トンガ火山噴火後の赤道プラズマバブルの発生について

#新堀　淳樹 [1)], 惣宇利　卓弥 [2)], 大塚　雄一 [3)], 西岡　未知 [4)],PERWITASARI　SEPTI[4)], 津田　卓雄 [5)], 熊本　篤志 [6)], 土屋　史紀 [7)], 松田　昇也 [8)], 笠原　禎也 [8)], 松岡　彩子 [9)], 中村　紗都子 [1)], 三好　由純 [1)], 篠原　育 [10)]
([1] 名古屋大学宇宙地球環境研究所,[2] 名大　ISEE,[3] 名大・宇地研,[4] 情報通信研究機構,[5] 電通大,[6] 東北大・理・地球物理,[7] 東北大・理・惑星プラズマ大気,[8] 金沢大学,[9] 京都大学,[10] 宇宙研／宇宙機構

Generation of equatorial plasma bubble after the 2022 Tonga volcanic eruption based on the analysis of Arase and GNSS-TEC data

#Atsuki Shinbori[1)],Takuya Sori[2)],Yuichi Otsuka[3)],Michi Nishioka[4)],SEPTI PERWITASARI[4)],Takuo Tsuda[5)],Atsushi Kumamoto[6)],Fuminori Tsuchiya[7)],Shoya Matsuda[8)],Yoshiya Kasahara[8)],Ayako Matsuoka[9)],Satoko Nakamura[1)],Yoshizumi Miyoshi[1)],Iku Shinohara[10)]
([1]Institute for Space-Earth Environmental Research, Nagoya University,[2]Institute for Space-Earth Environmental Research, Nagoya University,[3]Institute for Space-Earth Environmental Research, Nagoya University,[4]National Institute of Information and Communications Technology,[5]University of Electro-Communications,[6]Department of Geophysics, Graduate School of Science, Tohoku University,[7]Planetary Plasma and Atmospheric Research Center, Graduate School of Science, Tohoku University,[8]Kanazawa University,[9]Graduate School of Science, Kyoto University,[10]Japan Aerospace Exploration Agency/Institute of Space and Astronautical Science

Equatorial plasma bubbles (EPBs) are ”holes in the ionosphere” that occur in the equatorial ionosphere, where the electron density drops by two orders of magnitude compared to that in the surrounding area. Because the EPBs have a spatially disturbed electron density structure inside the depressed region, they severely affect satellite positioning and communications. Therefore, predicting and forecasting when and where plasma bubbles occur is one of the important issues in space weather research. On 15 January 2022, the explosive eruption of the undersea volcanic eruption off the coast of Tonga, which is said to occur once every 1,000 years, caused a powerful shock wave and pressure wave all over the world, and the pressure wave generated a high-speed tsunami. Upper atmospheric and ionospheric observations have confirmed that the eruption’s influence penetrated the troposphere and stratosphere to reach the ionosphere at the top of the atmosphere. Further, the eruption caused a plasma bubble in the equatorial ionosphere. In this study, we analyzed Arase and Himawari-8 satellite, ionosonde, and GNSS-TEC observation data to demonstrate that an air pressure wave triggered by the Tonga volcanic eruption could cause the generation of an equatorial plasma bubble. The most prominent observation result shows a sudden increase of electron density and height of the ionosphere several ten minutes to hours before the initial arrival of the air pressure wave in the lower atmosphere. The propagation speed of ionospheric electron density variations was ˜480 – 540 m/s, whose speed was higher than that of a Lamb wave (˜315 m/s) in the troposphere. The electron density variations started larger in the Northern Hemisphere than in the Southern Hemisphere. The fast response of the ionosphere could be caused by an instantaneous transmission of the electric field to the magnetic conjugate ionosphere along the magnetic field lines. After the ionospheric perturbations, electron density depletion appeared in the equatorial and low-latitude ionosphere of the Asia-Pacific region and extended at least up to +/-25^o in geomagnetic latitude. The apex altitude was estimated as 2000 km, corresponding to the lower plasmasphere. Such EPBs have been rarely observed except for a storm-time case. The above results observationally demonstrated the formation process of EPBs through the disturbances in the lower atmosphere, which had little observational support until now. It will greatly help in understanding the factors involved in generating ordinary EPBs. Further, our observational fact suggests that space weather research, focusing on the mechanism and forecast of EPB generated by solar activity, should also include natural phenomena occurring on the Earth’s surface, such as volcanic eruptions, in the research targets.

赤道プラズマバブル（EPB）は、赤道電離圏で発生する「電離層の穴」で、周辺に比べて電子密度が 2 桁ほど低下した構造を持つ。EPB は、その内部に電子密度の不規則構造をもつため、衛星の測位や通信に深刻な影響を与えることが知られている。そのため、プラズマバブルがいつ、どこで発生するかを予測・予報することは、宇宙天気研究の重要な課題の一つとなっている。2022 年 1 月 15 日、1000 年に一度といわれるトンガ沖の海底火山の爆発的噴火は、世界中に強力な衝撃波と圧力波をもたらし、圧力波によって高速伝搬する津波が発生した。この噴火の影響は対流圏、成層圏を超え、大気圏上部の電離圏に到達していることが超高層大気と電離圏観測で確認されている。さらに、この噴火は赤道電離圏にプラズマバブルを発生させた。本研究では、トンガ火山噴火に伴う気圧波が赤道プラズマバブルを発生させることを観測的に実証するために、あらせ衛星とひまわり 8 号機衛星、イオノゾンデ、GNSS-TEC の観測データを解析した。最も重要な結果は、気圧波が下層大気に最初に到達する数 10 分から数時間前に、電子密度と電離圏高度が急激に増加したことである。電離圏の電子密度変動の伝播速度は〜480〜540 m/s で、対流圏のラム波（〜315 m/s）よりも高速であった。その電子密度変動は、南半球よりも北半球で大きく始まる傾向にあった。その電離圏変動の高速応答は、電場が磁力線に沿って磁気共役電離圏に瞬時に伝達されることによって引き起こされたと考えられる。その電離圏擾乱の後、赤道域から

低緯度における電離圏に電子密度の減少がアジア－太平洋域で出現し、少なくとも地磁気緯度± 25° まで緯度方向に拡大していた。その最高高度は 2000km と推定され、プラズマ圏の下部に相当する。このような EPB は、磁気嵐時の事例を除くとほとんど観測されていない。上記の結果は、これまで観測的な裏付けが少なかった下層大気の擾乱を介した EPB の形成過程を、観測的に実証した。これは、通常の EPB の発生要因を解明するにあたり、大きく役立つと考えられる。さらに、今回の観測事実は、太陽活動によって発生する EPB の発生機構や予測に焦点を当てた宇宙天気研究において、火山噴火など地表で発生する自然現象も研究対象に含めるべきことを示唆する。

R005-39
B 会場 ：9/25　PM2 （15:45-18:15）
17:30〜17:45

HF ドップラー観測と GPS 電波掩蔽観測を用いた台風上陸に伴う電離圏擾乱の解析

#榎本　陸登 [1)], 中田　裕之 [2)], 細川　敬祐 [3)], 大矢　浩代 [4)]
[(1] 千葉大,[(2] 千葉大・工,[(3] 電通大,[(4] 千葉大・工・電気

Analysis of Traveling Ionospheric Disturbances associated with typhoons using HF Doppler and GPS radio occultation observations.

#Rikuto Enomoto[1)],Hiroyuki Nakata[2)],Keisuke Hosokawa[3)],Hiroyo Ohya[4)]
[(1]Graduate School of Science and Engineering, Chiba University,[(2]Graduate School of Engineering, Chiba University,[(3]Graduate School of Informatics and Engineering, University of Electro-Communications,[(4]Graduate School of Engineering, Chiba University

HF radio waves are usually reflected in the F region of the ionosphere. The reflection height of the radio waves is determined by ionospheric electron density. HF Doppler (HFD) sounding systems are able to capture the temporal variations of reflected altitudes as Doppler frequency. The temporal resolution of the HFD sounding system is several seconds, which is quite high compared to other ionospheric observation systems. The use of multiple receiving stations makes it possible to observe the distributions and movement of the disturbances in the horizontal direction. GPS radio occultation observation is a method used to investigate altitudinal variations in the ionosphere. This observation can observe the electron density at an altitude of 150-500 km. Because there has been no previous study of the three-dimensional spatial structure of ionospheric disturbances associated with typhoons, the purpose of this study is to analyze the structural characteristics of ionospheric disturbances associated with typhoons using HFD soundings and GPS radio occultation observations.

Typhoon strength is classified according to maximum wind speed by the Japan Meteorological Agency. This study analyzes typhoons with wind speeds of 33 m/s or higher, classified as strong typhoons. To investigate the disturbances by the HFD sounding system operated by the University of Electro-Communications and the other four institutes, the targets are the typhoons that have made landfall in Japan.

As an initial analysis, we analyzed the ionospheric disturbances associated with Typhoon No. 14 (Asian Name: NANMADOL) in 2022. This typhoon formed over the seas south of Japan on September 14, 2022, and made landfall in Kagoshima Prefecture on September 18 with a strong scale. We analyzed the short-wavelength component of the ionospheric disturbances using GPS radio occultation observations. The spectral intensities were compared using wavelets, and an increase in the intensity of the variations at wavelengths from 2 km to 32 km was confirmed on September 18. In the occultation observation at 13:00 UT on September 18, the observation path was quite close to the reflection point of the Onna Observatory of the HFD observation. Therefore, the temporal variation of the time-series data of the Doppler frequency obtained at Onna Observatory, an increase in the intensity with a period of around 10 mHz was observed in approaching the typhoon. Although the peak frequencies of variation intensities are different, it is natural to consider that typhoons cause these disturbances. In the future, we will analyze the spatial structure of the fluctuations and clarify the fluctuations of other target events.

通常 HF 帯電波は，F 領域電離圏で反射するが，その反射高度は電離圏電子密度で決まる。HFD 観測システムでは，反射高度の時間変化をドップラー周波数として捉えることが可能である。時間分解能は数秒程度であり，他の電離圏観測システムよりも高いという特長を持つ。また，複数の受信局を用いることで，平面方向の変動の分布・移動の観測が可能である。電離圏の高度方向の変動を調べるもう一つの観測方法として，GPS 電波掩蔽観測があげられる。この観測は高度 100~500km の領域での電子密度の高度分布を観測可能である。台風に伴う電離圏擾乱の 3 次元空間構造を調べた研究はこれまでにないことから，本研究では，HFD 観測と GPS 電波掩蔽観測を用いて台風に伴う電離圏擾乱の構造の特徴を解析することを目的としている。

気象庁では，台風の強さを最大風速によりランクづけしている。本研究では，強い台風と階級づけられている，風速 33 m/s 以上のものを解析対象としている。また，HFD 観測に見られる変動を調べるため，対象とする台風のうち，日本に上陸したものを扱っていく。

初期解析として， 2022 年台風 14 号（アジア名：NANMADOL）に伴う電離圏変動について解析を行った。この台風は，2022 年 9 月 14 日に日本の南海上で発生し，9 月 18 日に非常に強い勢力で鹿児島県に上陸した。まず、GPS 電波掩蔽観測により台風接近に伴う短波長成分の解析を行った。特に、9 月 18 日に観測された高度方向の電離圏擾乱をウェーブレットにより変動スペクトルを導出し，それらの変動スペクトル強度を比較したところ，波長 2~32 km の変動強度の上昇が確認された。9 月 18 日 13:00 UT の掩蔽観測では，HFD 観測の恩納観測点の反射点とかなり近い経路を通過したため，同時刻の HFD 観測の恩納観測点の時系列データについても解析を行ったところ，台風が接近する以前と比較して周期 10 mHz 前後の変動の振幅の上昇が観測された。それぞれの変動強度のピークは異なるものの，それぞれの変動強度の上昇が観測され，いずれも台風による変動であると考えられる。今後は，変動の空間構造についても解析を進め，他の対象イベントにおいても変動の様子を明らかにしていく予定である。

R005-40
B 会場 ：9/25　PM2 （15:45-18:15）
17:45〜18:00

HF ドップラー観測を用いた異なる経路に沿って伝搬した地震に伴う電離圏擾乱の解析

#清水　紘平 [1)], 中田　裕之 [1)], 細川　敬祐 [2)], 大矢　浩代 [1)]
([1] 千葉大,[2] 電通大

Analysis of ionospheric disturbances propagating along different paths due to earthquakes using HF Doppler observations

#Kohei Shimizu[1)],Hiroyuki Nakata[1)],Keisuke Hosokawa[2)],Hiroyo Ohya[1)]
([1]Graduate School of Science and Engineering, Chiba University,[2]Graduate School of Communication Engineering and Informatics, University of Electro-Communications

It is known that large-scale natural disasters such as earthquakes, tsunamis, and volcanic eruptions generate atmospheric waves, which cause ionospheric disturbances. The generation mechanisms of coseismic ionospheric disturbances can be classified into the following two categories.

(a) Rayleigh waves propagating on the earth's surface from the epicenter excite acoustic waves that reach the ionosphere
(b) Acoustic waves generated by ground motions at the epicenter reach the ionosphere directly

Although the characteristics of propagation along paths (a) and (b) have been analyzed in the previous studies, there are few studies that analyzed both types of disturbances generated by the an earthquake with an observation system. Therefore, the purpose of this study is to identify disturbances propagating along paths (a) and (b) using an HF Doppler (HFD) observation system, and to clarify the frequency characteristics of them.

HFD observation can observe the vertical motions of the ionosphere at the midpoint of transmitter and receives of radio waves at frequencies.

The observation system used in this study is conducted by the University of Electro-Communications and four other institutions. The transmitter is located at the Chofu campus of the University of Electro-Communications, and receivers used in this study are located at Iitate, Kakioka, and Oarai.

Propagation times of the acoustic waves along paths (a) and (b) were calculated and compared with HFD data. The propagation time along path (a) was calculated as the sum of the arrival time of the seismic wave just below the reflection point and the propagation time of the acoustic waves from the ground to the reflection points. The arrival time of seismic waves was determined using seismic data from F-net, a broadband seismic observation network operated by the National Research Institute for Earth Science and Disaster Prevention. The NRLMSISE-00 standard atmospheric model was used to obtain the vertical profiles of atmospheric temperature to calculate the acoustic wave propagation time. The propagation time along path (b) was calculated by ray tracing for the acoustic waves to reach each HFD reflection point.

In this study, frequency analysis data of HFD observation data and HFD waveform data were obtained for the Iwate Nairiku earthquake at 8:43 (JST) on June 14, 2008, the Sanriku-oki earthquake at 11:45 (JST) on March 9, 2011 and Hamadori earthquake at 17:16 (JST) on April 11, 2011.

In these data, there are two types of variations propagating along path (a) and path (b).The intensity of the disturbances was dominant in different frequency bands for the former and the latter, with the former being dominant in the broad frequency band from 20-60 mHz and the latter being dominant in the low frequency band below 20 mHz and in the high frequency band above 40 mHz.

In this study, the neutral air particle velocity along paths (a) and (b) is calculated from the Doppler frequency.

Assuming that the observed Doppler frequency is caused by acoustic waves propagating in the vertical direction or from the epicenter to the observation point, the neutral air particle velocity along paths (a) and (b) can be estimated by converting the plasma vertical velocity into the neutral air particle velocity.

Comparison of the neutral air particle velocities at the reflection heights of 5 MHz and 8 MHz radio waves at Iitate during the Sanriku-oki earthquake shows that the velocities for 8 MHz are smaller than those for 5 MHz. This result may be attributed to the attenuation of acoustic waves by the atmosphere. ☒ We will continue to analyze the characteristics of the vertically propagating acoustic waves excited by Rayleigh waves and the obliquely propagating acoustic waves generated by the ground motion at the epicenter by making comparisons for other events and observation points.

先行研究から、地震や津波、火山噴火などの大規模な自然災害により大気波動が生じ、電離圏擾乱が引き起こされることが知られている。その中でも、地震に伴う電離圏擾乱の発生メカニズムは大きく以下の 2 つに分類される。

(a) 震源遠方へ地表面を伝搬したレイリー波により励起された音波が直上の電離圏に到達する。
(b) 震央での地面動により生成された音波が直接電離圏に到達する。

これまでに (a)、(b) それぞれの経路に沿った伝搬特性について解析されてきたが、同一の地震から発生した両方の変動を同一の観測システムにて解析しているものは少なく、両者の違いについての解析は進んでいない。そこで、本研究では HF ドップラー (HFD) 観測システムを用いて、経路 (a)、(b) を伝搬した擾乱を識別し、それぞれの伝搬特性を明らかにすることを目的とする。

HFD 観測は電波が電離圏で反射する際にドップラー効果により生じる送受信周波数の差から電波の送受信点の中点における電離圏の上下動を観測するシステムであり、送信周波数によって反射される高度は異なる。本研究で用いる観測システムは電気通信大学他 4 機関で運用されており、最大 4 周波数の電波を受信可能である。本研究で用いた電波の送信局は電気通信大学調布キャンパスであり、受信局は飯舘、柿岡及び大洗を用いた。
また、本研究では経路 (a)、(b) それぞれでの伝搬時間を計算し、HFD データとの比較を行った。経路 (a) での伝搬時間は HFD 観測点直下に地震波が到達した時間と音波が HFD 反射高度まで伝搬する時間の合計として算出した。この際、地震波到達時間の同定には防災科学技術研究所が運用している広帯域地震観測網 F-net のデータを使用し、各 HFD 反射点に最も近い地震計に地震波が到達した時間をもとに HFD 観測点直下に地震波が到達した時間を決定した。また、音波伝搬時間の計算に必要となる高度別の大気温度パラメータの取得には NRLMSISE-00 標準大気モデルを用いた。経路 (b) での伝搬時間は、震央を波動源とし、音波が各 HFD 反射点まで到達する時間をレイトレーシングで算出した。

本研究では 2008 年 6 月 14 日 8:43 (JST) 発生の岩手内陸地震、2011 年 3 月 9 日 11:45 (JST) 発生の三陸沖地震、2011 年 4 月 11 日 17:16 (JST) 発生の浜通り地震について HFD 観測データと HFD 波形データの周波数解析データを得た。これらのデータでは、経路 (a) に沿って HFD 観測点まで伝搬した変動到達時間付近と経路 (b) に沿って HFD 観測点まで伝搬した変動到達時間付近にそれぞれ対応した変動が見られており、それぞれ経路 (a) に沿って伝搬した変動と経路 (b) に沿って伝搬した変動と考えられる。また、前者と後者では異なる周波数帯で変動強度が卓越しており、前者では 20-60 mHz での幅広い周波数帯での卓越が、後者では 20 mHz 以下の低周波数帯と 40 mHz 以上の高周波数帯での卓越が見られた。
したがって、これらの地震の HFD 観測ではレイリー波に励起された音波による擾乱と震源からの直接波による擾乱の両方が観測され、前者と後者では異なる周波数帯成分の卓越が見られるという結果が得られた。

また、本研究では経路 (a),(b) に沿って伝搬した音波に起因する中性粒子速度をドップラー効果による送信周波数と受信周波数のずれ (ドップラー周波数) から計算した。
ドップラー周波数はプラズマの移流と圧縮の影響を含んでいるため、移流と圧縮それぞれによる影響の割合を考慮することでプラズマの鉛直方向速度を計算できる。観測されたドップラー周波数を鉛直方向または震源から観測点に向かう方向に伝搬する音波によるものであると仮定し、プラズマ鉛直方向速度を中性粒子速度に換算することで経路 (a),(b) に沿った中性粒子速度を推定できる。
三陸沖地震時の飯舘における 5 MHz と 8 MHz 電波の反射高度での中性粒子速度を比較したところ、経路 (a),(b) の両方に関して 5 MHz よりも 8 MHz 高度における速度の方が小さいという結果が得られた。この結果は大気による音波の減衰に起因するものであると考えられる。☒今後他のイベント、観測点についても同様の比較を行い、レイリー波によって励起された鉛直方向に伝搬する音波と震央での地面動により生成された斜め方向に伝搬する音波の特性について解析を進めていく。

R005-P01
ポスター 3 ：9/26　AM1/AM2 （9:00-12:30）

南極・昭和基地における NO 分子の観測および NO 柱密度変動と高エネルギー電子の降り込みとの関係

#後藤　宏文 [1)], 水野　亮 [1)], 中島　拓 [1)], 長濱　智生 [1)]
(1 名大・宇地研

A study on the relationship between NO column density and high-energy electrons based on the mm-wave observation at Syowa station

#Hirofumi Goto[1)],Akira Mizuno[1)],Taku Nakajima[1)],Tomoo Nagahama[1)]
(1Institute for Space-Earth Environment Research, Nagoya University

We have carried out millimeter-wave spectroscopic observation of minor constituents in the middle atmosphere, such as nitric oxide (NO) and ozone, at Syowa Station (69.00^o S, 39.85^o E) in Antarctica since 2012 and at Tromsoe, Norway (69.35^o N, 19.14^o E) in the Arctic since 2016 to study the effects of energetic particle precipitation into the polar regions induced by the solar activity. We presented the results of short-term test observation of NO at Tromsoe, Norway, over 75 days from December 26, 2018, to March 10, 2019 (Goto et al., SGEPSS 2021). In this report, we will present the results of the analysis of the NO observation data over 10 days from March 22, 2023, to March 31, 2023, obtained by the multi-frequency millimeter-wave spectrometer (Mizuno et al., SGEPSS 2023), which started routine observations at Syowa in July 2022. Correlation studies between the NO column density, proxies of geomagnetic activities, and energetic particle precipitations were performed using the same analysis method applied to the Tromsoe data.

The FFT spectrometer used in this observation has a bandwidth of 2.5 GHz, which is 2.5 times broader than that of the spectrometer used in the Tromsoe observation, making it possible to simultaneously observe the spectra of six hyperfine structure lines of NO at relatively nearby frequencies. Averaging the column densities derived from these hyperfine structure lines is expected to improve the accuracy of determining column densities. Therefore, we derived NO column density at Syowa using 12-hour integrated six spectra at 250.796436 GHz, 250.436848 GHz, 250.440659 GHz, 250.448530 GHz, 250.815594 GHz, and 250.816954 GHz. As at Tromsoe, the atmospheric temperature in the region where NO is present was assumed to be a constant 200 K, and the NO emission lines were assumed to be optically thin. The average error in the column density this time was 0.73 times that at Tromsoe, which means that the error in the column density could be reduced while shortening the integration time, i.e., time resolution.

For the data analysis period, the Dst index decreased drastically from March 23 to March 24, 2023, peaking at about -150 nT. During the period, NO column density increased to $6.5*10^{14}$ cm^{-2} on March 24 and remained nearly constant before increasing further at the end of March 25 to a peak of about $1.2*10^{15}$ cm^{-2}. After that, it decreased to about the same level as on March 24 and remained almost constant until March 28. This suggests that NO may have increased due to electrons accelerated by the geomagnetic disturbance. Therefore, we compared NO column density with the electron flux data obtained by the MEPED 0^o telescope in the five POES/METOP satellites. For the comparison, we used the L-value and MLT of the satellite observations to select the electron flux data that were most likely to precipitate onto Syowa. As a result, it was found that the NO column density increased on March 24 and at the end of March 25 after the increase in electron flux observed by the satellites on March 23 and March 25, respectively. On the other hand, a more significant increase in electron flux was also observed on March 22, but there was no significant corresponding increase in NO column density. We will discuss the cause of the increase by referring to other observation data and report the correlation between the NO column density and energetic electrons.

太陽活動に伴って極域に降り込む高エネルギー粒子が NOx(窒素酸化物) やオゾンなどの中層大気中の微量分子に及ぼす影響を観測的に調べるため、我々は 2012 年から南極・昭和基地 (69.00° S, 39.85° E)、2016 年から北極域のノルウェー・トロムソ (69.35° N, 19.14° E) でミリ波分光観測を行っている。これまでに、トロムソについては 2018 年 12 月 26 日から 2019 年 3 月 10 日までの 75 日間にわたって実施した NO のテスト観測の結果を 2021 年の SGEPSS 講演会で報告した (後藤他、2021 年講演会参照)。今回は、昭和基地で 2022 年 7 月から定常観測を開始した多周波数ミリ波分光計（詳細は水野他、本年講演会参照）を用いて得られた NO の観測データの中から、2023 年 3 月 22 日から 31 日までの 10 日間にわたってトロムソで行ったのと同様の方法で解析を行い、NO 柱密度、Dst 指数、電子フラックスの時間変化を比較した。

今回の観測に用いた多周波数ミリ波分光計の FFT 分光計帯域は 2.5 GHz であり、トロムソでの観測で用いた分光計と比べ 2.5 倍の帯域を持つため、比較的近傍の周波数にある NO の 6 本の超微細構造線のスペクトルを同時観測することが可能となった。これらの超微細構造線から導出される柱密度を平均することで柱密度の決定精度が向上することが期待できる。今回の昭和基地での解析においては、250.796436 GHz、250.436848 GHz、250.440659 GHz、250.448530 GHz、250.815594 GHz、250.816954 GHz の 6 本に増やし、積分時間は 12 時間と短くした。NO が存在する領域の大気温度は一様に 200 K で、NO 輝線は光学的に薄いと仮定した。今回の柱密度の誤差の平均はトロムソでの観測の 0.73 倍となり、時間分解能を小さくしながら柱密度の誤差を小さくすることができた。

解析を行った期間には、Dst 指数が 3 月 23 日から 3 月 24 日にかけて急激に減少し、ピークは約-150 nT に達した。このとき、NO 柱密度は 3 月 24 日に $6.5*10^{14}$ cm^{-2} まで増加し、ほぼ一定の状態となってから 3 月 25 日にさらに増加し、ピークは約 $1.2*10^{15}$ cm^{-2} に達した。その後は 3 月 24 日とほぼ同じ値まで減少し、3 月 28 日までほぼ一定となった。以上より、磁場の擾乱により加速された電子により NO が増加した可能性が考えられる。そこで、5 機の POES/METOP 衛星に搭載された MEPED 検出器 0 度望遠鏡で得られた電子フラックスのデータと比較した。比較に当たっては、L 値および MLT の値で条件を与え、昭和基地に降り込んでくる可能性の高い電子フラックスデータを選定した。その結果、3 月 24 日と 3 月 25 日末の NO の柱密度の増加に対応する電子フラックスの増加がそれぞれ 3 月 23 日と 3 月 25 日に確認された。その一方、3 月 22 日にもそれらよりも大きい電子フラックスの増加が見られたが、NO の柱密度には対応する顕著な増加は見られなかった。今後、他の観測データも参照しその原因の考察を進め、NO 柱密度と高エネルギー電子の降り込みとの関係についてまとめて報告する予定である。

R005-P02
ポスター 3 ：9/26　AM1/AM2 （9:00-12:30）

ノルウェー・トロムソーのファブリ・ペロー干渉計で 2023 年 3 月 24 日に観測された 427.8nm 窒素分子イオンオーロラを通したイオンアップフローの分光計測

#菊池　大希 [1)], 塩川　和夫 [2)], 大山　伸一郎 [1)], 小川　泰信 [3)], 栗原　純一 [4)]
[(1] 名大 ISEE,[(2] 名大宇地研,[(3] 極地研,[(4] 情報大

Spectroscopic measurement of 427.8-nm aurora using a Fabry-Perot interferometer at Tromsoe, Norway on March 24, 2023

#Taiki Kikuchi[1)],Kazuo Shiokawa[2)],Shin ichiro Oyama[1)],Yasunobu Ogawa[3)],Junichi Kurihara[4)]
[(1]Institute for Space-Earth Environmental Research, Nagoya University,[(2]Institute for Space-Earth Environmental Research, Nagoya University,[(3]National Institute of Polar Research,[(4]Hokkaido Information Univeristy

Several satellite missions have reported the existence of ions that originated from Earth. Before OGO6 discover an abrupt enhancement of the N_2^+ density in the high latitude region during magnetic storms (Taylor et al., 1975), N_2^+ had been considered not to exist in high altitude regions due to its short lifetime. The OGO6 observation suggested that they are transported to high altitudes from Earth. Blue sunlit aurora seen before dawn has been considered as a consequence of the N_2^+ upflow. The wavelength of N_2^+ auroral emission observed from the ground becomes longer due to the Doppler shift when N_2^+ is moving upward. Fabry-Perot interferometer (FPI) can measure the velocity of ions from the amount of the Doppler shift. FPI observations of the 427.8 nm aurora have not been made due to its band structure. However, the establishment of this method makes it possible to observe N_2^+ upflow in the low-altitude ionosphere during aurora appearance. We observed the auroral 427.8 nm emission by FPI at Tromsoe, Norway, in winter of 2022-2023. The one-day average of N_2^+ upflow velocity from FPI observations was 202 m/s on March 24, 2023 (min Dst = -163 nT), while the temporal variation of the velocity suggests significant ambiguities of the measurements. We evaluate the reliability of these velocity measurements through model calculations of interference fringes considering the random noise and band emissions at multiple wavelengths of the 1st Negative Band of N_2^+.

地球の周辺の宇宙空間では 1960 年代から数々の人工衛星ミッションにより、磁気圏中で電離圏由来のイオンが観測されている。一方で、地球大気に大量に存在する窒素分子のイオンである N_2^+ はその存続時間が短いことから、高高度ではあまり見られないと考えられていた。しかし OGO6 衛星が磁気嵐時に電離圏高高度の領域で N_2^+ の分子イオン密度の急激な上昇を発見し (Taylor et al., 1975)、N_2^+ も高高度に輸送されている可能性が示唆された。

N_2^+ の上昇流により引き起こされている現象として、N_2^+ による太陽光の共鳴散乱による明け方の青いオーロラが挙げられる (Shiokawa et al., 2019)。共鳴散乱とは、N_2^+ 中の電子が太陽光によって励起され、その後、基底状態に戻るときにそのエネルギーを光として放出する現象である。N_2^+ が上昇しているとき、波長を地上から観測するとドップラー効果により長くなる。ファブリ・ペロー干渉計（FPI）はドップラー効果で変化した波長からイオンの運動速度を測定することができる。波長 427.8 nm のオーロラ発光はバンド構造を持っているため、これまで FPI 観測が行われてこなかった。一方で、この観測法が成功すれば、低中高度電離圏の N_2^+ の運動をオーロラ発生時に観測できるようになる。私たちは、2022-2023 年の冬、ノルウェーのトロムソで FPI を用いて波長 427.8 nm のオーロラを観測した。とりわけオーロラ活動が活発で共鳴散乱によるオーロラが観測された 2023 年 3 月 24 日 (min Dst = -163 nT)、 FPI による観測から窒素分子イオンの磁力線上向き方向の運動速度の一晩の平均は 202 m/s と算出されたが、各時刻に求められた風速は大きなばらつきを示した。本講演では、理論的に求められるフリンジに対する風速決定のモデル計算を通して、ランダムノイズの影響、N_2^+ の 1st Negative Band の複数波長の影響、という 2 つの観点からこの風速計測の誤差の評価を行った結果を報告する。

R005-P03
ポスター 3 ：9/26　AM1/AM2 （9:00-12:30）

Na ライダーの昼間観測に用いる Faraday filter の透過率詳細測定

#川原　琢也 [1)], 野澤　悟徳 [2)], 斎藤　徳人 [3)], 津田　卓雄 [4)], 高橋　透 [5)], 川端　哲也 [2)], 和田　智之 [3)], 小林　啓悟 [1)], 野村　俊介 [1)]
([1] 信州大・工,[2] 名大・宇地研,[3] 理化学研究所,[4] 電通大,[5] 電子航法研

Spatial transmission pattern measurements of a Faraday filter for Na lidar daytime observations

#Takuya Kawahara[1)],Satonori Nozawa[2)],Satonori Nozawa[3)],Takuo Tsuda[4)],Toru Takahashi[5)],Tetsuya Kawabata[2)],Satoshi Wada[3)],Keigo Kobayashi[1)],Shunsuke Nomura[1)]
([1]Faculty of Engineering, Shinshu University,[2]Institute for Space-Earth Environment Research, Nagoya University,[3]RIKEN Center for Advanced Photonics, RIKEN,[4]University of Electro-Communications,[5]ENRI

A Na lidar at Tromsoe is upgrading the receiver system for the thin Na atom observations in the lower thermosphere (<200km). The Na atom density at this altitude region is expected to be only ˜2-3 atoms/cm3 compared with ˜2,000 atoms/cm3 at the Na layer peak (˜90 km). To achieve the high S/N ratio measurement, even at nighttime, an ultra-narrowband optical filter, such as a Faraday filter, is necessary to reject the background skylight. The Faraday filter comprises a heated Na cell in a strong magnetic field (i.e., ˜200 mT) between two polarizers. The Faraday rotation and the Zeeman effect can achieve ultra-narrow optical bandpass (˜10 GHz or ˜0.01nm at 589 nm).

We assembled a transmission diagnosis system at 589 nm wavelength based on two narrowband DFB lasers (1064 nm and 1319 nm) at the RIKEN facility. We conducted the transmission profile measurements of the Faraday filter by changing the optical pass in the filter.

In this talk, we discuss the results of the transmission measurements and the filter's performances. We present a newly developed Na cell.

R005-P04
ポスター 3 ：9/26　AM1/AM2 （9:00-12:30）

電離圏中性大気観測に向けた中性質量分析器の開発

#米田　匡宏 [1)], 齊藤　昭則 [1)], 齋藤　義文 [2)]
([1] 京都大学大学院理学研究科,[2] 宇宙科学研究所

Development of a Neutral Mass Spectrometer for the Observation of the Ionospheric Atmosphere

#Masahiro Yoneda[1)],Akinori Saito[1)],Yoshifumi Saito[2)]
([1]Graduate School of Science, Kyoto University,[2]ISAS, JAXA

The ionospheric neutral atmosphere affects ionospheric currents through the collisions between plasmas, which makes it necessary to observe the neutral atmospheric density and composition to understand the ionospheric plasma phenomena. However, neutral mass spectrometers for the in-situ measurements of the ionospheric neutral atmosphere have rarely been installed on flying objects such as sounding rockets and low-earth orbit satellites in recent observations because they tend to be big and heavy. Some empirical models are used instead of actual observation data, but they refer to the old and limited observation data, and new observations are desired.

In our study, we are developing a small mass spectrometer for the observation of the ionospheric neutral atmosphere which can easily be installed on flying objects. The instrument is planned to be used for S-310-46 sounding rocket, which will be launched from Uchinoura, Kagoshima in the summer of 2024. The objective of the experiment is to reveal the formation process of daytime sporadic E layers and the instrument will provide the density profile of dominant components in the atmosphere such as O, O_2 and N_2 from about 90 km to 130 km. We are currently developing the flight model of the instrument for the experiment.

The mass spectrometer is based on TRITON, which is a time-of-flight neutral mass spectrometer developed by ISAS/JAXA for the Lunar Polar Exploration project (LUPEX) to measure water particles in lunar soil. In usual time-of-flight neutral mass spectrometers, particles are reflected one time, but TRITON and our instrument adopt the trajectory including three reflections, which enables a high mass resolution with a small size. We have finished designing and manufacturing the mass-analyzing part, and we will report the results of the tests.

At the same time, we are developing an inlet part called an antechamber. An antechamber is necessary to thermalize the particles which enter the instrument with the relative speed of the rocket. Furthermore, an antechamber can improve sensitivity because the inside density is enhanced compared to the outside density. We have finished designing considering these functions. In the rocket experiment, the measurement starts a few minutes after the launch and the contamination of the particles adsorbed on the inner wall of the antechamber can be a problem. In order to reduce the impact of the contamination, we plan to conduct baking with some heaters and nitrogen purge just before the launch. We will additionally report the results of some experiments which we made to evaluate the effect of these operations.

電離圏における中性大気はプラズマとの衝突を通して電離圏電流に影響を与えるため、中性大気密度や組成を観測することは電離圏プラズマ現象を捉える上で不可欠である。しかし、電離圏高度の中性大気をその場観測するための中性質量分析器は大型となる傾向にあり、近年では観測ロケットや低軌道衛星などの飛翔体に搭載されることは稀となっている。一方で、実際の観測データの代わりに用いられている経験モデルは主に古く限定された観測データを参照しており、新たな観測を行うことが望まれている。

そこで、本研究では飛翔体に手軽に搭載することができる小型の中性大気質量分析器の開発を進めている。開発中の装置は 2024 年夏に鹿児島県内之浦より打ち上げられる観測ロケット S-310-46 号機に搭載される予定である。当実験は昼間スポラディック E 層の生成過程の解明を目的としており、本装置は高度約 90km から 130km までの中性大気の主要成分である O や O_2、N_2 等の密度の高度プロファイルを得る。現在はロケット搭載用装置のフライトモデルを開発中である。

本装置は月極域探査ミッション LUPEX において地質中の水を探査することを目的として、宇宙科学研究所にて開発されている飛行時間型中性質量分析器 TRITON を基にしている。通常の飛行時間型質量分析器では粒子を一回反射させる経路が一般的であるが、本装置では三回反射させる経路を取り入れることで、小型ながらも高い分解能を実現している。質量分析部の設計、製造は終了しており、本発表では質量分析部試験の結果を報告する。

質量分析部と並行して、粒子を取り入れるための前室部と呼ばれる部分の開発も行っている。前室部は装置に対して飛翔体の速さの相対速度で入射してくる粒子を熱速度程度まで減速させるために必要となる。さらに、前室部内の密度は外部の密度より高まるため、感度が向上する。これらの機能を考慮して、前室部の形状設計を行った。また、ロケット観測においては打ち上げから数分で観測を開始するため、前室部内部に吸着した粒子の混入が問題となると考えられる。この影響を抑えるために、打ち上げ前にはヒーターによるベイキングや窒素パージを行う予定である。これらの効果を評価するための実験も行っており、併せて結果を報告する。

R005-P05
ポスター 3 ：9/26　AM1/AM2 （9:00-12:30）

ELF 電磁波観測によるスプライトがグローバルサーキットに与える影響に関する研究

#古谷　享一 [1)], 吉川　顕正 [2)], 池田　昭大 [3)]
([1] 九大,[2] 九大/理学研究院,[3] 鹿児島高専

A study on the impact of Sprites on the Global Electrical Circuit by ELF electromagnetic wave observation

#Uichi Furutani[1)],Akimasa Yoshikawa[2)],Akihiro Ikeda[3)]
([1]Kyushu University,[2]Department of Earth and Planetary Sciences, Kyushu University,[3]Kagoshima National College of Technology

ELF electromagnetic field data show instantaneously excited phenomena called ELF transients. Previous studies have suggested that ELF transients are closely related to sprite generation. However, further research is needed on its detailed relationship. In addition, it has been pointed out that sprites may contribute to the electrical coupling between the mesosphere and the ionosphere in the Global Electrical Circuit. It is important to understand sprites in considering realistic models of the Global Electrical Circuit. In this study, we analyzed magnetic field data of induction magnetometers during sprite generation to clarify the relationship between sprites and ELF transients and their role in the Global Electrical Circuit. As a result, ELF transients were observed in most sprites, but some were not observed. In this presentation, we will discuss the reasons why ELF transients associated with sprites are not always observed from two aspects: lightning discharges that cause sprites and the Global Electrical Circuits.

ELF 電磁場データには ELF トランジェントと呼ばれる瞬間的な現象が見られる。これまでの先行研究において ELF トランジェントはスプライトの発生に深く関連していることが示唆された。しかしながら、その詳細な関係性については更なる研究が必要である。また、地球規模の電流回路であるグローバルサーキットにおいて、スプライトが中間圏-電離圏間の電気的結合に貢献している可能性が指摘されており、その現実的なモデルを考えるうえでもスプライトを理解することが重要視されている。そこで本研究では、スプライトと ELF トランジェントの関係及びグローバルサーキットにおいて担う役割を明らかにすべく、スプライト発生時の誘導磁力計磁場データを分析した。その結果、ほとんどのスプライトで ELF トランジェントが観測されたが、一部観測されない例もあった。本発表では、スプライトに伴う ELF トランジェントが観測されない要因としてどのようなものがあるのか、スプライトを誘起させる雷放電とグローバルサーキットの二つの側面から議論する。

R005-P06
ポスター 3 ：9/26　AM1/AM2 （9:00-12:30）

冬季成層圏と夏季中間圏の半球間結合

#足立　拓馬 [1)], 三好　勉信 [1)]
([1] 九大・理・地球惑星

Interhemispheric coupling between winter stratosphere and summer mesosphere

#Takuma Adachi[1)],Yasunobu Miyoshi[1)]
([1]Dept. Earth & Planetary Sci, Kyushu Univ

Observations show that the temperature in the summer polar mesosphere are closely related with the temperature in the polar stratosphere. This phenomenon is called interhemispheric coupling, and its mechanism remains unclear. In this study, we examine the 6-year period from 2016 to 2022 using an atmosphere-ionosphere coupled model (GAIA model) (horizontal grid point count 128∗64, vertical resolution 150 layers). Detailed analysis was conducted for 2019 and 2020, when the SSW occurred in midwinter. Changes in the temperature, zonal and meridional winds, and vertical wind in the summer mesosphere during the SSW were studied. Our result indicates that the impact of the SSW on the summer mesospheric circulation has interannual variability. Furthermore, by comparing the present result with the observation by the Himawari satellite, we will discuss the interhemispheric coupling process during SSWs.

極中間圏雲などの観測から成層圏突然昇温（Stratospheric Sudden Warming：SSW）発生時に、夏季極域中間圏の温度が上昇するという観測結果が得られ、夏季中間圏高緯度域と冬季成層圏高緯度域の気温が関連していることが明らかになりつつある。この現象は、半球間結合と呼ばれ、そのメカニズムについては未だ仮説のままである。本研究では、全大気圏ー電離圏結合モデル（GAIA モデル）（水平格子点数 128 × 64、鉛直解像度 150 層）を用いて、2016 年〜2022 年の 6 年間を調べた。将来的に観測データと比較するためにこの 6 年間を用いた。本研究では、12 月終わりから 1 月に発生した SSW の影響について 2018 年 12 月〜2019 年 2 月、2020 年 12 月〜2021 年 2 月の二つの期間に絞って解析を進めた。二つの期間の温度、東西風、南北風、鉛直流をそれぞれ 6 年平均から引いて、変化を調べたところ、先行研究と同じような結果を得られた一方で、高度の面などの差異が見られ、年により SSW の中間圏への影響が異なる可能性が明らかとなった。そこで、本研究では、年による SSW の影響の違いについて、夏季中間圏循環がどのような影響を受けているかについて、子午面循環や波強制の変化に焦点を当てて解析を実施した。さらに、気象衛星ひまわりの観測データとも比較・検討することで結合メカニズムへの議論を深めていきたい。

R005-P07
ポスター 3 ：9/26　AM1/AM2 （9:00-12:30）

#津田　敏隆 [1)],Noersomadi Adi[2)],Nani Cholianawati[2)]
([1 京大・生存研,([2 インドネシア国立研究革新庁

A Relation between bending angle gradient of GNSS RO and refractive index gradient

#Toshitaka Tsuda[1)],Adi Noersomadi[2)],Cholianawati Nani[2)]
([1Research Institute for Sustainable Humanosphere, Kyoto University,([2National Research and Innovation Agency（BRIN)

This study is concerned with the bending angle of microwave, passing through the Earth's atmosphere in the GNSS radio occultation (RO) experiment. We focus on a relation between the height derivative of the bending angle with the refractive index gradient.

A refractive index model for a dry atmosphere is constructed at 0-110 km, employing a temperature profile published by NOAA. We assume concentric atmospheric layers with a height interval of 100 m, which are horizontally uniform. Using the Abel inversion, a bending angle profile is computed. We found that the bending angle is mostly contributed by the layers near the tangent height; 1/3, 1/2 and 4/5 of the bending angle is attributed to the height range about 1 km, 2 km and 7 km above the tangent point, respectively.

We developed a simple ray tracing model, where the bending is approximated by a circle within every atmospheric layers with a thickness of 100 m. Curvature of the ray is calculated, referring to the general relation between the impact parameter and the refractive index gradient (Lehn, 1985). By connecting partial pay paths at interface of the spheres, a smooth ray path is constructed for the tangent height ranging from 100 m above the ground up to 70 km altitude every 100 m. The ray tracing model is consistent with the Abel inversion result less than 1% of discrepancy, except below about 5 km altitude.

We found the refractive index gradient at the tangent altitude correlates reasonably well with the height derivative of the bending angle. Because the refractive index gradient in a dry atmosphere is mostly determined by the Brunt-Vaisala frequency squared, height derivative of the bending angle can be utilized as a measure of atmospheric stability.

In the retrieval procedure of GNSS-RO, observed bending angle is optimized by combining a model atmosphere at high altitudes for suppressing the effects of ionospheric noises, resulting in a possibility to induce artificial modification of the bending angle profile. This study suggests that the original bending angle without optimization is useful for detecting atmospheric thermal structure. We further apply this method to identify characteristics of the tropopause and stratopause using recent GNSS-RO data.

R005-P08
ポスター 3 ：9/26　AM1/AM2 （9:00-12:30）

#津田　卓雄 [1)], 安藤　芳晃 [1)], 中川　広務 [2)],Ward　William[3)], 堤　雅基 [4,5)], 穂積　裕太 [6,7)], 細川　敬祐 [1)], 村田　健史 [8)]
([1] 電通大,[2] 東北大,[3]University of New Brunswick（UNB),[4] 極地研,[5] 総研大,[6]National Aeronautics and Space Administration（NASA),[7]Catholic University of America（CUA),[8] 情報通信研究機構

Temperature retrieval in the middle atmosphere using Himawari-8/AHI limb-sounding data

#Takuo Tsuda[1)],Yoshiaki Ando[1)],Hiromu Nakagawa[2)],William Ward[3)],Masaki Tsutsumi[4,5)],Yuta Hozumi[6,7)],Keisuke Hosokawa[1)],Ken Murata[8)]
([1]University of Electro-Communications（UEC),[2]Tohoku University,[3]University of New Brunswick（UNB),[4]National Institute of Polar Research（NIPR),[5]Graduate University for Advanced Studies（SOKENDAI),[6]National Aeronautics and Space Administration（NASA),[7]Catholic University of America（CUA),[8]National Institute of Information and Communications Technology（NICT)

Himawari-8 is the Japanese Geostationary Earth Orbit (GEO) meteorological satellite, that is equipped with Advanced Himawari Imager (AHI). Himawari-8/AHI provides full disk images every 10 min in 16 observation bands, including three visible bands: blue (0.47 μ m), green (0.51 μ m), and red (0.64 μ m). These full disk images are normally used as nadir observations mainly for meteorological purposes. On the other hand, the full disk images by Himawari-8/AHI can also provide limb-sounding data utilizing the edges of images with near-global coverage. As an example, there are a couple of reports on polar mesospheric cloud (PMC) observations by Himawari-8/AHI limb-sounding.

In the present work, we consider temperature retrieval in the middle atmosphere as a further application using Himawari-8/AHI limb-sounding data. In the limb-sounding, Rayleigh scattering of the sunlight can be observed, and thus we can obtain height profiles of line-of-sight (LOS) integrated Rayleigh scattering signals. By inversion methods, such as the Abel transforms, the onion peeling, etc., the LOS-integrated signals can be converted into local signals, which could be considered to be proportional to the local number densities of the atmospheric molecules. Then, applying the Rayleigh scattering temperature lidar technique, height profiles of temperature can be derived from height profiles of the local signals under an assumption of the hydrostatic equilibrium. There are a couple of previous works demonstrating this kind of temperature retrieval method using limb-sounding data from low-Earth-orbit (LEO) satellites. On the other hand, there is no previous example of GEO satellites, which have an advantage in providing continuous observations from a fixed point in space. In the presentation, we will show our initial data analysis for temperature retrieval in the middle atmosphere using Himawari-8/AHI limb-sounding data, and discuss the potential of the retrieved temperature data.

R005-P09
ポスター 3 ：9/26　AM1/AM2 （9:00-12:30）

後期重爆撃期の天体衝突による地球大気の流体力学的大気散逸数値モデルの開発

#名和　樹生 [1)], 木村　智樹 [1)], 吉田　辰哉 [2)], 寺田　直樹 [2)]
([1] 東京理科大,[2] 東北大・理・地球物理

Development of a numerical model for atmospheric hydrodynamic escape in early Earth driven by celestial impacts

#Tatsuki Nawa[1)],Tomoki Kimura[1)],Tatsuya Yoshida[2)],Naoki Terada[2)]
([1]Tokyo University of Science,[2]Department of Geophysics, Graduate School of Science, Tohoku Universit

The primordial atmosphere of early Earth was likely formed from hydrogen-based solar nebula gas and water vapor and carbon dioxide ejected from the Earth's interior by celestial collisions and other events. The atmospheric gases were lost by hydrodynamic escape from the early Earth (Yoshida et al., 2020). About 3.8 billion years ago, when life emerged, the Earth was in the middle of or just after the Late Heavy Bombardment Period (LHBP) with frequent celestial impact events. Although many studies addressed atmospheric escape due to a single large-scale impact event during LHBP (Shuvalov et al., 2013), there has been no study for atmospheric escape due to frequent and small celestial impact events. Therefore, the total contribution of the celestial impacts to early Earth's atmospheric escape has yet to be quantified. In this study, we combined a numerical model of hydrodynamic escape due to solar X-ray - Ultraviolet (XUV) heating proposed by Yoshida et al. (2021) with our newly developed model for the atmospheric heating by small-scale frequent celestial impact events as an energy source, with which we assess the effect of celestial impact events on the Earth's atmospheric environment when life began. Based on the impact flux distribution measurement for the diameter of craters formed in the lunar Nectaris basin (Marchi et al., 2012) and the scaling law between the crater and impactor diameters (Morbidelli et al., 2018), we obtained a relation between the impactor diameter and impact flux during the late heavy bombardment. With the obtained impactor diameter-flux relation and an analytical model for the kinetic energy of an impactor entering the atmosphere (Collins et al., 2005), we derived the altitude distribution of the atmospheric heating rate by the impactors during celestial impact events over about 200 million years. As a result, the frequent and small celestial impacts during the late heavy bombardment were found to be a heating rate of ~10^(-10)[J/m^3/s] at altitudes of 0-500 [km]. Also, the instantaneous heating rate for a single small impact was ~10^3[J/m^3/s] at altitudes of 0-500 [km]. This is comparable to atmospheric heating rates of ~10^(-8) - 10^(-11)[J/m^3/s] at altitudes of 1000 - 190000 [km] due to the XUV heating during the same period. We are implementing this impactor heating rate model in the hydrodynamic escape model of Yoshida et al. (2021). The current status will be presented in this presentation.

原始地球大気は水素を主成分とする太陽系星間ガスと、天体衝突などで地球内部から噴き出した水蒸気や二酸化炭素が主体のガスで形成されていると考えられ、それらは特に初期地球では流体力学的散逸によって失われるとされている（Yoshida et al., 2020）。生命の誕生した約 38 億年前は後期重爆撃期の最中、もしくは直後であり、天体衝突が盛んであったと考えられる。一度の大規模な天体衝突イベントが引き起こす大気散逸を扱った研究は多くあるが（Shuvalov et al., 2013）、特定の期間の間頻繁に起こった天体衝突イベントを介した大気加熱による流体力学的大気散逸を扱った数値シミュレーションは先例がなく、初期地球大気散逸に対する天体衝突の影響の全容は解明されていない。そこで本研究では、先行研究 (Yoshida et al., 2021) で提案された、太陽極端紫外光 (XUV) 加熱に伴う流体力学的大気散逸の数値モデルに、新たなエネルギー源として小規模な天体衝突の際に大気に供給された熱エネルギーモデルを組み込むことによって、天体衝突による流体力学的大気散逸シミュレーションを行う。これにより、生命誕生時の地球大気環境において、天体衝突の及ぼす影響を評価する。まず、月のネクタリス盆地に形成されたクレーターの直径に対する衝突フラックス分布 (Marchi et al., 2012) と、クレーター直径と衝突天体の直径のスケーリング則 (Morbidelli et al., 2018) により、後期重爆撃期における衝突天体の直径とフラックスの関係式を求めた。そして天体の大気突入時の直径や運動エネルギー変化を記述した解析モデル (Collins et al, 2005)、に、得られた直径ーフラックスの関係式を組み込むことで、約 2 億年の間の天体衝突の際に、大気に供給される加熱率の高度分布を導出した。その結果、後期重爆撃期の天体衝突は、高度 0-500[km] で ~10^(-10)[J/m^3/s] の加熱率をもつことが分かった。これは同時期の、高度 1000-190000[km] における、太陽 XUV による大気加熱率~10^(-8) - 10^(-11)[J/m^3/s] と同程度である。また、1 回の小天体衝突による瞬間的な加熱率は~10^3[J/m^3/s] であり、太陽 XUV と比較して非常に高い加熱率である。この天体衝突熱源モデルを、Yoshida et al. (2021) のモデルに新たに組み込み、衝突加熱の効果を初めて入れた流体力学的大気散逸のシミュレーションを行う予定である。本発表ではその結果を報告する。

R005-P10
ポスター 3 ：9/26　AM1/AM2 （9:00-12:30）

ELFIN 衛星と EISCAT レーダーの観測結果を用いて解き明かす降り込み電子にはたらくミラー力が電子密度の高度分布に与える効果

#田中　友啓 [1)], 小川　泰信 [2)], 加藤　雄人 [3)], 吹澤　瑞貴 [2)],Artemyev Anton[4)],Angelopoulos Vassilis[4)],Zhang Xiaojia[5)]
[(1] 総研大,[(2] 極地研,[(3] 東北大・理・地球物理,[(4] カリフォルニア大学ロサンゼルス校,[(5] テキサス大学ダラス校

Effects of mirror force for precipitating electrons on altitude profiles of electron density with ELFIN and EISCAT observations

#Tomotaka Tanaka[1)],Yasunobu Ogawa[2)],Yuto Katoh[3)],Mizuki Fukizawa[2)],Anton Artemyev[4)],Vassilis Angelopoulos[4)],Xiaojia Zhang[5)]
[(1]The Graduate University for Advanced Studies, SOKENDAI,[(2]National Institute of Polar Research,[(3]Department of Geophysics, Graduate School of Science, Tohoku University,[(4]University of California, Los Angeles,[(5]University of Texas at Dallas

Energetic Electron Precipitation (EEP) causes various phenomena, such as aurora emissions and variations in atmospheric compositions via collisions with the atmosphere. To quantitatively study the effects of EEPs on the atmosphere is one of the essential fundamentals for understanding how precipitating electrons with various pitch angle distributions ionize the atmosphere. However, the basic processes involved in the propagation of precipitating electrons and the production of secondary electrons still need to be well understood. Katoh et al. [under review] recently suggested by numerical simulations that the magnetic mirror effect can vary the altitude profile of atmospheric ionization. Therefore, the purpose of this study is to understand observationally the mirror effects on atmospheric ionization so that we would verify the numerical simulation results.

In this study, we used simultaneous observation data of ELFIN satellites and EISCAT radars as well as numerical simulation data for connecting them. The ELFIN satellites consist of two CubeSats flying in formation on nearly identical orbits at an altitude of around 450 km, observing pitch-angle resolved fluxes of electrons in the 50 -7000 keV energy range from September 2018 to September 2022. We used altitude profiles of electron density at altitudes of 60 - 170km observed with the EISCAT Tromso UHF/VHF radars. We found 42 events which are simultaneously observed by EISCAT radar in Tromso [19.2 E, 69.6N] and ELFIN satellite in the region within $\pm$ 2 degree latitude and $\pm$ 5 degree longitude from Tromso. Among them, 33 events had significant ionization by EEP at altitudes below 100 km. We adopted the numerical simulation used in Katoh et al., which is a particle transport simulation using the Monte Carlo method. This simulation allows us to quantitatively investigate how the mirror force could affect the atmospheric ionization rate and production of secondary electrons, especially backscattering electrons. Specifically, we calculated, with the numerical simulation, the altitude profile of the collision rate of all the precipitating electrons under two conditions, with/without the mirror effect. Inputs of the energy and pitch-angle profiles of electron flux were used for the data observed by ELFIN satellites. We plan to compare and verify the characteristic of the altitude profile of the ionization-rate/electron-density based on that collision rate with that of electron density simultaneously observed by EISCAT radars.

First, we studied how the mirror effect varied the altitude profile of collision rate below 100 km using the 7th January 2021 simultaneous event. We found that the mirror effect made a difference in the collision rate if we considered the energy and pitch-angle profile of precipitating electron flux observed with ELFIN satellites. The collision rate with the mirror effect was about half of that without the mirror effect. As Katoh et al. suggested, electrons out of the loss cone reduce the collision rate at altitudes between 60 and 80km because they are bounced at a mirror point so that the number of electrons penetrating the low-altitude atmosphere decreases.

According to the result of the numerical simulation, it is useful to verify differences between with and without the mirror effect on the atmospheric ionization and the production of secondary electrons if many precipitating electrons have pitch angles near the loss cone angle. We found 4 events, 5th October, 27th November, 16th December in 2021, and 29th March in 2022, have distributions as mentioned.

In this presentation, we will discuss if the mirror effect makes some differences in atmospheric ionization by comparing with altitude profiles of the electron density simultaneously observed by EISCAT radar.

高エネルギー電子降下（Energetic Electron Precipitation; EEP）は、中性大気との衝突を介して、オーロラ発光や大気成分の変動といったさまざまな現象を引き起こす。様々なピッチ角分布で降下する電子が大気をどのように電離するかを理解することは、EEP による大気への影響を定量的に把握するうえで欠かせない基礎となる。しかし、降下電子の大気中の伝搬及び 2 次電子生成に関わる基本的なプロセスは、十分に理解されたとはいえないのが現状である。最近、Katoh et al. [under review] において、そのプロセスの１つである磁気ミラー効果の有無によって大気電離の高度分布が変わりうることが数値シミュレーションによって示唆された。そこで本研究は、その数値シミュレーション結果の検証を視野に入れて、磁気ミラー力の効果が大気電離に与える影響を観測的に明らかにすることを目的とする。

本研究では、ELFIN 衛星と EISCAT レーダーとの同時観測データ及び、その両者を繋ぐ数値シミュレーションデータ

を使用した。Angelopoulos et al.(2020) より、ELFIN 衛星は高度 450 km 付近をほぼ同一の軌道で編隊飛行する 2 基の CubeSat で構成され、50 -7000 keV のエネルギー帯の電子のピッチ角分解されたフラックスを 2018 年 9 月から 2022 年 9 月まで観測していた。EISCAT レーダーについては、トロムソ UHF/VHF レーダーで観測された電離圏高度 60-170 km の電子密度データを使用した。ELFIN 衛星がトロムソ [19.2 deg E, 69.6 deg N] から緯度± 2 度以内及び、経度± 5 度以内の上空を通過している間に、EISCAT と同時に観測しているイベントは 42 例存在した。その内、EEP による顕著な電離が高度 100km 以下に存在したイベントは 33 例であった。数値シミュレーションには、Katoh et al. で用いられたモンテカルロ法での粒子輸送シミュレーションを用いた。このシミュレーションにより、磁気ミラー効果の有無が、大気の電離率や 2 次電子生成（特に後方散乱電子の生成）にどのような影響を与えるかを定量的に調査できる。具体的には、ELFIN 衛星で観測された電子フラックスのエネルギーピッチ角分布と、1 電子当たりの衝突率を計算した数値シミュレーションを基に、大気へ降下する全電子による衝突率をミラー力の有無を区別して導出する。その衝突率に基づく大気電離率/電子密度の高度分布の特徴を、EISCAT レーダーで同時に観測された電子密度分布の特徴と比較・検証する。

まず 2021 年 1 月 7 日の同時観測イベントについて、前述の方法で 100km 以下の低高度における衝突率がミラー効果の有無によってどのように変化するかを検証した。その結果、実際の降下電子フラックスの観測値を基に計算した場合でも、ミラー力の有無により衝突率に違いが出ることが分かった。60-80km の高度においてミラー効果を考慮した場合の衝突率は、考慮しない場合の衝突率に対しておよそ 1/2 であった。Katoh et al. で示唆された通り、ミラー効果を考慮した場合に低高度で衝突率を低下させるのはロスコーン外にある電子であり、ミラー点で反射されることで低高度まで降り込む電子が減少することが理由である。

数値シミュレーションの解析結果から、ロスコーン付近のピッチ角をもつ電子が多く分布するイベントを用いることで、大気の電離率や 2 次電子生成においてミラー効果の有無による差を検証しやすいと考えている。そのようなピッチ角分布を持つ降下電子イベントを探した結果、2021 年 10 月 5 日、2021 年 11 月 27 日、2021 年 12 月 16 日、2022 年 3 月 29 日の 4 イベントが該当することが分かった。

本発表では、これらのイベントについて、EISCAT レーダーで同時観測された電子密度の高度分布データも組み合わせ用いることにより、磁気ミラー力の有無による特徴の違いや影響について議論することを予定している。

R005-P11
ポスター 3 ：9/26　AM1/AM2 （9:00-12:30）

#頭師　孝拓 [1)], 栗田　怜 [2)], 小嶋　浩嗣 [2)], 石坂　圭吾 [3)], 熊本　篤志 [4)], 浅村　和史 [5)], 笠原　禎也 [6)], 尾崎　光紀 [6)], 松岡　彩子 [7)], 野村　麗子 [8)], 田中　真 [9)], 横田　勝一郎 [10)], 阿部　琢美 [5)], 細川　敬祐 [11)], 小川　泰信 [12)], 齋藤　義文 [5)]
([1] 奈良高専,[2] 京都大学 生存研,[3] 富山県大・工,[4] 東北大・理・地球物理,[5] 宇宙研,[6] 金沢大,[7] 京都大学,[8] 宇宙航空研究開発機構,[9] 東海大,[10] 大阪大,[11] 電通大,[12] 極地研,[13] 極地研,[14] 極地研,[15] 宇宙研

Analysis of plasma waves observed by LFAS/WFC onboard the SS-520-3 sounding rocket

#Takahiro Zushi[1)],Satoshi Kurita[2)],Hirotsugu Kojima[2)],Keigo Ishisaka[3)],Atsushi Kumamoto[4)],Kazushi Asamura[5)],Yoshiya Kasahara[6)],Mitsunori Ozaki[6)],Ayako Matsuoka[7)],Reiko Nomura[8)],Makoto Tanaka[9)],Shoichiro Yokota[10)],Takumi Abe[5)],Keisuke Hosokawa[11)],Yasunobu Ogawa[12)],Yoshifumi Saito[5)]
([1]National Institute of Technology （KOSEN), Nara College,[2]Research Institute for Sustainable Humanosphere, Kyoto University,[3]Faculty of Engineering, Toyama Prefectural University,[4]Department of Geophysics, Graduate School of Science, Tohoku University,[5]Institute of Space and Astronautical Science, Japan Aerospace Exploration Agency,[6]Kanazawa University,[7]Graduate School of Science, Kyoto University,[8]Japan Aerospace Exploration Agency,[9]Tokai University,[10]Osaka University,[11]Graduate School of Informatics and Engineering, University of Electro-Communications,[12]National Institute of Polar Research,[13]National Institute of Polar Research,[14]National Institute of Polar Research,[15]Department of Solar System Sciences, Institute of Space and Astronautical Science, Japan Aerospace Exploration Agency

It is known that ions in Earth's upper atmosphere are accelerated and escape into space at the polar cusp region. The SS-520-3 sounding rocket was designed to understand the acceleration mechanism of escaping ions. Previous rocket experiments and satellite observations suggest that broadband extremely low frequency (BBELF) waves are involved in ion acceleration. For this reason, SS-520-3 is equipped with plasma wave and DC electric field instruments called the Low-Frequency wave Analyzer/ System (LFAS). The LFAS has two types of receivers, WaveForm Capture (WFC) and Electric Field Detector (EFD). The frequency range of the WFC is 10 Hz to 10 kHz, and that of the EFD is DC to 400 Hz. Both receivers obtain the electric field from two orthogonal pairs of dipole electric sensors. Due to telemetry limitations, the WFC performs single-channel waveform observations until 330 s after launch, and dual-channel observations between 330 s and 630 s, when the rocket is expected to be near apex height.

The SS-520-3 sounding rocket was successfully launched on November 4, 2021 from Ny Alesund, Spitsbergen, Norway. Two LFAS receivers operated successfully during the flight. However, due to sensor problems, two of the four sensor elements were not deployed and one was deployed later than planned. As a result, the LFAS observed the electric field in an orthogonal monopole configuration. From the observation result of the WFC, we found waveforms similar to the previously reported BBELF waves. However, the WFC waveform showed a large-amplitude, low-frequency, periodic noise originating from the undeployed antenna. We attempted to reduce the effect of noise by using EFD single probe data to analyze BBELF in more detail. In the presentation, we will show the detailed analysis result of the WFC observation data.

R005-P12
ポスター 3 ：9/26　AM1/AM2 （9:00-12:30）

SS-520-3 号機観測ロケット搭載 LEP で観測した極域カスプでの電子降下と低エネルギーイオン

#横田　勝一郎 [1)], 齋藤　義文 [2)], 浅村　和史 [3)], 松岡　彩子 [4)], 野村　麗子 [3)]
([1] 大阪大,[2] 宇宙研,[3] 宇宙研,[4] 京都大学

Electron precipitation and decelerated ion flux at the polar cusp observed by LEP on the SS-520-3 sounding rocket

#Shoichiro Yokota[1)],Yoshifumi Saito[2)],Kazushi Asamura[3)],Ayako Matsuoka[4)],Reiko Nomura[3)]
([1]Osaka University,[2]Institute of Space and Astronautical Science, Japan Aerospace Exploration Agency,[3]Japan Aerospace Exploration Agency,[4]Graduate School of Science, Kyoto University

The escape of the upper atmosphere is a universal phenomenon not only for the Earth but also for other terrestrial planets. Elucidating the physical mechanisms is important for understanding and predicting the atmospheric evolution that leads to the diversity of planetary atmospheres, and its scientific significance is not limited to the planets of the solar system. Scientific observations to verify theoretical studies are essential to elucidate the escape mechanism of the upper atmosphere, and the Earth's upper atmosphere is the most easily observable target among solar-system planets.

The SS520-3 sounding rocket experiment was conducted on November 4, 2021 at Ny-Alesund to observe in situ the acceleration and heating of outflowing ions at the top of the ionosphere above the Earth's cusp. One of the instruments was a low-energy particle experiment (LEP), which we developed.

The LEP is a pair of analyzers that analyze the energies of ions and electrons below 10 keV. The two analyzers are completely identical in shape, and both pass incident electrons and ions pass through ultra-thin carbon films and measure the secondary electrons emitted from them. Therefore, both detectors (MCPs) are of the same form for electron measurement, which is a characteristic of LEP. The SS520-3 sounding rocket experiment was also an opportunity to prove this new technology.

The SS-520-3 sounding rocket experiment was conducted as scheduled and the LEP acquired about 10 minutes of observation data. We report here the observations of accelerated electron precipitation and decelerated ion flux, which are considered to be the characteristics of the polar cusp.

超高層大気の流出現象は, 地球に限らず地球型惑星にとって普遍的な現象である. その物理機構を解明することは惑星大気の多様性をもたらす大気進化を理解・予測する上で重要であり, その科学的意義は太陽系の惑星に留まらない。この超高層大気の流出機構の解明には理論研究を検証する科学観測が必須であり, 地球の超高層大気が太陽系天体の中で最も観測が容易な対象である.

SS520-3 号機観測ロケット実験は地球カスプ上空電離層最上部における流出イオンの加速・加熱をその場観測することを目的としていて、2021 年 11 月 4 日に Ny-Alesund にて実施された。 観測装置の 1 つとして磁場・電場センサーと共に我々の開発した低エネルギー粒子計測器 (LEP) も搭載されていた.

LEP は 10 keV 以下のイオンと電子のエネルギー分析を行う一対の分析器である. 二つの分析器は完全に同一の形状であり、どちらも入射する電子とイオンを超薄膜カーボンに通過させて, そこから放出される二次電子を計測する。従って、検出器（MCP）は両者とも電子用の同一形態のものが用いられているのが LEP の特徴である. SS520-3 号機観測ロケット実験はこの新技術の立証の機会にもなった.

SS-520-3 号機観測ロケット実験にて LEP は予定通りの観測を行い、約 10 分間の観測データを取得した。2017 年に実施した性能試験データに基づき観測データの較正を行い、現在は SS-520-3 号機観測ロケット実験チーム内に公開している。LEP にて極域カスプの特徴とされる加速された電子降下や, 減速されたイオン降下などが観測されたので、ここに報告する.

R005-P13
ポスター 3 ：9/26　AM1/AM2 （9:00-12:30）

#大塚　雄一 [1),Fu　Weizheng[2)
([1 名大・宇地研,([2 名大・宇地研

Four-Minute Total Electron Content Fluctuations over Japan after the 2022 Hunga Tonga Hunga Ha'apai Volcanic Eruption

#Yuichi Otsuka[1),Weizheng Fu[2)
([1Institute for Space-Earth Environmental Research, Nagoya University,([2Institute for Space-Earth Environmental Research, Nagoya University

Ionospheric disturbances following impulsive events, such as earthquakes, volcanic eruptions, and powerful explosions, have been observed using various techniques. Fluctuations in the Total Electron Content (TEC) and magnetic field with a period of approximately 4 minutes are frequently observed following such ground-based disturbances. These 4-minute fluctuations are believed to be caused by the resonance of acoustic waves between the surface and lower thermosphere.

After the volcanic eruption of Hunga Tonga-Hunga Ha'apai on January 15, 2022, various ionospheric variations were observed. In this study, we analyzed TEC data collected from a dense Global Navigation Satellite System (GNSS) observation network operated by SoftBank Corp. Time resolution of the TEC data is 1 second. We observed intermittent TEC variations with a period of approximately 4 minutes over Japan between 11:30 and 13:30 UT on January 15, 2022. Our research aims to investigate the two-dimensional structures of these 4-minute TEC variations.

Acknowledgements: The SoftBank's GNSS observation data used in this study was provided by SoftBank Corp. and ALES Corp. through the framework of the "Consortium to utilize the SoftBank original reference sites for Earth and Space Science".

観測ロケットによる磁場データを用いたスポラディック E 層電流構造の解析

#奥田　隆一 [1)], 松岡　彩子 [2)], 熊本　篤志 [3)], 阿部　琢美 [4)]
([1] 京都大学,[2] 京都大学,[3] 東北大・理・地球物理,[4] ＪＡＸＡ宇宙科学研究所

Analysis of current structure in the sporadic E layer using magnetic data obtained by sounding rocket experiment

#Ryuichi Okuda[1)],Ayako Matsuoka[2)],Atsushi Kumamoto[3)],Takumi Abe[4)]
([1]Kyoto University,[2]Graduate School of Science, Kyoto University,[3]Department of Geophysics, Graduate School of Science, Tohoku University,[4]Institute of Space and Astronautical Science, Japan Aerospace Exploration Agency

The sporadic E layer is a region of high electron density that occurs suddenly and locally in the ionospheric E region, and is known to reflect radio waves in the VHF band (30 to 300 MHz). When the direction of the horizontal wind in the neutral atmosphere varies with altitude and has a shear structure along the vertical direction, ions above and below converge at an altitude between them and form a sporadic E layer, since their motion is affected by the earth's magnetic field (Wind Shear theory). The sporadic E layer appears at an altitude of about 100 km, where the means of direct observation is limited to sounding rockets. Due to the limited opportunities for direct observation, many things about the electromagnetic nature of the sporadic E layer remain unknown. It is meaningful to derive the altitude distribution of the electric current density from the magnetic field measured by sounding rockets for the advanced understanding of the sporadic E layer.

The sounding rocket S-310-38 was launched from Uchinoura Space Center (USC) in Kagoshima Prefecture on February 6, 2008 and reached an altitude of 160 km. The sporadic E layer was confirmed by imaging observation with a Magnesium Ion Imager (MII) and the electron density observation with an Impedance probe onboard the rocket. The rocket was equipped with a Digital Fluxgate magnetometer (DFG), that measures three orthogonal components of the magnetic field (one is along the rocket's axis and the others are in the spin plane around the axis) at a sampling frequency of 200 Hz. In order to subtract the modeled magnetic field and obtain the fluctuation component, it is necessary to determine the attitude of the rocket. Attempts to determine the attitude of the rocket were made by the observation with a star imaging attitude meter, but because the observation was in an area with too much sunlight, the information on the star positions could not be obtained and the attitude of the rocket could not be determined. The attitude of the rocket was estimated by assuming that the point the rocket axis was directed moved on a true circle by the precession motion of the rocket.

The sounding rocket S-520-29 was launched from USC on August 17, 2014 and reached an altitude of 243 km. The sporadic E layer was also confirmed by two MIIs and a Langmuir probe. Similar to S-310-38, the magnetic field observation was performed by a DFG at a sampling frequency of 200 Hz. S-520-29 was equipped with an attitude control system, and it was planned to direct the rocket's axis toward the zenith, but it did not work as expected. Although a very large precession with a radius of about 33 degrees occurred as a result, the attitude of the rocket was determined by the attitude sensor.

In this study, we analyzed the fluctuation component of the magnetic field measured during the flight, and derived the density of the electric current flowing inside and outside the sporadic E layer. Among the parameters included in the general Ohm's law equation expressing the electromagnetic relationship, the electrical conductivity is given by observations of the electron density and models. Although the electric field and the neutral wind velocity were not directly observed, their structure consistent with the current density distribution was inferred. Furthermore we discussed how the ionosphere is heated by converting the kinetic energy of ions and electrons into Joule thermal energy.

スポラディック E 層は電離圏 E 層に突発的かつ局所的に発生する電子密度が高い領域であり、VHF 帯（30〜300MHz）の電波を反射することで知られている。中性大気の水平風の方向が高度によって変わりシア構造を持つと、上下にあるイオンが地球磁場の影響を受けてその中間の高度に収束してスポラディック E 層が形成される（Wind Shear 理論）。スポラディック E 層は高度約 100km に出現し、直接観測の手段は観測ロケットに限られる。スポラディック E 層の中および周辺の電磁的な描像には未解明な部分が多く、観測ロケットによる磁場データから電流密度の高度分布を導出することは有意義である。

観測ロケット S-310-38 号機は 2008 年 2 月 6 日、鹿児島県内之浦宇宙空間観測所から打ち上げられ、高度 160km まで到達した。マグネシウムイオンイメージャ（MII）の撮像観測およびインピーダンスプローブの電子密度観測によって、スポラディック E 層の出現が確認された。同ロケットにはデジタル方式フラックスゲート磁力計 (DFG) が搭載され、サンプリング周波数 200Hz で磁場の直交 3 成分（1 つは機軸に沿った方向の成分、残り 2 つは機軸周りのスピン面内の成分）の測定を行った。測定した磁場からモデル磁場を引き変動成分を求めるためにはロケットの姿勢決定が必要である。星撮像姿勢計の観測により姿勢決定を試みたが、予想を上回る日照領域の影響を受けて、解析に使用しうるデータが得られずロケットの姿勢を決定できなかった。ロケットの歳差運動で機軸方向が真円を描くことを仮定して姿勢を決定した。

観測ロケット S-520-29 号機は 2014 年 8 月 17 日、鹿児島県内之浦宇宙空間観測所から打ち上げられ、高度 243km まで到達した。2 台の MII およびラングミュアプローブの電子密度観測により、同じくスポラディック E 層の出現が確認された。S-310-38 号機と同様に、DFG によってサンプリング周波数 200Hz で磁場観測を行った。S-520-29 号機には姿

勢制御装置が搭載され、ロケットの機軸が天頂を向く制御を行うことが計画されたが、姿勢制御装置が期待通りに動作しなかった。このため半径約 33 度の非常に大きな歳差運動を起こしたものの、姿勢センサにより観測ロケットの姿勢は決定された。

本研究では飛翔中の磁場データの変動成分の解析を行い、スポラディック E 層内外を流れる電流密度を導出した。一般的なオームの法則の式に含まれるパラメータの内、電気伝導度は電子密度の観測値とモデルで与えられる。電場と中性風速度は直接的には観測されていないが、電流密度分布と整合する電場と中性風速度の構造を推測した。また、イオンや電子の運動エネルギーがジュール熱に変換されることにより、電離圏がどのような加熱を受けるのか考察した。

R005-P15
ポスター 3 ：9/26　AM1/AM2 （9:00-12:30）

#古城　侑季 [1)], 齊藤　昭則 [1)], 西岡　未知 [2)]
([1] 京都大・理・地球物理,[2] 情報通信研究機構

Horizontal structures and movements of sporadic E layers observed with ionosonde receiver networks

#Yuki Kojo[1)],Akinori Saito[1)],Michi Nishioka[2)]
([1]Department of Geophysics, Graduate School of Science, Kyoto University,[2]National Institute of Information and Communications Technology

The sporadic-E (Es) layers are high plasma density layers that appear suddenly in the E region of the ionosphere, around 100 km altitude. It is known that tidal winds play a major role in the formation and movement of Es. The horizontal movement of Es has been studied with various observational methods and numerical simulations. Continuous TEC observation has been used to capture the horizontal structure of Es, although Es height cannot be measured. Es height is important because wind is critical to the motion of Es and the distribution of wind is dependent on height. The advantage of ionosonde observation is the ability to measure the altitude. Ionosonde network can detect horizontal structure and movement of Es. However, the distances among four ionosonde facilities of NICT in Japan are longer than typical Es scale, so it is hard to investigate horizontal movement of Es. In this study, we performed multistatic observations with two networks of ionosonde and receivers to investigate the horizontal structure and movement of Es over Japan.

In the observation networks, two ionosonde receivers are newly installed around ionosonde of NICT Radio Observation Facilities at Yamagawa, Kagoshima in June 2023. They are located at Aso and Miyazaki, performing a tristatic observation. The distance is 190 km between Yamagawa and Aso, and 100 km between Yamagawa and Miyazaki. Radio waves emitted from the ionosonde are reflected by the Es layers above the midpoint between the ionosonde and the receiver, and the reflected waves are received by the receiver, which measures the electron density of the Es above the midpoint. We compare the data from the ionosonde vertical observations with the data over the midpoints obtained from the receivers. The horizontal scale of the Es layers is estimated by determining whether the same Es layer is observed at multiple observation points based on the correlation between the density and altitude changes of Es. In the tristatic observation, the direction and velocity of Es horizontal movement are also calculated from the difference in observation time at each site. This network will make simultaneous observation with sounding rocket experiment, RIDE campaign to be launched from JAXA Uchinoura Space Center in Kagoshima in the summer of 2024.

Another ionosonde network consists of an ionosonde at Kokubunji, Tokyo and a receiver at Oarai, Ibaraki, performing a bistatic observation. The distance between ionosonde and receiver is 120 km.

In this study, we will discuss the horizontal structure and horizontal movement of the Es layer with data from these two ionosonde networks.

R005-P16
ポスター 3 ：9/26　AM1/AM2 （9:00-12:30）

昭和基地で観測された Ca+ 層とスポラディック E 層の比較

#江尻　省 [1,2], 西山　尚典 [1,2], 津田　卓雄 [3], 津野　克彦 [4], 古城　侑季 [5], 齊藤　昭則 [5], 西岡　未知 [6], 阿保　真 [7], 川原　琢也 [8], 小川　貴代 [4], 和田　智之 [4], 中村　卓司 [1]
([1] 極地研,[2] 総研大,[3] 電通大,[4] 理研,[5] 京都大・理・地球物理,[6] 情報通信研究機構,[7] 都立大・システムデザイン,[8] 信州大・工

Comparison between the Ca+ and the sporadic E layers observed at Syowa

#Mitsumu K. Ejiri[1,2],Takanori Nishiyama[1,2],Takuo T. Tsuda[3],Katsuhiko Tsuno[4],Yuki Kojo[5],Akinori Saito[5],Michi Nishioka[6],Makoto Abo[7],Takuya D. Kawahara[8],Takayo Ogawa[4],Satoshi Wada[4],Takuji Nakamura[1]
([1]National Institute of Polar Research,[2]Graduate University for Advanced Studies, SOKENDAI,[3]University of Electro-Communications,[4]RIKEN, RAP,[5]Department of Geophysics, Graduate School of Science, Kyoto University,[6]National Institute of Information and Communications Technology,[7]Graduate School of System Design, Tokyo Meteropolitan University,[8]Faculty of Engineering, Shinshu University

Sporadic E (Es) layer is the thin layer of enhanced electron density forms at the height between 90 and 120 ☒ km in the mesosphere and lower thermosphere (MLT) region. The wind shear theory is widely accepted as the mechanism of the formation of the Es layer in the mid-latitudes and the daytime Es has usually higher plasma density than the nighttime Es. Among the ions that drift vertically due to the vertical shear of neutral horizontal winds, the long-lived ions that form the core of the Es layer are metal-atom ions supplied by meteoroids to the MLT region. On the other hand, the Es layer in the auroral zone is usually seen during the night hours and has been mostly associated with magnetic and auroral activity. It is known that the value of foEs obtained by ionosonde observation increase with the motion of an auroral arc or band from a low elevation angle to a position near the zenith. However, it is unknown if there is a contribution of the metal-atom ions to formation and lasting of the Es in the auroral zone as in the mid-latitude. A resonance scattering lidar developed by the National Institute of Polar Research (NIPR) was installed at Syowa (69S, 40E), Antarctic in 2017 and successfully obtained Ca^+ density profiles 6 nights in total in Spring of 2017 and 2018. In this presentation, we will discuss a relationship between a metal-atom ion and the Es layer by comparing the temporal variation of Ca^+ density with foEs data obtained by the NICT ionosonde at Syowa Station.

R005-P17
ポスター 3 ：9/26　AM1/AM2 （9:00-12:30）

HF ドップラー観測システムによる電離層 FM-CW 距離測定の試み

#並木　紀子 [1)], 細川　敬祐 [1)], 野崎　憲朗 [1)], 坂井　純 [1)], 冨澤　一郎 [1)], 有澤　豊志 [1)]
[1) 電通大]

Trial of Ionospheric FM-CW Distance Measurement by HF Doppler Observation System

#Noriko Namiki[1)],Keisuke Hosokawa[1)],Kenro Nozaki[1)],Jun Sakai[1)],Ichiro Tomizawa[1)],Toyoshi Arisawa[1)]
[1)The University of Electro-Communications]

Observations of ionospheric disturbances using the High Frequency Doppler (HF Doppler: HFD) sounding have been carried out in various latitudes since the early 1960s. In Japan, ob-servations have continued for the past ˜50 years, and the Doppler shifts imposed at the time of reflection at the ionospheric E and F regions have been used to study traveling ionospheric disturbances (TIDs), sporadic E (Es), and various ionospheric phenomena caused by energy input from the magnetosphere or lower atmosphere. The University of Electro-Communications (UEC) started HFD observations using the standard radio JJY (Communica-tions Research Laboratory) in 1977, and has conducted multipoint observations by operating a number of receivers at multiple stations in Japan. After the stop of HF JJY transmission, in order to continue ionospheric researches using HFD, the experimental radio transmission station JG2XA was newly established in 2001 which employs radio waves at 5006 kHz and 8006 kHz, which are close to the frequencies used by JJY. An overview of the HFD project data from the experiments are available at ”http://gwave.cei.uec.ac.jp/˜hfd”.

Since the beginning of this transmitting station, CW for Doppler observation and Morse code as an identification signal for the transmitting station are transmitted. The Doppler shift from the target is obtained by receiving CW reflected at the ionosphere, which has a reflec-tion surface in a specific electron density region. However, which reflection mode of the target resulted in the data was often determined by empirically or through comparison with another observation.

The following requirements are needed to improve the transmitter system: 1) need to be consistent with the existing observation data, 2) need to measure the reflection altitude quantitatively with a distance resolution of several kilometers, and 3) need to meet domes-tic radio regulations to obtain an additional radio wave license.

To measure the propagation distance, FM-CW is considered with a sweep range of 150 kHz and repetition of 20 Hz (Namiki et al., JpGU 2022). Frequency and time will be synchronized between transmitter and receiver precisely via GPS. An indoor experiment was conducted by transmitting conventional CW and additional FM-CW signal together. Both ranging and Doppler signal were detected simultaneously by a receiver with an additional sweep frequency converter (Namiki et al., SGEPSS, 2022).

An addition of the FM-CW radio type and a change of the transmitting system were approved in March 2023. Transmission with the new system has been operational and the received data is being compared with the previous Doppler data. Since the start of the operation of the new system, -3 mHz steady deviation has been observed for both the 5006 and 8006 kHz transmission. This frequency bias is attributed to the frequency generator in the new system and is confirmed to be negligible for usual Doppler measurement within $\pm$ 4 Hz Doppler range (Namiki et al., JpGU, 2023).

If we measure the ionospheric height at a distance of about 80-570 km with our FM-CW ranging technique, the frequency of the baseband signal at the receiver side will range from 1.6 kHz to 15 kHz, which is far from the Doppler frequency range of $\pm$ 4 Hz. There is a need for receiving system different frequency processing to handle the ranging signal. We report the results of a study of data processing method for the coexistence of new FM-CW ranging and conventional CW Doppler observation.

短波ドップラー（HF Doppler: HFD）法を用いた電離層擾乱の観測は、1960 年代から様々な緯度帯において継続的に行われてきた。日本においても、過去 50 年ほどにわたって観測が継続され、電離圏 E、F 領域からの反射波に印可されたドップラーシフトを用いて、伝搬性電離圏擾乱やスポラディック E 現象、磁気圏もしくは下層大気からのエネルギー流入に伴う変動の研究が行われてきている。

電気通信大学では、1977 年から短波標準電波 JJY（通信総合研究所) を利用した HFD 観測を開始し、反射波を国内の複数点で受信することによる多点観測を実施してきた。短波 JJY が廃止された後、2001 年からは、HFD による電離圏研究の継続のために、従来使用していた周波数に近い 5006 kHz と 8006 kHz の連続波 (Continuous Wave：CW) を送信する実験局 JG2XA を設置し、送受信局の運用を続けている。HFD プロジェクトの概要と測定データは”http://gwave.cei.uec.ac.jp/˜hfd”にて公開されている。当設備では初期より、観測用の CW と送信局の識別信号として

のモールス信号が送信され、見かけ上特定の電子密度領域での反射面をもつ電離圏で反射された CW を受信して、ターゲットからのドップラーシフトが得られている。しかしながら、そのデータがどの反射モードのターゲットから生じた結果であるのかは、経験的に推測するか別の観測データとの比較で決定することが多かった。

送信設備改良への要求としては、(１）従来の観測データとの整合性がとれること、（２）従来経験的に推測していた現象の高度を、周波数ごとに異なる見かけの反射高度として数 km の距離分解能で定量的に測定すること、（３）国内無線局の基準を満たして電波型式追加と構成機器変更の認可を取得すること、が挙げられた。

そこで、従来設備のデジタル化と高精度化への置き換えに合わせ、観測システムへ測距機能を追加するため電波高度計として普及している低出力でも感度の得られる FM-CW 型式の追加を検討した。GPS で離れた送受信点の時刻同期をとり、HF 帯 FM-CW による電離圏の距離測定を行うために、ターゲットの出現高度と仮の変動速度から見積もって 150kHz の帯域を 20Hz で掃引することを検討した (Namiki et al., JpGU, 2022)。FM-CW による電離圏距離測定の検討を元に、室内で現行の受信システムにミキサーを追加した疑似距離測定実験を行い、現在ホモダイン検波で動作している CW ドップラー受信システムに物理的に装置を追加したヘテロダイン検波であっても、CW と FM-CW の同時観測が可能であることを確認した (Namiki et al., SGEPSS, 2022)。

この間、新送信設備のスプリアス基準を満たす変更工事を施し、2023 年 3 月に FM-CW 電波型式の追加と設備一式の更新が正式に認められた。新送信設備の実運用が開始され、新旧切替の前後で従来のドップラー観測データとの比較を行ったところ、複数の受信点と周波数で-3mHz の定常的なずれが認められたが、送信機の基準クロックがルビジウムから GPS へ置き換わった影響と考えられた。± 4Hz 範囲のドップラーシフトを観測するうえでは、無視できる程度の変化であることを確認した (Namiki et al., JpGU, 2023)。送信機の基準信号としてルビジウムと GPSDO を比較した結果、周波数発生装置内のバイアスであることが判明した。送信設備の改良は段階的に進められ、現在は CW を常時発信しながら FM-CW とモールスの送信を自動的に定時切替装置や保護装置の追加に取り組んでいる。距離測定のためには、送信機側の電波追加と同時に、受信機側の設定変更も必要とされる。実空間を飛来した電波の予測される高度は 80-570km 程度となることから、距離が周波数に変換された場合 1.6kHz から 15kHz の値域をとることが想定される。現在± 4 Hz を表示するクイックルックとは別の処理を施したうえで可視化し、距離情報を抽出する仕組みが求められている。受信アンテナ系統は共通のものを利用し、150 kHz 掃引の FM-CW と従来の CW ドップラー観測とを共存させるためのデータ処理方法を検討した結果について報告を行う。

R005-P18
ポスター 3 ：9/26　AM1/AM2 （9:00-12:30）

EISCAT_3D レーダー観測に向けた 1 局・複数ビーム観測による電離圏イオン速度再構成手法の検討

#吹澤　瑞貴 [1)], 小川　泰信 [1)], 西村　耕司 [2)], 西山　尚典 [1)], 橋本　大志 [1)], 津田　卓雄 [3)]
([1] 極地研,[2] 京大,[3] 電通大

Feasibility study of ionospheric ion velocity reconstruction method for monostatic and multi-beam EISCAT_3D radar observation

#Mizuki Fukizawa[1)],Yasunobu Ogawa[1)],Koji Nishimura[2)],Takanori Nishiyama[1)],Taishi Hashimoto[1)],Takuo Tsuda[3)]
([1]National Institute of Polar Research,[2]Kyoto University,[3]University of Electro-Communications

EISCAT_3D radar (E3D) is the world's first multi-static phased-array incoherent scatter radar to observe the three-dimensional (3-D) distribution of ionospheric physical parameters with high temporal resolution. E3D is planned to consist of a central active (transmitting/receiving) site ("core") and four receive-only sites. Currently, the core site in Skibotn, Norway (geographic latitude (GLAT): 69.340 degrees, geographic longitude (GLON): 20.313 degrees), and receiving sites in Karesuvanto, Finland (GLAT: 68.463 degrees, GLON: 22.458 degrees) and Kaiseniemi, Sweden (GLAT: 68.267 degrees, GLON: 19.448 degrees) are under construction. The E3D is capable of deriving the 3-D distribution of ionospheric ion velocity vectors from multi-beam observations from at least three stations. These observations will contribute to the understanding of the magnetosphere-ionosphere-thermosphere coupling process. The E3D observation is scheduled to start in 2024 with one station, followed by a three-station observation system. In this study, a method to reconstruct the 3-D distribution of ionospheric ion velocity vectors from line-of-sight (LOS) ion velocity observation data by monostatic and multi-beams was investigated.

In the Common Program of E3D, which is the common experiment to all member countries of the EISCAT Scientific Association, a total of 27 beams (10 low-elevation beams, 10 high-elevation beams, and 7 meridional beams) are suggested to be used for observations. For the low-elevation beams, the azimuth and zenith angles were determined so that the beam points are equi-latitudinally spaced on the meridian +/-150 km east-west from the core site at an altitude of 250 km. The azimuth and zenith angles of the high-elevation beams were then determined by tracing the magnetic field lines from the 110 km altitude of these beams to the 250 km altitude and passing through these points. For the meridian beams, we determined four beams with elevation angles of 30 and 60 degrees for azimuth angles of 0 and 180 degrees, respectively; two beams with vertical and magnetic zenith directions; and two beams with an azimuth angle of 180 degrees and elevation angle of 60 +/- 6 degrees.

From the LOS ion velocity observations at an altitude of 250 km by the 27 beams determined in this way, the ion velocity vectors were derived using data from three adjacent observation points. The number of grids (north-south x east-west) connecting the three adjacent points was 8 x 2 grids for a range of +/-30 km in the east-west direction from the core site and 6 x 4 grids for a range of +/-150 km. The spatial resolution in the north-south direction was approximately 30 km and 60 km, respectively. In order to generate pseudo-E3D observation data, the atmosphere-ionosphere coupling model GAIA (Ground-to-topside model of Atmosphere and Ionosphere for Aeronomy) was used. The projected component of the GAIA's ion velocity to the 27 beam directions in E3D was obtained as the E3D LOS ion velocity observation data. The ion velocity vectors were then derived from the pseudo-E3D observation data at three adjacent points. As a result, the original GAIA data were reproduced well. However, since this derivation assumes that the ion velocity is constant at the three adjacent points, it was confirmed that the error tends to be large at the edge of the field of view, where the spacing between the three beams is large.

As another method, a linearly constrained least-squares problem is set up and the ion velocity vector is derived using the Lagrange multiplier method. As a constraint condition, the ionospheric ion velocity above the 200 km altitude is assumed to follow the E x B drift, and the rotation and divergence of the ion velocity in the horizontal plane are given zero based on Gauss's law and Faraday's law under the conditions of electric neutrality and a steady state magnetic field. Under these conditions, we are considering problem setups that minimize the first- and second-order derivatives of the ion velocity in the spatial direction. In the presentation, we will also show the results of these methods.

The dataset used for this study is from the GAIA project carried out by the National Institute of Information and Communications Technology, Kyushu University, and Seikei University.

EISCAT_3D レーダー (E3D) は電離圏物理量の 3 次元分布を高時間分解能で観測する世界初の複数局フェーズドアレイ式非干渉散乱レーダーである。E3D は 1 つの送受信局と 4 つの受信局から構成される計画であり、現在は 1 つの送受信局（主局、シーボトン：北緯 69.340 度、東経 20.313 度）と 2 つの受信局（カレスバント：北緯 68.463 度、東経 22.458 度、カイセニエミ：北緯 68.267 度、東経 19.448 度）の建設が進んでいる。E3D は少なくとも 3 地点からの複数ビーム観測により電離圏イオン速度ベクトルの 3 次元分布を導出することが可能である。電離圏のイオン速度の 3 次元分布が分かれば電離圏電場や熱圏中性風の分布の推定が可能となり、磁気圏–電離圏–熱圏結合過程の理解に貢献することが期

待される。E3D による観測は、まず主局のみの 1 局方式による共同利用を 2024 年に開始予定であり、その後 3 局方式による観測運営体制が整えられる予定である。そこで、本研究では 1 局・複数ビームによる視線方向のイオン速度観測データから電離圏イオン速度ベクトルの 3 次元分布を再構成する手法の検討を行なった。

E3D の Common Program と呼ばれる EISCAT 科学協会全加盟国の共通実験では、低仰角 10 本、高仰角 10 本、子午線上 7 本の合計 27 本のビームを使った観測が提案されており、それらのビームの方位角と天頂角をまず決める必要がある。低仰角のビームについては、高度 250 km において送信局から東西方向に± 150 km の子午線上においてビーム点が等緯度間隔となるようにビームの方位角と天頂角を決定した。次にこれらのビームの高度 110 km 地点から高度 250 km まで磁力線を辿り、その点を通るように高仰角ビームの方位角・天頂角を決定した。子午線上のビームについては、方位角 0 度、180 度それぞれについて仰角 30 度、60 度の 4 本、鉛直方向、磁気天頂方向の 2 本、そして方位角 180 度、仰角 60 ± 6 度の 2 本とした。

このように決定した 27 本のビームによる高度 250 km における視線方向イオン速度観測から、隣接する 3 点の観測データを用いてイオン速度ベクトルの導出を行った。隣接する 3 点を結んだグリッド数（南北×東西）は、主局から東西方向に± 30 km の範囲では 8 × 2 グリッド、± 150 km の範囲では 6 × 4 グリッドとなった。南北方向の空間分解能はそれぞれ約 30 km と約 60 km となった。擬似的な E3D 観測データを作成するために、大気圏–電離圏結合モデル GAIA (Ground-to-topside model of Atmosphere and Ionosphere for Aeronomy) を用いて電離圏イオン速度ベクトルの 3 次元分布を生成し、E3D の 27 本のビーム方向の射影成分を求めた。そして、隣接する 3 点のデータからイオン速度ベクトルを導出した。その結果、元の GAIA データをよく再現することができたが、この導出では隣接する 3 点でイオン速度が一定と仮定しているため、3 点のビームの間隔が広い視野の端では誤差が大きい傾向が確認された。

また、別の手法として、線形拘束付き最小二乗問題を設定し、ラグランジュ未定乗数法を用いてイオン速度ベクトルを導出する手法の検討を行っている。拘束条件としては高度 200 km 以上の電離圏イオン速度が E × B ドリフトに従うと仮定し、電気的中性条件や磁場定常状態を仮定した際のガウスの法則とファラデーの法則から水平面内のイオン速度の回転や発散が 0 という条件を与え、この条件下でイオン速度の空間方向の 1 階微分や 2 階微分を最小化するような問題設定を検討している。当日の発表ではこれらの手法の検討結果についても示す予定である。

本研究で利用したデータセットは、国立研究開発法人情報通信研究機構、九州大学、成蹊大学による GAIA プロジェクトから提供されたものである。

R005-P19
ポスター 3 ：9/26　AM1/AM2 （9:00-12:30）

南極昭和基地大型大気レーダーによる電離圏沿磁力線不規則構造のイメージング観測

#香川　大輔 [1)], 橋本　大志 [2)], 齊藤　昭則 [3)], 西村　耕司 [4)]
([1] 京大・理,[2] 極地研,[3] 京都大・理・地球物理,[4] 京都大・生存圏研究所

Imaging Observation of Ionospheric Field Aligned Irregularities by the PANSY radar at Antarctic Syowa Station

#Daisuke Kagawa[1)],Taishi Hashimoto[2)],Akinori Saito[3)],Koji Nishimura[4)]
([1]Kyoto University Graduate School of Science,[2]National Institute of Polar Research,[3]Department of Geophysics, Graduate School of Science, Kyoto University,[4]Research Institute for Sustainable Humanosphere, Kyoto Univ.

Program of Antarctic Syowa MST/IS radar (PANSY radar) is the large atmospheric and VHF-band radar located at the Antarctic Syowa Station. This radar has the capability of observing plasma quantities at altitudes of 100-500km using the ionospheric incoherent scatter (IS). In 2015, the PANSY radar performed the first ionospheric IS observation in the Antarctica.This radar also has a frequency of 47MHz, so it can observe the echoes of field aligned irregularities (FAIs) in E-region. If FAIs have a space scale of half wavelength of radio waves, they are coherently backscattered, so the PANSY radar observes the coherent echoes from 3-meter-scale FAIs in E-region. In order to suppress contamination from the FAI echoes during the IS observation, Hashimoto et al.(2019) separated the FAI echoes from IS echoes by the multichannel signal processing technique using the antenna array for observing FAIs (”FAI array”). On the other hand, if we utilize this method to observe FAIs, we can resolve E-region FAIs in detail and measure their motion.

PANSY radar has the array for observing meteors (Meteor array) as well as the FAI array. The FAI array has the degree of freedom only of azimuth angles because its antennas are positioned linearly, whereas the Meteor array can observe FAIs three-dimensionally because the five antennas of the Meteor array are positioned areally. Therefore, we expect that we transmit the radio waves using the FAI array and receive the FAI echoes using the Meteor array. However, it is expected that the Fourier imaging or the Capon imaging cannot accurately measure the spatial structures caused by the antenna pattern. FAI echoes are generally observed if the conditions that radio waves are perpendicular to FAI are satisfied. The grating lobes, however, are generated because the distance of adjacent antenna are wide, so it is considered that the ”ghosts” are also mistakenly generated in the non-echoing region. Therefore, due to remove their effects and provide the accurate spatial structure, we conducted deconvolution based on ”Matching Pursuit”. In this algorithm, we subtract the receive pattern of the Meteor array in each iteration. This algorithm makes smaller the responses of the non-mainlobe region, such as grating lobes and sidelobes, because the antenna pattern are subtracted, so we can suppress the ”ghosts” and conduct high-resolution FAI imaging observation.

In this presentation, we will introduce the result of application of imaging method based on the ”Matching Pursuit” which can remove the effects of the antenna pattern and conduct accurate and high-resolution FAI observation.

南極昭和基地大型大気レーダー (PANSY レーダー) は、南極の昭和基地に設置されている大型 VHF 帯大気レーダーである。本レーダーは電離圏非干渉性散乱 (IS) を用いて地表 100km から 500km におけるプラズマ物理量を観測することが可能であり、2015 年には南極で初となる電離圏 IS 観測が開始された。また、47MHz の周波数を用いているため、E 領域における沿磁力線不規則構造 (Field Aligned Irregularity; FAI) エコーの観測も可能である。FAI がレーダー電波の半波長の空間スケールを持つとき、電波をコヒーレントに散乱するため、PANSY レーダーでは約 3m スケールの E 領域 FAI からのコヒーレント・エコーを観測できる。Hashimoto et al.(2019) では、この FAI エコーの混入による IS 観測への干渉を除去するため、PANSY レーダーに備えられた FAI 観測用アンテナアレイ（以下、FAI アレイ）を用いた多チャンネル信号処理技術により、異なる角度からの信号（IS エコーと FAI エコー）を分離した。一方、FAI の観測に主眼を置いて同様の手法を用いれば、E 領域 FAI を詳細に解像し、その運動を観測することが可能である。

PANSY レーダーには FAI アレイのほか、流星観測用アレイ（以下、流星アレイ）も備えられている。FAI アレイは直線状に配置されているため自由度は方位角方向にしか持たないのに対し、流星アレイは 5 本のアンテナが面的に配置されているため、流星アレイを用いることで FAI の立体的な位置情報を得ることができる。そのため、本研究では FAI アレイを用いて電波の送信を行い、流星アレイを用いて FAI からの反射波の受信を行うことを想定する。しかし、観測された FAI に対して Fourier 法や Capon 法等でエコー到来方向を推定すると、アンテナパターンに起因した空間構造の不確定性が発生することが想定される。本来、FAI はレーダー電波と地磁気の磁力線が直交するところで観測されるはずであるが、流星アレイのアンテナ間隔が大きいためにグレーティングローブを生じ、これによってそれ以外の方位にも偽像が生じると考えられる。そこで、その影響を除去し真の空間構造を推定するために、本研究では マッチング追跡に基づいたデコンボリューション処理を行った。本アルゴリズムでは、毎回のイタレーション処理において、流星アレイによる

受信パターンを組み合わせたパターンを差し引いている。これにより、グレーティングローブやサイドローブといったメインローブ以外の領域でもアンテナパターンが考慮されて自動的に応答値が小さくなるため、偽像を抑えつつ高分解能なFAI のイメージング観測が可能となる。

本発表では、アンテナの放射パターンの影響を除去し FAI の正確かつ高分解能に観測できる、マッチング追跡に基づいたイメージング手法の適用について、シミュレーション結果を紹介する。

R005-P20
ポスター 3 ：9/26　AM1/AM2 （9:00-12:30）

#PERWITASARI　SEPTI[1)],Hozumi　Kornyanat[1,2,3)], 西岡　未知 [1)]
[(1] 国立研究開発法人 情報通信研究機構,[(2]NASA Goddard Space Flight Center,[(3]Catholic University of America

Development of an Autonomous Method for Equatorial Spread-F from SEALION Ionosonde Data

#SEPTI PERWITASARI[1)],Kornyanat Hozumi[1,2,3)],Michi Nishioka[1)]
[(1]National Institute of Information and Communications Technology,[(2]NASA Goddard Space Flight Center,[(3]Catholic University of America

We have developed an automatic detection method for nighttime (1800-0600 LT) equatorial spread-F (ESF) from SEALION (SouthEast Asia Low-latitude Ionospheric Network) FMCW ionosonde data. ESF in this study is classified into three categories: range (Q), frequency (F), and mixed (M). We compared our result with the manual scaling in March and September 2013. The comparison with the manual scaled data shows ˜91%, 85%, and ˜89% match for Q, F, and M types, respectively. We analyzed the seasonal and local time variation at Chiang Mai in 2013. The seasonal and local time variation shows a good agreement with the previous studies which indicate high occurrence during equinoxes and pre midnight. The longitudinal and latitudinal variations were analyzed by comparing three different stations: Chiang Mai, Chumphon, and Cebu. The results show that the occurrence is significantly higher in Chumphon and Cebu which are located near the magnetic equator.

R005-P21
ポスター 3 ：9/26　AM1/AM2 （9:00-12:30）

電離圏現象が高精度衛星測位に与える影響

#西岡　未知 [1)], 津川　卓也 [1)]
[(1] 情報通信研究機構

Effects of ionospheric phenomena on precise positioning

#Michi Nishioka[1)],Takuya Tsugawa[1)]
[(1]National Institute of Information and Communications Technology

“Council for the advancement of space weather forecast” was held in the first half of 2022 by the Ministry of Internal Affairs and Communications.
（https://www.soumu.go.jp/main_sosiki/kenkyu/space_weather/index.html）
In the council, “Working group on space weather alert criteria” was established and a new alert system was discussed. It is reported that there is no clear international space weather standard for positioning derived from user-side requirements and the threshold for issuing a warning should be quantitatively determined.
(https://www.soumu.go.jp/menu_news/s-news/01tsushin05_02000047.html)

In this study, we focused on real-time kinematic (RTK) positioning, which uses dual frequency for precise positioning. RTK positioning errors were analyzed with GEONET observation network data developed by the Geospatial Information Authority (GSI）. Two GEONET stations with a distance of 10 km or less between the stations were selected. One station is used as a reference point whose position was already know and the other is used as an assumed station whose station was unknown. The RTK positioning was conducted for the assumed station, and the fix rate of the positioning was analyzed. It was found that fix rates declined during daytime in spring and fall, and nighttime in summer. The former coincides with a period when ionospheric total electron contents are large, while the latter coincides with a period when medium scale traveling ionospheric disturbances often appears.

In this presentation, the effects of ionospheric phenomena on precise positioning will be clarified based on the results of RTK positioning accuracy analysis as a start point of determining the threshold for a new alert system.

電離圏を通過する電波は、電離大気によって伝搬遅延を受ける。電離大気の空間勾配が特に大きい場合は、地上における受信強度が著しく低下する。そのため、GNSS 等を利用した衛星測位では、電離圏の時空間変動の影響を受けてその精度が劣化する場合がある。衛星測位が測位分野の主要な測位手法となる状況の下、2022 年 1 月より総務省にて開催された「宇宙天気予報の高度化の在り方に関する検討会」（https://www.soumu.go.jp/main_sosiki/kenkyu/space_weather/index.html）では、宇宙天気の影響を受ける社会インフラの一つとして測位分野が挙げられ、そのリスクに着目した予報・警報について議論された。その結果、電離圏現象に基づいた指数・基準は存在するが、測位への影響を明確にする予警報の基準が未設定のため、早急に設定する必要があると報告された。測位手法には様々あるが、最も予警報の基準策定の必要性が高いとされた測位手法が二周波精密測位である (https://www.soumu.go.jp/menu_news/s-news/01tsushin05_02000047.html)。

本研究では、二周波精密測位であるリアルタイムキネマティック測量（RTK 測量）に着目し、国土地理院の展開する GEONET 観測網データを用いて、電離圏擾乱時の RTK 測位誤差について解析を行った。GEONET 観測網のうち、観測点間の距離が 10km 以下の 2 観測点を選び、一方を位置が既知の基準点、他方を位置が未知のみなし観測点として、みなし観測点における RTK 測位の解のフィックス率を解析した。その結果、春および秋の昼間、および、夏の夜間にフィックス率が低下することが明らかになった。前者は全電子数の大きい時期と一致し、後者は中規模伝搬性電離圏擾乱の発生時期と一致する。本発表では、RTK 測位の精度解析結果に基づき、電離圏現象が厚生緯度衛星測位に与える影響を明らかにし、測位分野における宇宙天気予警報の基準策定の足掛かりとする。

R005-P22
ポスター 3 ：9/26　AM1/AM2 （9:00-12:30）

GAIA 極域変動版を用いた大規模磁気嵐中の NmF2 と TEC の異なる振舞の調査

#垰　千尋 [1)], 陣　英克 [1)], 品川　裕之 [2)], 三好　勉信 [3)], 藤原　均 [4)]
([1] 情報通信研究機構,[2] 九州大学国際宇宙惑星環境研究センター,[3] 九大・理・地球惑星,[4] 成蹊大学

Investigation of different behaviors of TEC and NmF2 during large geomagnetic storms using polar variable GAIA

#Chihiro Tao[1)],Hidekatsu Jin[1)],Hiroyuki Shinagawa[2)],Yasunobu Miyoshi[3)],Hitoshi Fujiwara[4)]
([1]National Institute of Information and Communications Technology,[2]International Research Center for Space and Planetary Environmental Science, Kyushu University,[3]Department of Earth and Planetary Sciences, Faculty of Sciences, Kyushu University,[4]Seikei University

Behaviors of observed total electron content (TEC) and maximum F-region electron density (NmF2) are similar during medium geomagnetic storms while they are sometimes different during large geomagnetic storms. More significant NmF2 decrease during TEC increase has been reported for more penetration electric field, higher electron temperature case, and morning sector of the initiation of the geomagnetic storms, from model experiments [Jin et al., 2008].

We are extending the GAIA, Ground-to-Topside Model of Atmosphere and Ionosphere for Aeronomy, to include the magnetospheric variation via electric field deposition and auroral electron precipitation at the polar region and penetration of the electric field toward mid-to-low latitude. Using the polar variable GAIA, we have investigated the behavior of TEC and NmF2 during large geomagnetic storms. Evaluation of the model and 3-dimensional distribution of the electron density during the events will be discussed in the presentation.

磁気嵐時における中緯度域の電離圏全電子数 (TEC) と F 領域最大電子密度 (NmF2) の変化は、中規模の磁気嵐時には類似するが、大規模な磁気嵐時には異なる変化が観測される場合がある。TEC が増大する反面 NmF2 が一時減少する振舞について、極域からの侵入電場が大きいほど、背景電子温度が高いほど、また、日本上空では発生タイミングが朝側である場合ほど、NmF2 の減少傾向が大きくなることがモデル実験で報告されている [Jin et al., 2008]。

我々は、対流圏から熱圏までの全球の大気圏と電離圏の主要な大気物理・化学過程を解くモデルである GAIA (Ground-to-Topside Model of Atmosphere and Ionosphere for Aeronomy) に、極域電場およびオーロラ降込みの変動と電場の中低緯度への侵入効果を含めるよう改良を行っている。この GAIA 極域変動版を用いて、大規模磁気嵐イベントにおける TEC と NmF2 の振舞について調査した。イベント再現性のモデル評価およびモデルで得られた変動時の電子密度３次元分布について発表で議論する。

R005-P23
ポスター 3 ：9/26　AM1/AM2 （9:00-12:30）

#惣宇利　卓弥[1)], 新堀　淳樹[2)], 大塚　雄一[3)], 西岡　未知[4)],PERWITASARI　SEPTI[5)], 熊本　篤志[6)], 土屋　史紀[7)], 松田　昇也[8)], 笠原　禎也[9)], 松岡　彩子[10)], 中村　紗都子[11)], 三好　由純[12)], 篠原　育[13)]
([1] 名大　ISEE,[2] 名古屋大学宇宙地球環境研究所,[3] 名大・宇地研,[4] 情報通信研究機構,[5]NICT,[6] 東北大・理・地球物理,[7] 東北大・理・惑星プラズマ大気,[8] 金沢大学,[9] 金沢大,[10] 京都大学,[11]IAR&ISEE,[12] 名大 ISEE,[13] 宇宙研／宇宙機構

Characteristics of Mid-Latitude Plasma Bubble During a Geomagnetic Storm on March 23-24, 2023 using GNSS and Arase Satellite Data

#Takuya Sori[1)],Atsuki Shinbori[2)],Yuichi Otsuka[3)],Michi Nishioka[4)],SEPTI PERWITASARI[5)],Atsushi Kumamoto[6)],Fuminori Tsuchiya[7)],Shoya Matsuda[8)],Yoshiya Kasahara[9)],Ayako Matsuoka[10)],Satoko Nakamura[11)],Yoshizumi Miyoshi[12)],Iku Shinohara[13)]
([1]Institute for Space-Earth Environmental Research, Nagoya University,[2]Institute for Space-Earth Environmental Research, Nagoya University,[3]Institute for Space-Earth Environmental Research, Nagoya University,[4]National Institute of Information and Communications Technology,[5]National Institute of Information and Communications Technology,[6]Department of Geophysics, Graduate School of Science, Tohoku University,[7]Planetary Plasma and Atmospheric Research Center, Graduate School of Science, Tohoku University,[8]Kanazawa University,[9]Emerging Media Initiative, Kanazawa University,[10]Graduate School of Science, Kyoto University,[11]Nagoya University,[12]Institute for Space-Earth Environement Research, Nagoya University,[13]Japan Aerospace Exploration Agency/Institute of Space and Astronautical Science

After sunset, a plasma density depletion (plasma bubble) often occurs at the bottom of the F region over the equator. Plasma bubbles are sometimes extended from the equator to mid-latitudes during geomagnetic storms. Many researchers have studied the characteristics of the mid-latitude plasma bubbles during geomagnetic storms using in-situ satellite observation data. The longitudinal width of mid-latitude plasma bubbles remains unknown, since inclinations of the ionospheric satellites are too low to adequately observe the mid-latitude ionosphere. In this study, we report characteristics of the mid-latitude plasma bubble during a geomagnetic storm on March 23 and 24, 2023, using the Global Navigation Satellite System (GNSS) and the Arase satellite data. We used Total Electron Content (TEC) and Rate of TEC Index (ROTI) derived from GNSS data, along with electron density estimated from the in-situ plasma wave data observed by the Arase satellite.

ROTI enhancements, associated with plasma bubbles, appeared over the magnetic equator in the evening sector around 00:30 UT on March 24 during the main phase of the geomagnetic storm. The enhanced ROTI region extended to the mid-latitudes around 45 N in geomagnetic latitudes in (or within) the American sector. The TEC depletion region also extended to the mid-latitudes. During this time, the Arase satellite passed through the northern part of the mid-latitude plasma bubble around 35 N in geomagnetic latitudes at an altitude of ˜500 km. The electron density showed a depletion from 8.65x10ˆ11 m-3 to 5.65x10ˆ11 m-3 (˜40% decrease). The location of electron density depletion corresponded to the enhanced ROTI and decreased TEC regions. The estimated longitudinal width of the electron density depletion was approximately 535.5 km.

Previous studies based on high inclination satellites such as DMSP and Swarm have reported spatiotemporal variations of mid-latitude plasma bubbles during geomagnetic storms. However, these satellite data cannot provide the longitudinal distribution of the plasma bubble, and the longitudinal structure of the plasma bubble remained unknown. For the first time, the present study revealed the longitudinal distribution of the mid-latitude plasma bubble during the geomagnetic storm, with the Arase satellite observation data. Our analysis results indicate that the longitudinal width of the electron density depletion at the mid-latitudes as observed by the remote sensing observation data (GNSS) corresponds to that as seen in the in-situ observation data (Arase satellite).